Spring 2018

Investigation of the Homologs Rad51 and Dmc1 Role in Cell Division and Homologous Recombination

Amaal Abulibdeh
Missouri State University, Abulibdeh31@live.missouristate.edu

INVESTIGATION OF THE HOMOLOGS RAD51 AND DMC1 ROLE IN CELL DIVISION AND HOMOLOGOUS RECOMBINATION

A Master's Thesis

Presented to

The Graduate College of

Missouri State University

In Partial Fulfillment

Of the Requirements for the Degree

Master of Science, Cell and Molecular Biology

By

Amaal A. Abulibdeh

May 2018

INVESTIGATION OF THE HOMOLOGS RAD51 AND DMC1 ROLE IN CELL DIVISION AND HOMOLOGOUS RECOMBINATION.

Biomedical Sciences

Missouri State University, May 2018

Master of Science

Amaal A. Abulibdeh

ABSTRACT

RecA-like proteins homologs Rad51 and Dmc1 (disruption of meiotic control) promote recombination between homologous chromosomes by repairing programmed DNA Double-Strand Breaks (DSBs). Dmc1 is a Recombinase involved in meiosis-specific repair of DSBs, whereas Rad51 has been found to be involved in meiotic and non-meiotic DSBs repair. Previous studies showed that when *RAD51* is overexpressed, interhomologous recombination still occurs even when *DMC1* is knocked out. Dmc1 and Rad51 have not been fully characterized in the ciliate *Tetrahymena thermophila*. In order to more fully investigate the role of Rad51 and Dmc1 in Homologous Recombination Repair (HHR), this work focuses on using a model organism, *T. thermophila*, to further elucidate the contribution of Rad51 and Dmc1 in DNA repair following various genotoxic stressors (H_2O_2, MMS, and UV radiation). Bioinformatics was used to illustrate the extensive conservation of the Rad51 and Dmc1 homologs in various organisms and between one another. Expression of *RAD51* and *DMC1* was shown to be altered following exposure to H_2O_2, MMS, and UV radiation, and that the *RAD51* expression was significantly higher than Dmc1 expression levels following all DNA damaging agents. Localization studies using Green fluorescent protein (GFP) and Red fluorescent protein (RFP) tagged to *RAD51* or *DMC1* and introduced back into *T. thermophila* revealed that Rad51 does not localize to the micronucleus or macronucleus following exposure to MMS. Tagging revealed that Dmc1 may localize in the micronucleus without DNA damage but does not localize after MMS treatment. Both proteins showed localization outside the nuclei, suggesting expression of the tagged Rad51 and Dmc1 in *T. thermophila*.

KEYWORDS: Rad51, Dmc1, Homologous Recombination, DNA repair, *Tetrahymena thermophila.*

This abstract is approved as to form and content

_____

Joshua J. Smith, PhD
Chairperson, Advisory Committee
Missouri State University

INVESTIGATION OF THE HOMOLOGS RAD51 AND DMC1 ROLE IN CELL DIVISION AND HOMOLOGOUS RECOMBINATION.

By

Amaal A. Abulibdeh

A Masters Thesis
Submitted to the Graduate College
Of Missouri State University
In Partial Fulfillment of the Requirements
For the Degree of Master of Sciences, Cell and Molecular Biology

May 2018

Approved:

_____
Joshua J. Smith, PhD

_____
Colette M. Witkowski, PhD

_____
Amanda C. Brodeur, MD, PhD

_____
Julie Masterson, PhD: Dean, Graduate College

ACKNOWLEDGEMENTS

First, I would like to express my sincere gratitude to my advisor Dr. Joshua J. Smith for the continuous support of my study, for his patience, motivation, and immense knowledge. His guidance helped me in all the time of research and writing of this thesis. I could not have imagined having a better advisor and mentor for my master study.

Besides my advisor, I would like to thank the rest of my thesis committee: Dr. Amanda C. Brodeur, for her insightful comments and encouragement, and Dr. Colette M. Witkowski for steering me in the right direction whenever I needed it.

I would like to thank the members of Smith Lab for their help during the research that went into this Thesis. I would especially like to thank Jeremy Tee for designing GFP and RFP epitope tags.

Finally, I must express my very profound gratitude to my parents and to my husband, Amjed, for providing me with unfailing support and continuous encouragement throughout my years of study. This accomplishment would not have been possible without them.

TABLE OF CONTENTS

LIST OF TABLES

LIST OF FIGURES

LIST OF APPENDICES' FIGURES

INTRODUCTION

The Pathways of Double-Strand DNA Breaks

Deoxyribonucleic acid (DNA) is the genetic material stored within the nucleus of the cell, and the preservation of this genetic information requires not only the accuracy of its copying during DNA replication, but also the availability of multiple DNA repair processes to cope with any loss of genomic material. Unlike any other molecules, DNA requires a single strand of DNA as a template and a region of a few base pairs long on a double-strand of DNA to start the synthesis of a new strand. Once DNA starts forming a new strand, it is partially broken down to monomers and the other strand is used as a template to make a new copy of double-strand of DNA (Aerssens et al., 2001). DNA is continually exposed to the endogenous and exogenous DNA damaging agents, leading to mitotic cell death, permanent cell cycle arrest, and changes that lead to carcinogenesis through (translocations, inversions, deletions), or consequently induction of apoptosis.

Damage to DNA can result from either physical mutagens that cause covalent modifications between neighboring pyrimidine nucleotides resulting in pyrimidine dimmers: (6-4) pyrimidine photoproducts, and cyclobutane pyrimidine dimmers (CPDs), or chemical mutagens (alkylating and oxidizing agents) that intercalate or covalently bind to DNA to produce a specific mutational signature (Hakem, 2008; Helleday et al., 2014; Rothkamm et al., 2003). Mechanisms of DNA repair provide high fidelity and genome integrity (Waters, 2006). Probably one of the most severe type of DNA damage is double-strand breaks (DSBs) that result in loss and rearrangement of genomic sequence. Exogenous agents such as ionizing radiation and chemotherapeutic drugs generate reactive oxygen species and mechanical stress on the chromosomes. Sometimes, when the DNA replication forks face single strand breaks during initiation of the recombination

between homologous chromosomes, DSBs occur, leading to loss/amplification of chromosomal material or to tumorigenesis, if the deleted chromosomal region encodes a tumor suppressor protein (Khanna and Jackson, 2001).

DSBs are initiated when the two complementary sequences of the DNA double helix are broken at sites that are close enough to one another, and base paring is insufficient to keep the two strands of DNA together. Consequently, the two DNA ends generated by DSBs perform a perilous recombination with other sites in the genome. In addition to interfering with transcription or replication of genes, they are disrupted in this process, leading to hybrid proteins or inappropriate activation of genes. One cellular response to DSBs is activation of the DNA repair proteins ataxia-telangiectasia mutated (ATM), which is one of these crucial molecules recruited to the site of DNA double-strand breaks (Maréchal, 2013). Once DSBs occur, ATM phosphorylates downstream substrates such as p53, BRCA1, and NBS1, causing multiple effects on the DNA repair process. ATM deficiency leads to the development of cancer and neurodegenerative syndrome called Ataxia Telangiectasia (A-T), resulting in hypersensitivity to ionizing radiation and chemical agents that yield DNA DSBs.

Two major DNA repair pathways have evolved to cope with DSBs. DSBs are repaired by either Non-Homologous End-Joining (NHEJ) or Homologous Recombination Repair (HRR). Both these pathways are very distinct from one another and function in different ways to effect DNA double-strand breaks repair.

Non-Homologous End Joining

Non-Homologous End Joining is the simplest mechanism that is used at different points of the cell cycle when sister chromatids are not available to be used as homologous recombination templates. It rejoins two ends of a broken DNA molecule without the requirement for homologous sequences between the ends. It involves XRCC4-LIG4 complex, DNA-dependent protein kinase (DNA-PK) holoenzyme of catalytic subunit DNA-PKc, and DNA end-binding heterodimer Ku70-Ku80 (Davis, 2013). The basic mechanism of NHEJ is described in Figure 1. The core component of NHEJ is the Ku protein, a heterodimer of two subunits called Ku70 and Ku80. It binds the ends of a broken DNA strand for repair, protecting them from degradation. The mammalian Ku protein forms a complex with the DNA dependent protein kinase (DNA-PKcs); the serine/threonine kinase is activated in the presence of the DNA ends. Ku protein recruits DNA-PKcs to the broken DNA strands, which together form the DNA-PK holoenzyme. Two relative proteins of DNA-PKcs are implicated in responses to DNA damage such as ATM and ATR. Those proteins are kinases and physically recruited to the site of DNA damage. ATM binds to the DNA and phosphorylates p53 protein in response to DSBs, and ATR phosphorylates the p53 in the same fashion. DNA-PKcs phosphorylates proteins bound to the DNA around the break. Then a complex of MRE11, XRS2 and RAD50, which possesses exonuclease, endonuclease and unwinding activity, localize to site of DNA double-strand breaks in mammalian. The human Mre11 protein has nuclease activity and Nbs1 seems to replace Xrs2. This complex trims the DNA ends to create single-stranded overhangs before they can be rejoined. Another factor possesses hydrolytic activity called Artemis as shown in Figure 1B, can process DNA DSBs before NHEJ occurs (Jackson, 2002; Featherstone et al., 1999). Finally, ligase IV stimulates

DNA end-ligation, which functions in a tight complex with protein XRCC4 (Ramsden et al., 1998). XRCC4 is a substrate for DNA-PKcs that might regulate the activity of the ligase.

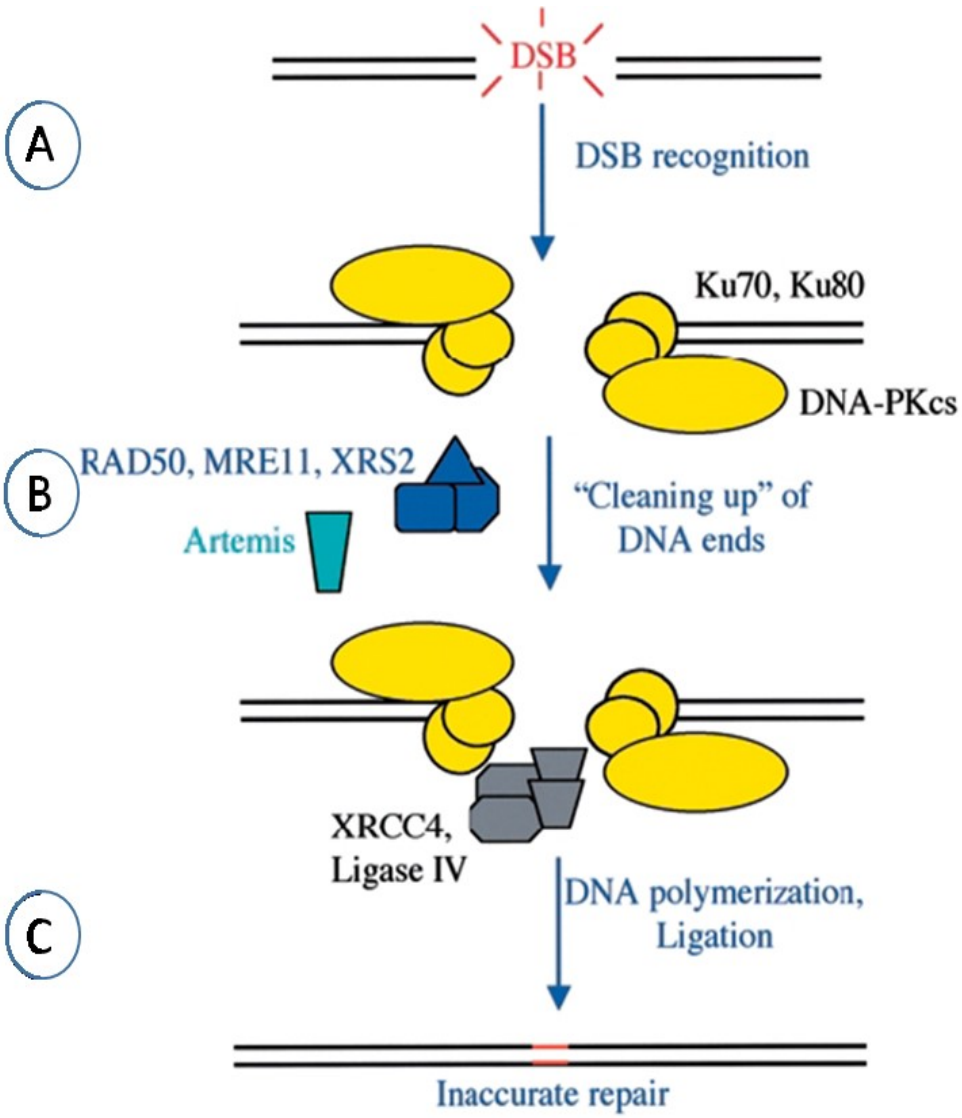

Figure 1: Schematic of Non-Homologous End Joining Pathway. NHEJ requires several factors to rejoin the two broken ends of the DNA after inducing DSBs. **(A)** DSB recognition, a heterodimer of two subunits (Ku70 and Ku80) that quickly binds to free ends to recruit DNA-PKcs; **(B)** Processing of DSB ends, Ku recruits XRCC4 along with DNA ligase IV, and DNA-PKcs-mediated phosphorylation of XRCC4 may influence its activity. The MRE11-RAD50-XRS2 complex contains xo- and endo-nuclease and helicase activity that processes the DNA ends before ligation. Complex DNA damage may be processed via the DNA-PKcs-mediated recruitment of the nuclease Artemis; **(C)** Sealing of DSB, ligase IV then brings about the physical relegation of the DNA ends. In many cases, NHEJ may also require the actions of a DNA polymerase(s) (Jackson, 2002).

Homologous Recombination Repair

The homologous recombination repair (HRR) pathway maintains genomic integrity during both meiosis and mitosis, and it provides a template-dependent repair and is tolerance of complex DNA damage including DNA gaps. The HRR pathway is activated when the cell is in the late S/G2 phase, and the template has recently been duplicated. This mechanism requires the damaged chromosome to enter synapsis with an undamaged DNA strand, which shares extensive sequence homology. The HRR pathway can be divided into three steps. In the first step, presynaptic, multiple nucleases resect both ends of a DNA double-strand break to generate 3' ssDNA overhangs and enable the Rad51 recombinase nucleoprotein filament to search for homology as illustrated in Figure 2A. The second step is synapsis where the formation of a D loop takes place, and the invading strand serves as a primer for DNA synthesis (Figure 2B). During the third step, a postsynaptic step, the intact DNA structure is restored (Figure 2D). An essential event in the presynaptic step is the nucleolytic resection of the DNA DSBs in the 5' to 3' by a complex containing Rad50, Mre11 and Xrs2 (NBS1 in human) and the complex is responsible for sensing DNA breaks, activating the checkpoint, and controlling the end resection (Sebesta et al., 2016). Also, the replication protein A (RPA) binds to 3' ssDNA overhangs for nucleation of the Rad51 recombinase. There are different recombination mediators that are required to load Rad51 onto ssDNA tails such as Rad52, Rad54, and Rad55-Rad57 complex (Gasior, 1998; Sung P, 1997; Ogawa et al., 1993).

Notably, Rad52 binds to DNA DSBs leading to competition with Ku for DNA ends that may determine which one of the two DNA DSBs repair pathways is applied (Lieber MR. 2010). Rad52 helps in binding of the DNA and Rad51 as well as RPA through different domains (Seong et al., 2008). After formation of the Rad51

nucleoprotein filament, nucleofilament interacts with an undamaged DNA molecule to search for homologous sequences within the genome during the synapsis step. Once homology is found, the transient structure known as the D-loop is formed.

Before any extension of the D-loop by replication factors, Rad54 translocase should free the 3'-OH of the invading strand to prime DNA synthesis off the template duplex DNA. Next, the replication factory C (RFC) clamp loader loads PCNA onto the D-loop to allow DNA polymerase δ to extend the D-loop (Li and Heyer, 2008; Li and Heyer 2009). Some studies have shown that other polymerases are involved in HRR such as polymerase η and polymerase κ, which function in the DNA repair by translesion synthesis (Sebesta et al., 2011). Finally, the 3' end of the damaged DNA is extended by a DNA polymerase that copies the information from the undamaged DNA strand, and later the ends are ligated by DNA ligase I as shown in Figure 2 (Jackson SP, 2002). During migration, Holliday junctions (HJs) allow a branch migration process to occur where the strands move through the junction point. After migration, HJs are resolved by cleavage or ligation to yield two intact DNA helixes.

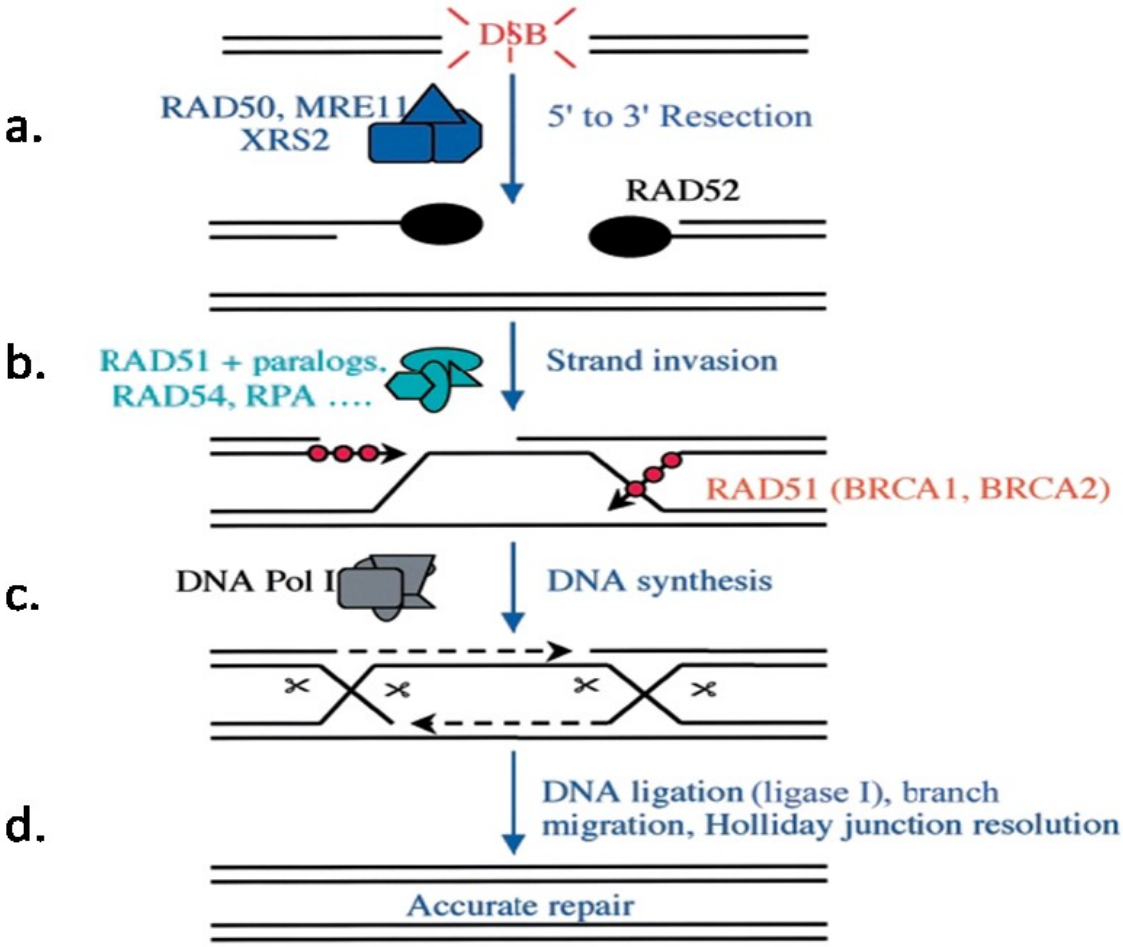

Figure 2. The main steps of the DNA DSBs repair pathway of HRR. Upon DNA damage, the free ends of a DSB are first processed by an exonuclease. **(A)** The first step, presynaptic, the nucleolytic resection of the DNA DSBs in the 5' to 3' by a complex containing Rad50, Mre11 and Xrs2 takes place to generate 3' ssDNA overhangs; **(B)** RPA binds to 3' ssDNA overhangs for nucleation of the Rad51 recombinase; recombination mediators are required to load Rad51 onto ssDNA tails such as Rad52, Rad54, and Rad55-Rad57 complex for Rad51 nucleoprotein filament; **(C)** The second step is synapsis. Rad51 nucleoprotein filament searches for homologous sequence within an undamaged DNA sequence and D loop is formed; invading strand serves as a primer for DNA synthesis and the 3' end of the damaged DNA is extended by a DNA polymerase; **(D)** During the third step, postsynaptic, the intact DNA structure is restored, and gaps are filled with DNA ligase I. Holliday junctions allow a branch migration process to occur and then resolved by cleavage to yield an intact DNA helix (Jackson SP, 2002).

Eukaryotic Homologs of RecA: Rad51 and Dmc1

Rad51 and Dmc1 recombinases are the eukaryotic homolog of *Escherichia coli* RecA strand transfer enzyme that can promote the DNA double-strand breaks repairing through homologous recombination by catalyzing efficient homologous pairing (Dresser,1997). The yeast and the human Rad51 and Dmc1 proteins are closely related to RecA at the amino acid level (Appendix B - Figures B1 & B2), where human Rad51 and Dmc1 share about 54% of their amino acids (Masson et al., 2001). It is unknown why eukaryotic cells possess two RecA homologs. However, there are obvious differences in their expression profiles. Some co-localization studies show the appearance of Rad51/Dmc1 foci in meiosis of yeast coinciding with the presence of DNA DSBs (Bishop, 1994). The assembly of Rad51 foci in yeast requires different proteins such as Rad55, Rad52, and Rad57 (Gasior et al., 1998). In addition, it was found that Dmc1 foci are detectable in *rad51* mutant during meiotic prophase, and Rad51 foci are normal in *dmc1* mutants, indicating that the assembly of Rad51 protein on the chromosomes is independent of the DMC1 function.

The Dmc1-independent assembly of Rad51 is also seen in a *dmc1* knockout mouse (Bishop, 1998; Pittman et al., 1998). These findings led to a conclusion that Rad51 and Dmc1 function independently, rather than forming a heteromeric nucleoprotein filament containing both proteins at DNA DSBs site. However, other studies have been proposed that the budding yeast *rad51* mutant is defective in Dmc1-focus formation (Shinohara et al., 1997), indicating that Rad51 promotes Dmc1-assembly. The presence of several Rad51 paralogs in higher eukaryotes with weaker homology to the catalytic domain of Rad51 such as XRCC2 and XRCC3 suggests that some of these factors may interact directly with Rad51 and help in the assembly of Rad51 nucleoprotein filament

(Liu N, 2002). Studies on mouse cells that lack either XRCC2 or XRCC3 have showed a reduction in the rate of HRR as seen in cells lacking Rad51.

In mitotic cells, Rad51 is required to be oriented towards inter-sister recombination (Masson et al., 2002), but meiotic recombination is dependent upon both Rad51 and Dmc1 where Dmc1 might help to direct Rad51 towards inter-homologous recombination (Schwacha et al.,1997), while Rad51 promotes the formation of Dmc1-ssDNA filaments (Cloud, 2012). A previous study in yeast has found that the meiotic phenotypes of the *rad51* and *dmc1* single mutants appear to be similar in which both accumulate DNA DSBs to levels higher than normal (Bishop et al., 1992; Schwacha et al., 1997), and they exhibit a significant reduction homologous pairing and delayed synapsis (Rockmill et al., 1995). Human Rad51 and Dmc1 proteins are with DNA-dependent ATPase activity and possess the ability to promote homologous DNA pairing and strand reactions in vitro (Tanaka et al., 2002).

Interestingly, the three proteins, Rad51, Dmc1, and RecA share two highly conserved motifs, Walker A and Walker B for ATP binding and hydrolysis (Chang et al., 2015). This indicates the significant functional similarities of the two proteins (Rad51 and Dmc1) to RecA. However, Rad51 and Dmc1 have an additional N-terminal region that is absent in RecA, and they lack an extended C-terminal region found in RecA (Figure 3C; Yu et al., 2001).

The difference between the two recombinases Rad51 and Dmc1 is still not well understood. These proteins share sequence, structural homology, and a close functional relationship, but they have some differences in the location of expression and also the structure itself. The biochemical analysis of Rad51 is well advanced, but much less is known about the Dmc1 protein. Electron microscopic observations of human Rad51

revealed that it forms helical filaments in ssDNA in the presence of ATP, which carries out a strand exchange reaction (Okorokov, 2010). Like Rad51, RecA binds DNA to form helical nucleoprotein filaments. Surprisingly, Dmc1 forms an octameric ring structure (an eight-subunit ring with a central hole) on the DNA, and these rings are often found to form short filaments composed of stacked rings (Figure 3A-B). The biological significance of these structures remains to be elucidated. DNA passes through the central channel of Dmc1, and the rings may open to encircle the DNA.

Although much emphasis is often placed on the deleterious effects of DSBs, they are not always harmful to the cell. Elevated levels of Rad51 expression could be beneficial where DSBs occurs naturally. Also, meiotic recombination is involved in genetic diversity and potential evolutionary. On the other hand, the opposite of that statement is true. Some human cancer types exhibit overexpression of RAD51 to very high levels in the absence of DNA damage agents, suggesting that overexpression of Rad51 may support the cancer development in tumor cells (Li et al., 2017).

Overexpression of Rad51 will cause lower homologous recombination efficiency and reduced viability (Kim et al., 2001). Tumors with high level of a Rad51 expression exhibit serious pathologic features (Qiao et al., 2005). Conversely, the expression of Rad51 is reduced in some sporadic cancer cells. On the other hand, nothing reported about DMC1 expression happens to be related to cancer. Indeed, a physical analysis revealed that *rad51* and *dmc1* mutants accumulate DSBs (Shinohara et al.,1992). In addition, in *S. cerevisiae*, *dmc1* mutation triggers cell cycle arrest and a reduction in

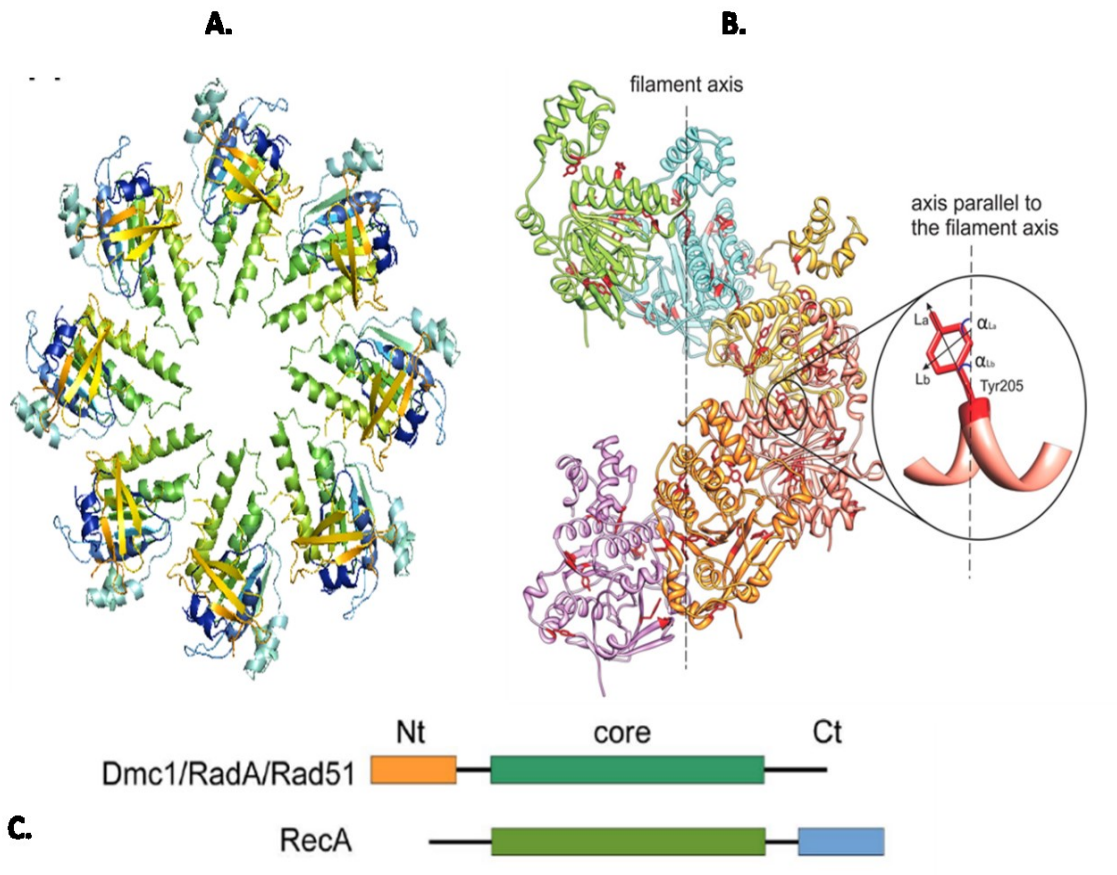

Figure 3. Comparison of Rad51 Model with Dmc1 Structure and Schematic Representation of the Domain Organization of the RecA/ Rad51 Recombinase family. (A) The Octameric Ring Structure of Dmc1. **(B)** The helical filament structure of Rad51**. (C)** Schematic representation of the domain organization Rad51/Dmc1 and RecA. The N-terminal domain (Nt) of Rad51/Dmc1 is in orange; the C-terminal domain of RecA is in blue and the core domain is in green. RadA is RecA protein homolog from the archaeon *Sulfolobus solfataricus* (Reymer et al., 2009; Okorokov et al., 2010)

chromosome synapsis (Bishop et al.,1992). In mice, a *dmc1* knockout is viable, but unable to reproduce since the reproductive organs are smaller than normal (Yoshida et al.,1998). This is expected because Dmc1 protein takes place at the time of recombination of the homology search, so absence of Dmc1 will result in the absence of the interaction between non-homologous strands. Meiotic arrest occurs in both *rad51* and *dmc1* mutants but more largely is in *dmc1* mutant. Placing Rad51 mutation into *dmc1* strain weaken the arrest phenotype in the same level *rad51* single mutant does (Shinohara et al.,1997). These results raise the possibility that Rad51 is required for persistent meiotic arrest in a *dmc1* mutant.

Since both Rad51 and Dmc1 are involved in HRR, *rad51* mutants are much more sensitive to DNA-damaging agents such as Methyl Methanesulfonate (MMS). In this study, the expression of Rad51 was induced by introducing the cells into MMS agent to damage the DNA. Tumor-associated variants in human RAD51 have a change in the catalytic activities of the Rad51-DNA filaments, and therefore it affects the efficacy of HRR and promote the genomic instability (Ristic et al.,2005). The exact cause of Rad51 overexpression is not known, but there are important clues. For example, the wild-type p53 protein directly interacts with the Rad51 protein, suppressing the transcriptional regulation of *RAD51* (Buchhop et al., 1997). Considering this, tumors suppress the function of p53 and hence upregulate *RAD51* expression. Also, many factors such as a transcriptional activator protein (AP2) in combination with p53 down-regulates *RAD51* transcription (Hannay et al., 2007). In addition to p53 interaction, Rad51 interacts with peptides derived from Brca2 but no direct interaction has been reported with Brca1 (Mizuta et al., 1997; Sharan et al.,1997). A recent work has found a strong links between HRR and the breast cancer susceptibility proteins (Brca1 and Brca2) and loss of function

of either one will reduce the efficiency of accurate homology directed DNA repair. The main defect between the interaction of Rad51 and Brca2 and the influence of these tumor suppressors exert over *RAD51* activity lead to genome instability in these cell line in Rad51-mediated DNA repair systems (Tarsounas et al.,2004; Jasin M, 2002). Moreover, there is evidence that oncogenic fusion tyrosine kinase BCR/Abl, the result of translocation, increases the *RAD51* expression (Slupianek et al., 2001), and maybe c-AbI is involved in up-regulating *RAD51* transcription (Choudhury et al., 2009).

Interestingly, the heterodimeric Hop2-Mnd1 complex are required for normal progression of meiotic recombination (Petukhova al et.,2003), and mutations in Hop2 have been found in early onset familial breast and ovarian cancer patients (Peng et al., 2013). In general, better understanding of how *RAD51* expression is up-regulated should be useful in the analyses of primary tumors and help to determine potential treatment modalities.

Hop2-Mnd1 Complex

The heterodimeric Hop2-Mnd1 complex is a conserved recombinase cofactor that stabilizes the presynaptic filament. It promotes the capture of the double-stranded DNA partners by the recombinase filament to assemble the synaptic complex (Chen et al., 2004; Bugreev et al., 2014). The mammalian Hop2-Mnd1 complex physically interacts with Rad51 to stabilize their function in mediating homologous pairing between the recombining DNA molecules to form the D-loop. However, it appears to interact with Dmc1 in *S. pombe* (Ploquin et al., 2007). The X-ray scattering analysis revealed that Hop2-Mnd1 complex is a V-shaped molecule that regulates ATP and DNA binding by Rad51 and Dmc1. Recent work has provided an evidence for the existence of three

distinct DNA binding domains in Hop2-Mnd1 complex. It binds to dsDNA preferentially over ssDNA (Pezza et al., 2006). Specifically, N-terminal region of Hop2 and Mnd1 prefers dsDNA, but the C-terminal region of Hop2 has a preference for ssDNA (Zhao et al., 2014). Based on new studies, Hop2 can bind DNA, but only Mnd1 seems to interact with hRad51 once HRR is elevated (Chi et al., 2007). Genetic studies in *S. cerevisiae* have found that *hop2* mutants arrest in the meiotic prophase, DSBs are not repaired, and more frequently synapsed with a non-homologous counterpart (Leu et al., 1998). Similarly, *mnd1* mutants arrest before the first meiotic division and confers very similar phenotypes to that of *dmc1* mutants (Henry et al., 2006). Both *hop2* and *dmc1* mutants accumulate unrepaired DSBs and show strong prophase arrest. Importantly, mutations in *hop2* have been found in different types of cancer such as early onset familial breast (Peng et al., 2013) and XX ovarian dysgensis (Zangen et al.,2011; Zhao, et al.,2015).

Tetrahymena thermophila as a Model Organism

Tetrahymena thermophila is a free-living unicellular eukaryote that belongs to the ciliated protozoa (Eisen, J.A. 2006). It grows rapidly to high density over a wide range scale; it has locomotory and oral cilia that organized into membranelles to sweep food particles into oral cavity (Peterson et al.,2002). It is greatly used in research because it possesses special advantages for the study of regulated secretion, ciliary motility, chromatin function, and regulation (Orias, 2000). In addition to that, it is easily manipulated by genetic techniques such as, epitope tagging under the cadmium-induced promoter *MTT* (Shang at el.2002) by inserting transgenes into the non-essential *BTU1* locus, transformation, knockout, knock in gene, suppression and inducible gene expression (Eisen J.A.2006). Homologous recombination allows any region of the

genome to be targeted for manipulation. The reason behind using *T. thermophila* as a model in this project is that it exhibits nuclear dimorphism in which each cell has two nuclei, the micronucleus (MIC) and the micronucleus (MAC). The MIC is a germline that passes the genetic information by conjugation in *T. thermophila* life cycle, and it is in the form of heterochromatin containing five pairs of chromosomes, and therefore it is silent, except during meiosis. However, the DNA of the MAC is in the form of euchromatin consisting of approximately 180 chromosomes (Orias, 2012), transcriptionally active, and it divides amitotically. Studying Rad51 and Dmc1 in *T. thermophila* has a great advantage for being Dmc1 a meiosis-specific and only expressed in the micronucleus during conjugation, and Rad51 is expressed in both MAC and MIC. The life cycle of *Tetrahymena* consists of an alternation of haploid and diploid stages with the reference to the germline. Conjugation is the sexual stage of the *Tetrahymena* life cycle where two starved cells pair of complementary mating type form a junction for exchanging genetic information shown in Figure 4. Then, it is followed by micronuclear meiosis, producing four haploid nuclei, but only one of them is functional and three of four haploid nuclei are degraded. This is the stage at which homologous meiotic recombination occurs and Dmc1 localizes to this structure. During mitosis, the functional micronuclei undergo mitosis producing two gamete pronuclei. Gamete nuclei are exchanged and fused to form the zygote nucleus, which undergoes two mitosis rounds. This is the stage at which site-specific DNA rearrangements and mating type determination occur in the MAC. The nuclei produced by mitosis differentiate into new micronuclei and macronuclei. Exconjugant separation occurs, in which the old macronucleus and one of the two new micronuclei are destroyed. Then each exconjugants undergoes the first postzygotic cell

division generating four karyonide cells, each consists of both new MAC and MIC. Finally, these cells continue multiplication by binary fission (Orias, 2012).

Meiosis in *Tetrahymena thermophila*

Unlike many other eukaryotes, meiosis in Tetrahymena occurs in MIC, whereas the MAC degenerates and a new MAC is recreated from the MIC. Meiosis doesn't involve synaptonemal complex (SC), and it elongates the nuclei during prophase to 50 fold, twice the length of the cell. All the centromeres are arranged at one end of the nucleus, and the telomeres gather at the opposite end (Wolfe et al.1976; Loidl and Scherthan.2004). This meiotic bouquet arrangement (crescent; Ray, 1956) promotes homologous pairing and crossing over (Wolfe et al.1976). Reaching MICs their maximal elongation during DSBs is initiated by nuclease Spo11 protein that is removed at 5' end and 3' ssDNA overhangs must be generated. Shortening, widening the DNA, and limiting the homology search to essentially one-dimensional space are required to perform homologous meiotic recombination in a few hours. Chiasmata is needed for separation of meiotic bivalents to avoid aneuploidy. A defect in chiasma structure will result in the separation of bivalents into univalents due to the deficiency in HOP2 function. In general, completion of meiosis prophase takes around 3.5 hours.

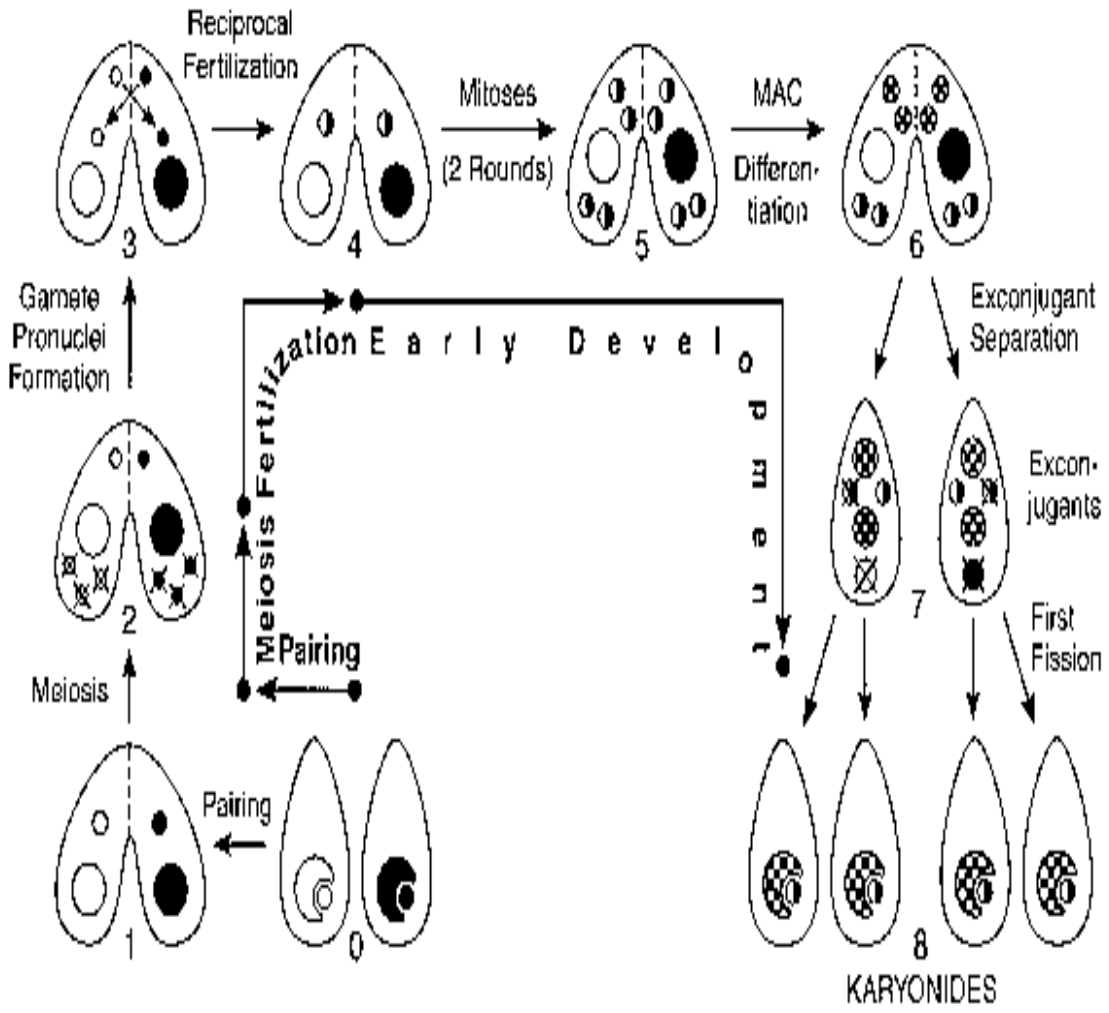

Figure 4. The *Tetrahymena thermophila* life cycle. Vegetatively growing cells reproduce asexually. Conjugation is the sexual stage of the *Tetrahymena* life cycle where two starved cells pair of complementary mating type form a junction for exchanging genetic information.in the first step, the micronuclear meiosis produces four haploid nuclei (HRR occurs at this step), but only one of them is functional and others are degraded. The functional micronuclei undergo mitosis producing two gamete pronuclei. Gamete nuclei are exchanged and fused to form the zygote nucleus, which undergoes two mitosis rounds. The nuclei produced by mitosis differentiate into new micronuclei and macronuclei. Exconjugant separation occurs; the old macronucleus and one of the two new micronuclei are destroyed. Then each exconjugants undergoes the first postzygotic cell division generating four karyonide cells, each consists of both new MAC and MIC. Finally, these cells continue multiplication by binary fission (Orias, 2012).

The Recombinase Proteins and Hop2-Mnd2 Complex in *Tetrahymena thermophila*

T. thermophila Rad51 cDNA has 996 base pairs coding for a protein of 331 amino acids with a mass of 36.3 kDa, whereas the sequence of *T. thermophila Dmc1* cDNA has 1,071 base pairs coding a protein of 356 amino acids with a mass of 37 kDa (Tetrahymena Genome Database, http://www.ciliate.org) (Stover et al.2006). Immunostaining and protein tagging demonstrated that numerous DSB-dependent Dmc1 foci is formed on chromatin in elongating prophase I of meiosis, whereas weak Rad51 foci appear only in shortening nuclei after maximal elongation (Howard et al.,2011). Localization and nuclear elongation begin 2 hours after meiosis induction, and this explains the reason behind the presence of Dmc1 foci peaks at that time. Similarly, Rad51 expression peaks during prezygotic development in conjugating Tetrahymena (Marsh et al., 2000). A proximity ligation assay detected large amounts of Dmc1 protein signals with meiotic nuclei, whereas Rad51 protein signals was more common in somatic nuclei, not detected on meiotic chromatin (Howard et al., 2011). This supports the hypothesis that Dmc1 is meiosis-specific because it localizes to the micronucleus during conjugation. However, Rad51 localizes to the micronucleus (Smith et al., 2004). In the absence of Dmc1, efficient Rad51-dependent repair takes place via the sister chromatid, but the chromosomes remain univalent, suggesting minimal Rad51 protein is required for the repair of meiotic DSBs and homologous crossover does not occur. Also, the inter-homolog repair deficit in *dmc1* mutant meiosis is consistent with a requirement of Dmc1 to homolog between recombination partners. Basically, Dmc1 is more efficient than Rad51 in searching similar but non-identical DNA sequences at DSBs (Lee et al., 2015).

In response to treatment with MMS, Rad51 protein levels increased followed by localization in the macronucleus (Campbell and Romero.1998). In the absence of Rad51,

chromosomes of metaphase meiosis I were fragmented and pulsed-field gel electrophoresis exhibited that DNA is permanently broken (Howard et al.,2011). In contrast, Dmc1 foci form independently of Rad51. Dmc1 nucleoprotein filaments can be formed without the participation of Rad51, but they are inefficient for strand exchange, therefore, Rad51 is required for the repair of meiotic DSBs (Brown et al.,2015).

The phenotypic of *rad51* knockout in the developing macronuclei displays an increase in the cell mass and macronucleus volume, greater than wild-type cells. The absence of Rad51 in progeny cells prevents the initiation of first vegetative division and leads to developmental arrest (Marsh et al., 2001). Also, a phenotype of overexpression Rad51 results in cells without macronuclei due to the defect in the initiation of macronuclear elongation (Figure 5; Dr. Smith J, Unpublished Data). These results support the idea that Rad51 participate in a cell cycle progression and inhibition of micronuclear elongation during DNA damage.

Hop2 (for homologous pairing 2; also known as TBPIP, and as PSMC3IP in mammals; Neale et al., 2006) binds as a complex with Mnd1 and enhances the processing of meiotic DSBs. It was reported that Hop2-Mnd1 complex stabilizes the Rad51 and Dmc1-ssDNA nucleoprotein filaments and enhance their ability to invade duplex DNA (Chi et al., 2007). In *Tetrahymena*, meiotic Hop2 protein is specific for Dmc1 nucleoprotein filaments, and the ubiquitous version of Hop2 protein functions with Rad51 in inter-sister repair. Since Hop2-Mnd1 is involved in meiotic recombination, any mutation in *HOP2* will cause severe pairing defects. In the absence of meiotic Hop2, the

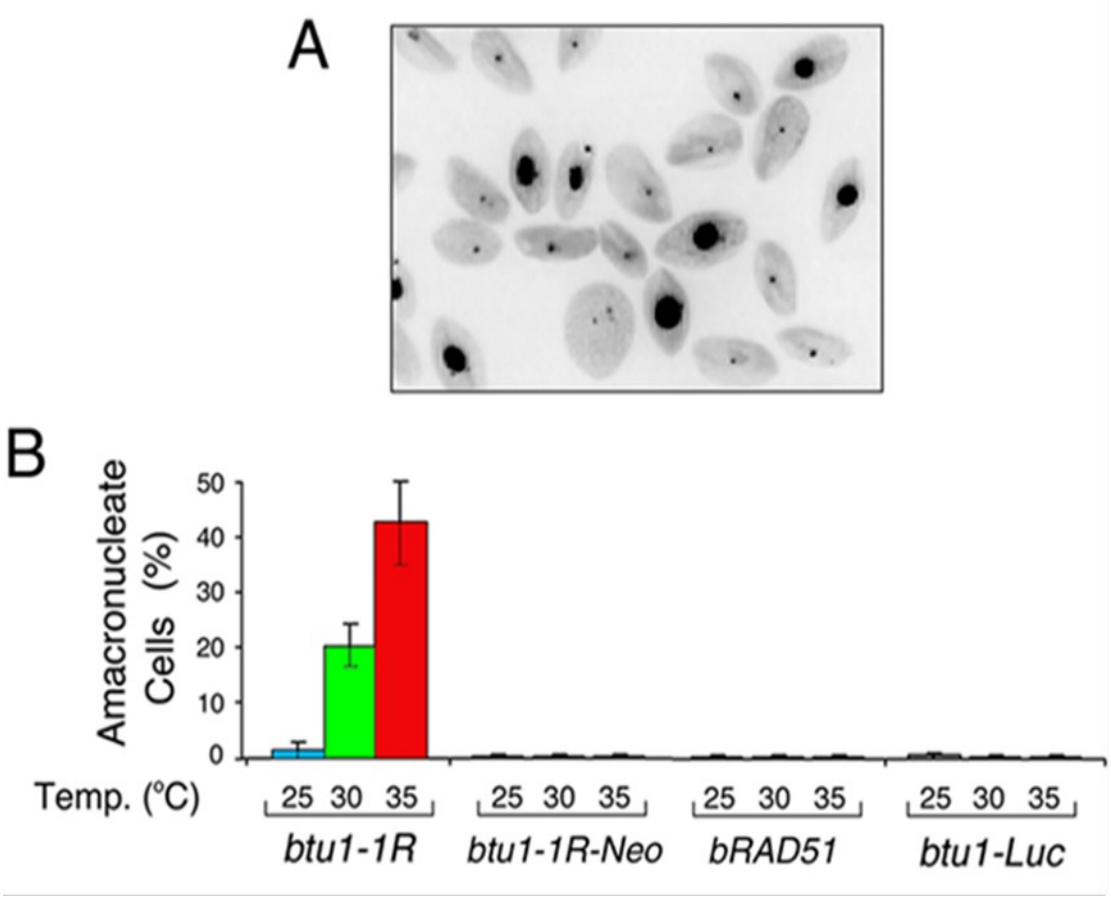

Figure 5. Overexpression of RAD51 causes an amacronuclear cell phenotype. (A) RT-PCR for CU522 (*btu1-1*), *btu1-1R* (*RAD51* overexpression), *btu1-Luc* (Luciferase overexpression) with and without reverse transcriptase (AMV). No product was detected for *btu1-1R*, *btu1-Luc* showing that 100% of the *btu1-1* allele was assorted away. None of the samples without AMV showed any amplification. **(B)** Graph of the percentage of amacronucleate cells observed at 25°C, 30°C, and 35°C. The amacronucleate phenotype was tested for in *bRAD51 (RAD51* driven by *RAD51* promoter), *btu1-Luc*, *btu1-1R*, and *btu1-1R-Neo* (*btu1-1R* disrupted with Neo cassette) (Unpublished data).

early meiotic development of MICs was normal, and DSBs are repaired normally. However, chromosomes remain univalent at metaphase I (Mochizuki K. 2008). The protein family database (Pfam) has reported two *Tetrahymena* Hop2 homologs and two Mnd1 homologs. My goal is to confirm this hypothesis using bioinformatics data.

Purpose Statement

The purpose of this study is to investigate the homologs Rad51 and Dmc1role in homologous recombination repair. The results of previous studies initially indicated that Dmc1 does not localize to either micronucleus or macronucleus after treatment with MMS. However, the expression of *Dmc1* increases after the treatment and may not be involved in the actual repair process. It probably plays role in regulating *RAD51* expression levels, therefore this study aims to further characterize the relationship between Dmc1 and Rad51 to better understand the factors that are involved in regulating their expression during DNA repairing damage. First, the amino acid sequences of Dmc1 and Rad51 homologs in *T. thermophila* and different higher and lower organisms were analyzed using bioinformatics techniques to determine the functional conservation. Quantitative Reverse Transcriptase Polymerase Chain Reaction (qRT-PCR) was used to explore *DMC1* and *RAD51* expression levels in response to DNA damage caused by MMS, H_2O_2, and UV. Transformation of *DMC1* and *RAD51* genes with different epitope tags (2HA, Flag) into *T. thermophila* was done to perform western-blot analysis. Localization studies of Dmc1 and Rad51 in response to MMS damage was performed using fluorescence microscopy using Green/Red Fluorescent Protein (GFP/RFP) Tags. These results will provide insight into the relationship between Dmc1 and Rad51 and their role in DNA repair in *T. thermophila*.

MATERIAL AND METHODS

Tetrahymena thermophila Strain and Growth Conditions

Tetrahymena thermophila strains CU522 and CU725 (*T. thermophila* Stock Center, Cornell University) containing the mutant *btu-1* gene (K350M) that confers paclitaxel sensitivity, were grown in 2% PPYS (2% bacto proteose peptone, 0.2% bacto yeast extract, 0.1% sequestrene) with 1x Penicillin/Steptomycin/Fungizone (PSF) (Thermo Scientific HyClone, Logan, UT, Cat #SV30079.01) at 30 ^{o}C incubator without shaking. Further details on each strain and construct used for this project are noted below in Table 1.

Cryopreservation of *Tetrahymena thermophila*

RAD51 and *DMC1* constructs were grown in 20 mL of 2% PPYF and 1x PSF in a 30 ^{o}C shaking incubator. The cells were counted using a hemacytometer and diluted to $2x10^5$ cells/mL. Then, 10 mL of the culture was centrifuged at 3,000 rpm for 3 min (Marathon 21000R, Fisher Scientific). Pallets were resuspended in 10 mL of 10 mM Tris-HCL pH 7.5 and starved at room temperature for 3 days. Cells were centrifuged again at 3,000 rpm for 3 min (Marathon 21000R, Fisher Scientific) and resuspended in 2 mL of DMSO solution [12.1 mL 10 mM Tris-HCL pH 7.5, 1.9 mL dimethyl sulfoxide (DMSO)]. Immediately, 300 μL was aliquoted into cryovials and allowed equilibrate at RT for 30 min. The vials were placed in a Nalgene 5100 Cryo 1 ^{o}C freezing container (Cat.# 5100-0001) and stored overnight at -80 ^{o}C . The next day, the vials were placed in the liquid nitrogen to be used for further studies

Table 1: *T. thermophila* Stains.

Name	Genotype	Phenotype	Description
CU522	MIC: *mpr1-1/mpr1-1, btu1-1::btu1-1M350K/btu1-1::btu1-1M350K*. MAC: *btu1-1::btu1-1M350K*	6-methylpurine resistant, paclitaxel sensitive, vinblastine resistant	*BTU1* mutant used for transformation of epitope tagging constructs
CU725	MIC: *chx1-1/chx1-1 btu1-1::btu1-1M350K/btu1-1::btu1-1M350K* MAC: *btu1-1::btu1-1M350K*	Cyclohexamide, paclitaxel sensitive, vinblastine resistant	*BTU1* mutant used for transformation of epitope tagging constructs
2HA-RAD51	MAC: *btu1-1M350K ::2HA-RAD51*	Paclitaxel resistance	Expresses 2HA-tagged RAD51, CU522 background
2HA-DMC1	MAC: *btu1-1M350K ::2HA-DMC1*	Paclitaxel resistance	Expresses 2HA-tagged DMC1, CU522 background
FH6-RAD51	MAC: *btu1-1M350K :: FH6-RAD51*	Paclitaxel resistance	Expresses FH6-tagged RAD51, CU725 background
FH6-DMC1	MAC: *btu1-1M350K :: FH6-DMC1*	Paclitaxel resistance	Expresses FH6-tagged DMC1, CU725 background
GFP-RAD51	MAC: *btu1-1M350K :: GFP-RAD51*	Paclitaxel resistance	Expresses GFP-tagged RAD51, CU725 background
GFP-DMC1	MAC: *btu1-1M350K :: GFP-RAD51*	Paclitaxel resistance	Expresses GFP-tagged DMC1, CU725 background
RFP-RAD51	MAC: *btu1-1M350K :: RFP-RAD51*	Paclitaxel resistance	Expresses RFP-tagged RAD51, CU522 background
RFP-DMC1	MAC: *btu1-1M350K :: RFP-RAD51*	Paclitaxel resistance	Expresses RFP-tagged DMC1, CU522 background

LR Clonase™ Reaction

LR Clonase™ II enzyme mix (Invitrogen, Cat. #11791100) was made to generate an expression clone between an entry clone and a destination vector shown in Figure s.4-13. pMTFH6-GTW, pBM2HA-GTW (Washington University in St. Louis), pBMRFP-GTW, and pBMGFP-GTW (constructed by Jeremy Tee, Missouri State University, Springfield, MO) were used as a destination vector to insert pENTR-RAD51 and pENTR-DMC1 into the vector. Each reaction of 5x solution contained: 2 µL/150 ng PENTR-plasmid, 1 µL destination vector (200 ng/µL of HA and FLAG; 400 ng/µL of RFP and GFP); and brought to 4 µL total volume with nuclease-free water. Then 1 µL of LR Clonase™ II enzyme mix to the reaction was added and kept overnight at room temperature. The next day, 0.5 µL 2µg/µL Proteinase K solution was added to terminate the reaction and incubated at 37 ° C for 30 min.

Electroporation Transformation of *E. coli*

LR clones reactions were transformed into electrocompetent *E. coli* cells (DH10B). A mix of 50 µL of DH10B cells and 1 µL of the LR clonase reaction were placed to a chilled electroporation cuvette (Fisher). Samples were electroporated at the following setting: 2.5 kV voltage, 200 ohms resistance, and 25 µF capacitance (BIO-RAD Gene Pulser II Electroporation System.) Recording time was between (4-5 ms); Cells were transferred into 1 mL of LB media and allowed to recover for one hour at 37 ˚C. After recovery, 100 µL of cells were plated onto LB-Amp plate (1% w/v bacto-tryptone, 1% NaCl, 0.5% yeast extract in water with 100 µg/mL ampicillin) and allowed to grow overnight at 37 °C. The next day, different colonies were picked and surviving

colonies were screened by plasmid isolation and restriction enzyme digests for presence of *DMC1* or *RAD51*.

Midiprep DNA Purification

Positive constructs were selected to perform a Midiprep DNA isolation. Media (25 mL) of LB+AMP (1% w/v bacto-tryptone, 0.5% yeast extract, 1% NaCl in water with 100 µg/mL ampicillin)was inoculated with *E. coli* DH10B cells expressing the FH6, RFP,2HA, GFP epitope tags fused to both DMC1 and RAD51 genomic DNA (gDNA) sequence (see Appendix A for construct maps). The culture was placed in the 37°C shaking incubator (220 rpm) to grow overnight. Samples were centrifuged at 6,000 rpm for 10 min (Marathon 21000R, Fisher Scientific) and the supernatant was removed; cells were resuspended in 3.5 mL of Sucrose Lysis Buffer(8% sucrose, 0.5% Triton X-100, 50 mM EDTA, 10 mM Tris pH 8.0 in water) and 250 µL of 10 mg/mL Lysozyme were added to microcentrifuge tubes. Cells were incubated at room temperature for 5 min and were then placed in 99˚C water for one minute. The samples were then centrifuged for 15 min. The pellets of cell debris were removed and 400 µL of 3 M NaOAc (pH 5.1), 2.2 mL of Isopropanol were added. Next, plasmid DNA was allowed to precipitate at RT for 5 min followed by centrifugation at 13300 rpm for 10 min. The supernatant was removed and the pellets were washed with 1 mL of 70% Ethanol and allowed to air dry before being resuspended in 300 µL of 1x TE (pH 8.0). Purified sample was treated overnight with RNase A (10 mg/mL) (1 µL per 100 µL sample). An equal volume of Phenol:Chloroform: Isoamyl alcohol (25:24:1) extraction to an aqueous solution of lysed cells was added and vortexed vigorously to mix the phases. Then the samples were centrifuged for 5 min at 13,000 rpm (Spectrafuge 24D, Labnet International) followed by

pipetting off the top aqueous layer and transferred to a clean microcentrifuge. The sample was mixed with1/10th volume of 3 M sodium acetate and 2.5 times the total volume of 100 % chilled ethanol were added, mixed by inversion, and incubated overnight at -20°C. The following day, extra salt was washed after 10 min of centrifugation with 1 mL of 70% ethanol and centrifuged again for 10 min at 4°C (Spectrafuge 24D, Labnet International). The dried pellet was dissolved with 150 µL of nuclease-free water. The purified plasmid was quantified by a NanoDrop 2000 Spectrophotometer (Thermo Scientific, Waltham, MA) which was diluted to between 2 to 3 µg/µL for all samples. Then DNA was confirmed by restriction enzyme digestion as follows: 0.5 µL specified restriction endonuclease, 2 µL SmartCut Buffer, and 2 µL purified plasmid DNA were combined and brought to 20 µL total volume with nuclease-free water. After incubation 2 hours to overnight in a 37°C water bath, 10X RNase Sample Dye (2 µL of 10X for a final concentration 1X) was added to 20 µL reaction. 1% agarose gel with 5 µg/mL Ethidium bromide (EtBr) was run at 120 V for 45 min. The visualized DNA fragments (Fotodyne Incorporated; Gel Logic 200 Imaging System, Kodak) was compared with the predicted band size on gel using SnapGene program.

Biolistic Transformation of *Tetrahymena thermophila*

The DNA constructs were linearized with restriction enzymes KpnI and SacI; each reaction had (2.5 µL SacI, 2.5 µL KpnI, 100 µg purified plasmid, 20 µL SmartCut and all were brought to 200 µL total volume with nuclease-free water.). The reactions then were incubated overnight in water bath at 37°C. The next day, Phenol: Chloroform: Isoamyl alcohol (25:24:1) extraction and ethanol precipitation was performed to precipitate the purified constructs and incubated overnight at -20°C. The pellet was

precipitated by removing ethanol and 10 μL Tris-EDTA pH 8.0 (TE) was added. The reaction was diluted to a final concentration of 2.0 μg/μL and confirmed the linearization using 1% agarose gel. *Tetrahymena* strains CU522 and CU725 were grown in 100 mL cultures (2% PPYF with 1x PSF) to a density between 1-3x10^5 cells/mL. Cells were centrifuged at 3,000 rpm for 3 min (Marathon 21000R, Fisher Scientific) and the media was removed and replaced with 10 mM Tris-HCl pH 7.5, and were allowed to starve at 30˚C for 18 hours without shaking. The starved cells were counted using a hemacytometer and centrifuged at 3,000 rpm for 3 min (Marathon 21000R, Fisher Scientific). The pellet was resuspended in ~2 mL of 10 mM HEPES (pH 7.5) to a density of 1x10^7 cells/mL. The starved cells were placed onto a Petri dish (100 mm diameter) that contained a presoaked a sterile whatman 114 filter paper with 2 mL of 10 mM HEPES (pH 7.5). The linearized plasmid constructs (2 μL) for transformation were coated onto 1 μm gold beads (25 μL of 1.5 mg of beads in 50% glycerol) with the addition of 25 μL of 2.5 M CaCl2 and 10 μL of 100 mM spermidine. The mix was then vortexed at 4˚C for 30 min before being centrifuged briefly for 5 seconds at 13300 RPM (Spectrafuge 24D, Labnet International). The supernatant was removed and the beads were washed with 100 μL of 70% ethanol once followed by a wash with 100 μL of 100% ethanol. Finally, the beads were suspended back into 25 μL of 100% ethanol and were then added to a macrocarrier and allowed to dry.

Constructs were introduced into *T. thermophila* biolistically with the BioRad Gene Gun™, using a pressure of 900 psi and a vacuum of 27 mm Hg according to manufacturer's instructions. Previously, a steel macrocarrier holder, yellow plastic macrocarrier, a metal stopping screens, and the red plastic cap were sterilized by 100 % ethanol in a laminar flow hood. The plastic rupture disks were sterilized using 100%

isopropanol. The DNA-bead mixture (25 μL) was allowed to dry onto the marocarrier. The parts of the gen gun were assembled and the DNA was shot into *T. thermophila* cells. After transformation, the cells on the filter paper were transferred into a flask containing 50-mL of pre-warmed 2% PPYF with 1X PSF and then incubated at 30 °C for 6 hr. without shaking. The cells were treated with 20 μM Paclitaxel (Pac; LKT Laboratories). Then they were plated onto three 96-well plates at 100 μL/well and incubated at 30 °C in humidity chamber. After 7 days of Pac selection for transformants, wells with growth were re-plated into new 2% PPYF with 1X PSF in 48-well plates (500 μL/well) in 20 μM Paclitaxel containing meeting. Then a second round of selection in 24-well plates (1.0 mL/well) in 40 μM Paclitaxel containing media was performed. Cells that were able to grow at 40 μM Paclitaxel were then selected for experiments and 10-mL 1% PPYS stock tubes with 1X PSF were started in 15-mL conical tubes.

Bioinformatics

The protein sequences of Rad51 (TTHERM_00142330), Dmc1 (TTHERM_00459230). Hop2a (TTHERM_00794620), Hop2b (TTHERM_01190440), Mnd1(TTHERM_00300660), and Mndp1 (TTHERM_00382290) in *T. thermophila* were retrieved from the Tetrahymena Genome Database (http://ciliate.org;Stover et al, 2006). Those sequences of proteins were compared with similar proteins from other species using NCBI protein database. An EXPASY Proteomics Tools Prosite database (http://www.prosite.espasy.org) was used to obtain the functional domains in the original protein and homologs sequences. The T-COFFEE database analysis (http://www.tcoffee.vitalit.ch/apps/tcoffee/do:regular) was used to align sequences and analyze the conserved domains among the homologs. CLUSTALW

(http://www.genome.jp/tools-bin/clustalw) was used to align all selected sequences and obtained clustalw.aln file, which uploaded to construct phylogenetic tree using Mega7.0 program (http://www.megasoftware.net). Unweighted Pair Group Method with Arithmetic Mean (UPGMA) was the evolutionary tree used predicting the likelihood of branch formation based on 500 replicates

qRT-PCR

To determine the expression of *RAD51* and *DMC1*, gene sequences were obtained from the *Tetrahymena* Genome Database (http://www.ciliate.org;Stover et al. 2006). Primers were designed previously using the Primer3 program, ordered from Integrated DNA Technologies (Coralville, IA) and then reconstituted in nuclease free-water to prepare a 200 µM stock primers and a 20 µM working stock. Two primer sets for both RAD51 and DMC1 were previously ordered. The RAD51-2 primers spans the second intron of *RAD51*, but RAD51-1 spans the first intron. The DMC1-1 primers span the second intron of *DMC1*), and the DMC1-2 span the third and the fourth introns. The sequences of all primers are given in Table.2.

To check which of RAD51 primers work, quantitative real-time PCR (qRT-PCR) was used in a MiniOpticon Real Time PCR system (Bio-Rad) using (10 µL 2x Ssofast EvaGreen supermix (Bio-Rad, Hercules, Ca, Cat. #172-5200), 0.5 µL of each forward and reverse primers, 1.0 µL *T. thermophila* cDNA or gDNA, and brought to 20 µL total volume with nuclease free-water). The optimal annealing temperature for both primers was determined to be 56 °C (A. Maltzman MSCMB Thesis,). The reactions were run on a thermocycler according to the following protocol: 98°C for 2 min; 98°C for 5 sec; 56°C for 20 sec; go back to step 2, repeat 39 times; 56°C for 10 sec; 95°C; 4°C forever. The

results were analyzed and confirmed the primers using the Bio-Rad CFX Manager program. PCR products were run on a 1.5% agarose gel and visualized using a UV transillumiator to verify the amplification of both *RAD51* and *DMC1*.

The complementary DNA (cDNA) was prepared for qRT-PCR, wild-type CU428 was treated with 10 mM Methyl Methanesulfonate (MMS), 1 mM hydrogen peroxide (H_2O_2), or 100 J/m^2 ultraviolet light (UV) and allowed to recover for 0-4 hrs. A Reverse Transcriptase cocktail was made (Qiagen RNeasy Mini Kit. Valencia, CA, Cat. #74104) per reaction (4 µL 5x an Avian Myeloblastosis Virus (AMV), 4 µL 25 mM MgCl2, 2 µL 10 mM dNTPs, 1 µL RNasin, 1 µL 7.5 U/µL AMV RT, 2 µL 50 µM Oligo dTVN, 4 µL RNase-free H2O, 2 µL total RNA), then put in a thermocycler as following: 42°C for 25 min; 99 °C for 5 min; 4 °C for 5 min. Samples was stored at -20 °C after adding equal volume of RNase free-water (20 µL).

The relative expression of RAD51 and DMC1 was estimated in response to MMS, UV, and H_2O_2 at 0, 1, 2, 3, and 4 hrs. Untreated samples were used as control, and histone heterochromatin protein 1 (HHP1) housekeeping gene primers were used to normalize each treatment sample expression levels and treatments were made relative to the untreated samples. Actin 1 (ACT1) primers were used for a standard curve of known amounts of genomic DNA from 0.1-1000 ng to construct a standard curve so Starting Quantity values could be obtained for each run in order to be able to compare runs done at different times with different batches of SsoFast Evagreen Master Mix.

Table 2: Quantitative RT-PCR Primers

Target	Primer sequence (5'-3')
DMC1-1	Forward: GAATAGAGTCTCAAAGCATAACAG Reverse: TATTCACCCTCCATTCCGTAGTG
DMC1-2	Forward: GCTGAATTTAATATCGCAGTG Reverse: TACAAATAAGGTGAATCAACCAGC
RAD51-1	Forward: TTGAAACAGGCTCTCTCACTG Reverse: CATTCGGATTACATCCTCAAGAAT
RAD51-2	Forward: CTGCAGCTGAATACTATGTAAAGAGA Reverse: ATCCTTCACCACCACCCTTT
HHP1	Forward: TTAGCAATGATAAACCTTCAGAC Reverse: TGTGTAAAGAGATTTTCCATC
ACT1	Forward: TGAATTAAAGGCTTACAAGGAATC Reverse: CACACTTCATGATAGAGTTGAAGG

Damage Treatment for RNA Extraction

Positive transformants were grown in 10 mL media with 2% PPYF and 1x PSF, diluted to $1x10^5$ cells/mL, and treated with 10 mM MMS. The cells were incubated in the shaking incubator at 30°C at 100 rpm until the RNA isolation time points (1, 2, and 3 hours) from both the treated and untreated cells. At each time-point, the cells were centrifuged at 3,000 rpm for 3 minutes (Marathon 21000R, Fisher Scientific), media was decanted and cells were resuspended in 600 µL of lysis buffer containing 10 µL Beta-mercaptoethanol (βME) per 1 mL of RNeasy Lysis Buffer (RLT). A sterile 70% ethanol (600 µL) was added to homogenized cells and moved to a spin column placed in a 2 mL collection tube, followed by centrifugation at 13,300 rpm for 30 sec. (Spectrafuge 24D,

Labnet International) and flow through was discarded. Next, column was washed once with 700 µL of Buffer RW1 followed by two washes with500 µL Buffer RPE. Column was centrifuged at 13,300 rpm for 2 min. The spin column was placed in a new collection tube followed by centrifugation at full speed for 1 minute and 50 µL of nuclease-free water was placed and allowed to be incubated at RT for 2 min. The samples were centrifuged at maximum speed for 1 minute and saved with flow through on at -80 ^{o}C.

Fluorescence Microscopy

GFP and RFP transformants were prepared by placing them in 10 mL of 2% PPYF, 1X PSF at 30 ^{o} C. Cadmium chloride ($CdCl_2$ 1.5 µg/mL) induced the cells and incubated at 30°C for 2 hrs. The cells were treated with 10 mM MMS for 1 to 4 hrs. at each time point, 1 mL of the cells was removed and centrifuged at 3,000 rpm for 3 min, and media was decanted away and later cells were transferred to microcentrifuge tubes. The cells were resuspended in 0.5 mL 10 mM Tris-HCL (pH 7.5) and 1 µL of 1 mg/mL 6-diamidino-2-phenylidole (DAPI) (3.7% formaldehyde, 0.1 µ/mL DAPI) was added to stain the cells for 15 min at RT. The samples were centrifuged at 3,00 rpm for 3 min and the supernatant was removed. Highly concentrated cells (2 µL) and 3 µL of 2% methylcellulose were placed on a glass microscope slide. The cells were visualized under 1000x magnification with oil immersion on an Olympus BX60 Fluorescence Microscope.

Protein Isolation

FLAG and 2HA transformants were grown in 5 mL of 2% PPYF and 1x PSF in a 30 °C shaking incubator overnight and treated with 1.5 µg/mL $CdCl_2$ for 2 hrs. The cultures were centrifuged at 3,000 rpm for 3 min (Spectrafuge 24D, Labnet

International), decanted supernatant, and resuspended in 5 mL of 10mMTris-HCL (pH 4.5). Cells were centrifuged, decanted supernatant, and resuspended in 1 mL of 10 mM Tris-HCL (pH7.4). Cells were transferred to a 1.5 mL microcentrifuge tube and spun at 5,000 rpm for 2 min at 4°C (Spectrafuge 24D, Labnet International) . The supernatant was removed and 600 µl of Breaking Buffer (350 mM NaCl, 40 mM HEPES (pH 7.5), 1% TritonX-100, 10% glycerol, 1 mM DTT and water to 100 mL total volume) with 1x Protease inhibitors (Roche, Mannheim, Germany, Cat. #11873580001) was added. The lysed cells were vortexed for 1 min at 4 °C, then centrifuged at 13,000 for 15 min(Spectrafuge 24D, Labnet International). The supernatant was removed and protein extracts were quantified using Bio-Rad 500-0006 Protein Assay. A standard curve was made using bovine serum albumin (BSA) standards to determine the concentration of protein in each sample.10 mg/mL BSA stock (Hercules, CA, Cat. #500-0002) was diluted to 100 µg/mL in water (2µl 10 mg/mL BSA and 198 µl water). The diluted BSA was diluted to make 10, 8, 4, 2, and 0 µg/mL standards; 5 µl of each dilution was added to 795 µL water and 200 µL Bio-Rad protein assay reagent (Hercules, CA, Cat. #500-0006). The absorbance of the solution was measured at wavelength of 595 nm and standard curve was created. Protein samples were diluted 1:5 to 1:25 and 5 µL of protein extract was used to measure the absorbance as above. The concentration of each extract was determined by linear regression using standard curve and analyzed by western blot.

RESULTS

Bioinformatics

The first step in the analysis of Rad51 and Dmc1 sequences is to search the protein databases for similar sequences. A high degree of similarity score across the entire sequence set within a given alignment indicates structural and functional importance of that gene. Rad51 and Dmc1 proteins are very well conserved among various species. The protein sequences of Rad51 and Dmc1 homologs were aligned using T-COFFEE to identify the most highly conserved amino acid residues (Appendix B). Multiple sequence alignment for Rad51 homologs shows 92% similarity. Individual species' scores ranged from ninety-three to seventy-one. Alignment of the Dmc1 homologs has an overall score of 90.4%, with scores ranging from ninety-one to seventy-two. As a result, the similarity, substitutions of an amino acids with similar properties (e.g. acidic amino acids), among Rad51 homologs is higher than Dmc1 homologs (Appendix B - Figures B1 & B2). *S. cerevisiae* Rad51 has high similarity sequence of 93% compared to other species. Also, it is found that *T. thermophila* Rad51 sequence shows homology of 92% with Rad51 homology of *H. sapiens, M. musculus, D. rerio, X. laevis. D. melanogaster, and Paramecium*. However, X. laevis Dmc1 shows 91% similarity, and the other homologs received very good score between 87 to 90%, confirming the highly conserved nature of the Rad51 and Dmc1.

To further support T-COFFEE alignment results, *T. thermophila* Dmc1 has 42% identity (refers to the number of amino acids which are exactly conserved), and 61% similarity to *T. thermophila* Rad51. *T. thermophila* Dmc1 has 43% identity and 64% similarity to *H. sapiens* Dmc1 with an E-value: 1e-92 (the lower the E-value, the more

probably it is a homolog). Additionally, it has 40% identity and 53% similarity to *E. coli* RecA with a very low E-value: 0.018 (Altschul et al.2005).

T. thermophila Rad51 and Dmc1 proteins along with the potential homologs were evaluated to determine if they contained similar domains utilizing the ExPASy Proteomics Tool PROSITE. All the homologs were found to possess the same conserved RECA2 and RECA3 domains (Figure 6). RECA-2 domain is for ATP binding and hydrolysis, located in the N-terminal part of the Rad51 and Dmc1 proteins, whereas RECA3 domain is for nucleotide binding, located in the C-terminal region. Continually, T-COFFEE revealed the presence of Walker A and Walker B motifs (black box) in all Rad51 and Dmc1 homologs (Appendix B - Figures B1 and B2). The *E. coli* sequence GPESSGKT matches the consensus sequence of amino acids (G/A) XXXXGK(T/S) for the Walker A motif (also called the P-loop or phosphate binding loop), where X is any amino acid (Koonin et al., 1995). Another nucleotide binding motif, the Walker B that is characterized by ZZZZD/E, where is Z is a hydrophobic amino acid followed by an acidic residue (usually aspartate) (Koonin, 1993; Koonin, 1993b; Leipe et al., 2002). The Walker A and Walker B motifs are found in the RECA2 domain at a highly conserved residue of the N-terminal region of Rad51 and Dmc1 proteins, providing a possible explanation for the regulation of DNA binding by phosphorylation within the N-terminal domain.

Given the high level of conservation of both proteins, phylogenetic tree was constructed to confirm the homology of Rad51 and Dmc1 and all homologs (Figure 7). In the majority of the organisms looked at Rad51 and Dmc1 branch closely together (*Homo sapiens, Mus musculus, Xenopus laevis, Arabidopsis thaliana, Drosophila melanogaster, Dictyostelium discoideum, Paramecium tetraurelia, Caenorhabditis elegans*) showing the

high conservation of the two RecA protein paralogs in those species. For some other organisms the Dmc1 sequences have diverged significantly from their Rad51 paralogs, which can be seen in by the distant branching clade of four Dmc1 homologs (*Danio rerio, Saccharomyces cerevisiae, Schizosaccharomyces pombe, and Zea mays*). This is also to a little lesser extent true for *T. thermophila* Dmc1 that is closer to the main eukaryotic Rad51/Dmc1 clade but still branches off away from the main group and the *T. thermophila* Rad51 homolog (Figure 7). Additionally, *E. coli* RecA was used to root the tree and show the relative divergence of the Dmc1 and Rad51 paralogs in eukaryotes.

RNAseq of *RAD51* shows it contains two introns unlike *DMC1* that are composed of four introns (Figure 8). RNAseq coverage and transcript data indicated that there are three exons in *RAD51*, and five exons in *DMC1*. The RNAseq coverage for *DMC1* displayed some coverage over the area of the second intron, where it should not be present.

Further information was collected to identify the expression patterns for *RAD51* and *DMC1* using microarray data obtained from the Tetrahymena Functional Genome Database (http://tfgd.ihb.ac.cn, Figure 9). Based on microarray expression profiling data, *DMC1* is not expressed in *T. thermophila* during logarithmic growth and starved condition, but it starts to increase drastically at 2 to 4 hours during conjugation (Figure 9B), and then decrease during conjugation with a later secondary peak between 12-16 hours. However, *RAD51* expression profile has more expression during logarithmic growth and a broad increase during starvation peaking at 9 hours (Figure 9A). During conjugation *RAD51* follows the same pattern as *DMC1* peaking around 4 hours and later around 14 to 16 hours. Notably, *RAD51* is expressed in all conditions, where it peaks and drops at different time points, but *DMC1* is expressed only during conjugation.

Apparently, this expression pattern reveals that expression of *DMC1* is specific for conjugation of the cell cycle.

Following the Rad51 and Dmc1 analysis, Hop2 and Mnd1 proteins were investigated in *T. thermophila*. Hop2 and Mnd1 are meiosis proteins that act together in a complex to stabilize Rad51 and Dmc1 activity. Unlike other species studied thus far, *T. thermophila* has two HOP2 paralogs, of which TTHERM_01190440 (*HOPP2*) protein has the best e-value, 1e-10 (Appendix B - Table B1). The second Hop2 paralog (*HOP2*), TTHERM_00794620, had a lower e-value, 5e-05 (Appendix B - Table B1), but the microarray expression data mimicked more that of DMC1 (data not shown). In accordance with the presence of two *Tetrahymena* Hop2 homologs, two Mnd1 homologs were also found, TTHERM_00300659 (*MND1*; once TTHERM_00300660 but reannotation split into two genes) that has a role in meiotic pathway and TTHERM_00382290 *(MNDP1*), which is a ubiquitously expressed (Appendix B - Table B1 and data not shown). This raises the possibility that a meiotic and a ubiquitous Mnd1p-Hop2p complex exists.

RAD51 and DMC1 Plasmid Purification and Transformation into *Tetrahymena thermophila*

To verify that the constructs were successfully containing DMC1 and RAD51 genes, they were digested with restriction enzymes and run on agarose gel to observe the predicted fragment sizes using SnapGene program (Appendix A - Figures A1-10). *E. coli* expressing a plasmid containing FLAG-His6 epitope tag fused to the DMC1 genomic DNA (gDNA) and plasmid expressed 2HA tag fused to either DMC1-cDNA or DMC1-gDNA were gifted as a frozen glycerol stocks (E. Gallichotte, Joint Science Department

of Claremont McKenna, Pitzer, and Scripps Colleges, Claremont, CA). They are under inducible Metallothionein (MTT) promoter and a selectable marker for Pac resistance. A plasmid containing GFP epitope tag fused to the DMC1 was obtained from collaborators (Dr. Emily Wiley, Claremont College, Claremont, CA), and GFP-RAD51 and FH6-RAD51 constructs were prepared by former MSU Cell and Molecular Biology undergraduate (Gregory R. Fuller). SnapGene program used to predict the expected DNA fragments to confirm the constructs. These constructs were thawed from liquid nitrogen container. After two attempts of thawing the cells, they were found dead. The *E. coli* contain the constructs were frozen in glycerol at - 80°C, so they were allowed to grow overnight in shaking incubator at 37°C. The purified DNA was digested with appropriate restriction enzymes to check for the presence of the correct restriction fragment length polymorphism (RFLP) for the constructs. FH6-DMC1 and 2HA-DMC1 constructs were confirmed as predicted (Figure 10). The other constructs of GFP-RAD51, GFP-DMC1, FH6-RAD51, and 2HA-DMC1 did not match with the predicted RFLP patterns (Figure 11). LR Clonase reaction and electroporation of *E. coli* cells (DH10B) was done to create an expression vector of GFP-DMC1, GFP-RAD51, RFP-DMC1, RFP-RAD51, but multiple attempts of transformation were unsuccessful (Figure 11). Due to the large plasmid size of pBMTTmCherry-GTW and pBMTTGFP-GTW there was some complications in getting fused *DMC1* and *RAD51* occurred. The pENTR-RAD51 and pENTR-DMC1 were purified Fresh and the LR Clonase was done using new destination vectors, pBMGFP-GTW and pBMRFP-GTW (provided by Jeremy Tee, Cell and Molecular Biology undergraduate in Dr. Josh Smith's lab) and pBMFH6-GTW and pBM2HA-GTW (provided by Dr. Josh Smith, Missouri State University) were fused to either *RAD51* or *DMC1* (Figure 10). Plasmid isolation and restriction enzyme digestion

revealed the predicted RFLPs indicating that the plasmids were correctly constructed (Figure 10). Further LR Clonase reaction was preformed to fuse RFP epitope tag to

Species	*RAD51*		*DMC1*	
	Domains	Size (aa)	Domains	Size (aa)
Tetrahymena thermophila		331		356
Homo Sapiens		339		339
Mus Musculus		339		339
Danio rerio		340		342
Caenorhabditis elegans		362		357
Xenopus laevis		336		336
Drosophila melanogaster		336		336
Saccharomyces cerevisiae		334		334
Schizosaccharomyces pombe		358		332
Dictyostelium discoideum		351		351
Arabidopsis thaliana		342		342
Paramecium		337		337
Zea mays		340		344
	RECA			
Escherichia coli			353	

Figure 6. Protein Domains in Dmc1 and Rad51. PROSITE images showing functional domains RECA-2 (grey) and RECA-3 (green) in the Dmc1 and Rad51 homologs from various species, and the RecA protein in *Escherichia coli*. The size of the protein (amino acids; aa) was also listed for each homolog.

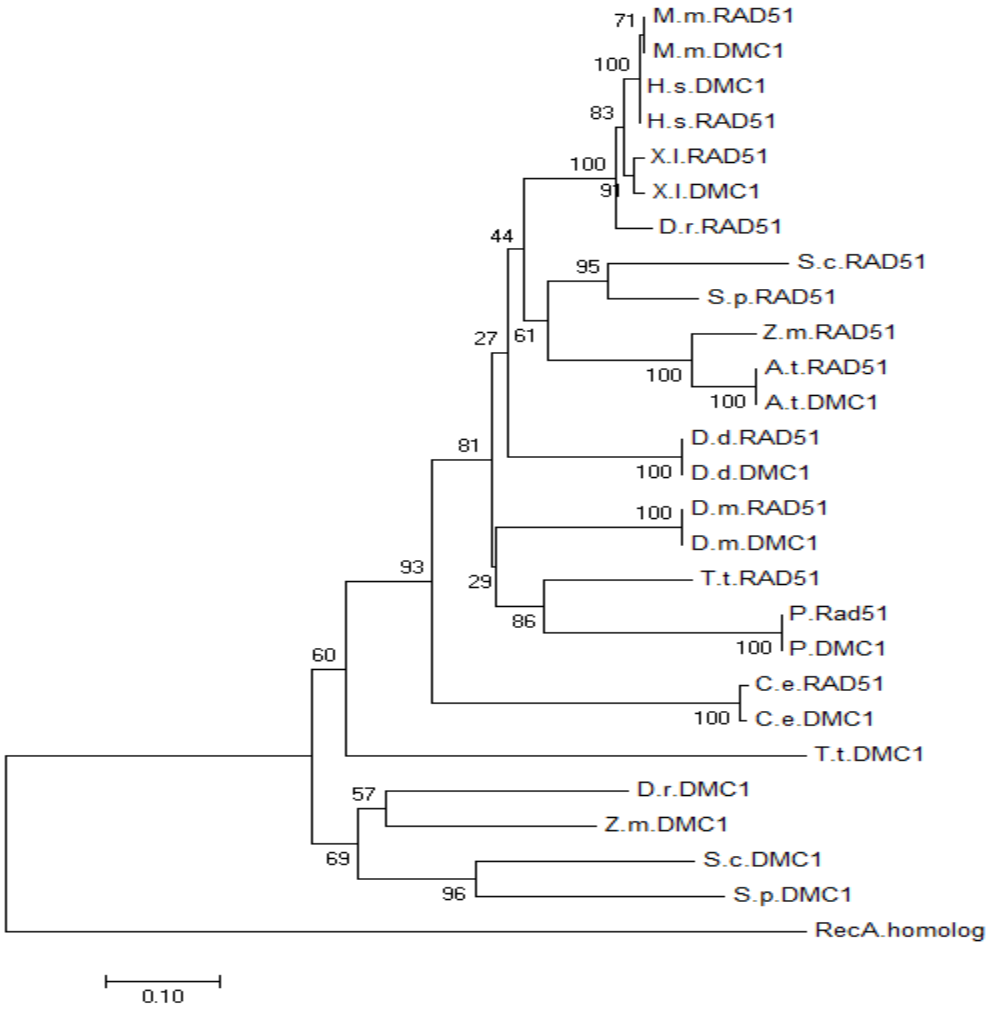

Figure 7. Unweighted Pair Group Method with Arithmetic (UPGMA) Bootstrapped Phylogenetic tree for possible *T.thermophila* Rad51 and Dmc1 homologs. Tree was constructed using UPGMA method in the MEGA7.0 program with 500 bootstrap replicates. The scientific species names are abbreviated: *T.thermophila (T.t), Schizosaccharomyces prombe (S.p), Drosophila melanogaster (D.m), Danio rario (D.r), Saccharomyces cerevisiae (S.c), Arabidopsis thaliana (A.t), Zea mays (Z.m), Caenorhabditis elegans (C.e), Xenopus laevis (X.l), Dictyostelium discoideum (D.d), Homo sapiens (H.s), Mus musculus (M.m), Paramecium tetraurelia (P).*

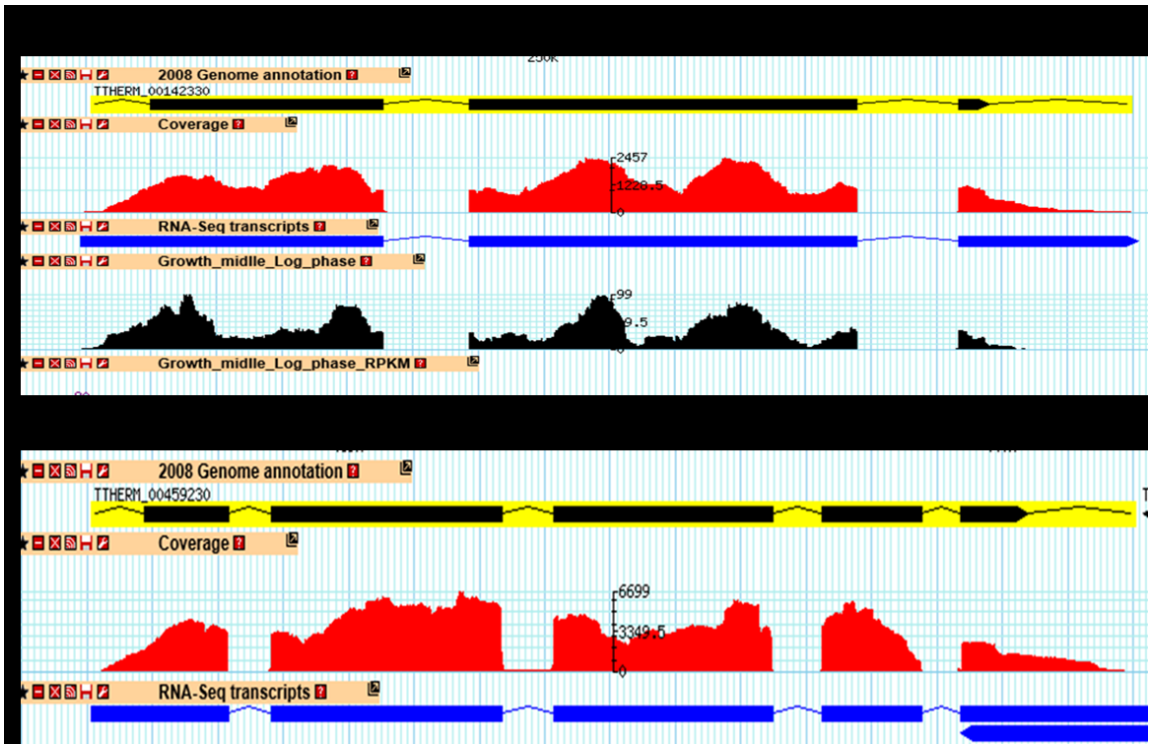

Figure 8. ***Tetrahymena thermophila*** **RNAseq data of** ***RAD51*** **and** ***DMC1***.
Estimated coverage of each gene is displayed in red**. (A)** *RAD51* RNAseq expression data**. (B)** *DMC1* RNAseq expression. Predicted annotation of gene sequence is displayed in black above red coverage. The red peaks indicates the presence of RNA expression and corresponds with coding regions and stay within the boundaries of the exons. The region between the exon is the intron and no RNAseq coverage should be observed in this region if a true intron. The coverage was assembled using the annotated genome to predict the RNA transcript for each gene (Blue). The RNAseq data was retrieved using TetraFGD RNAseq database.

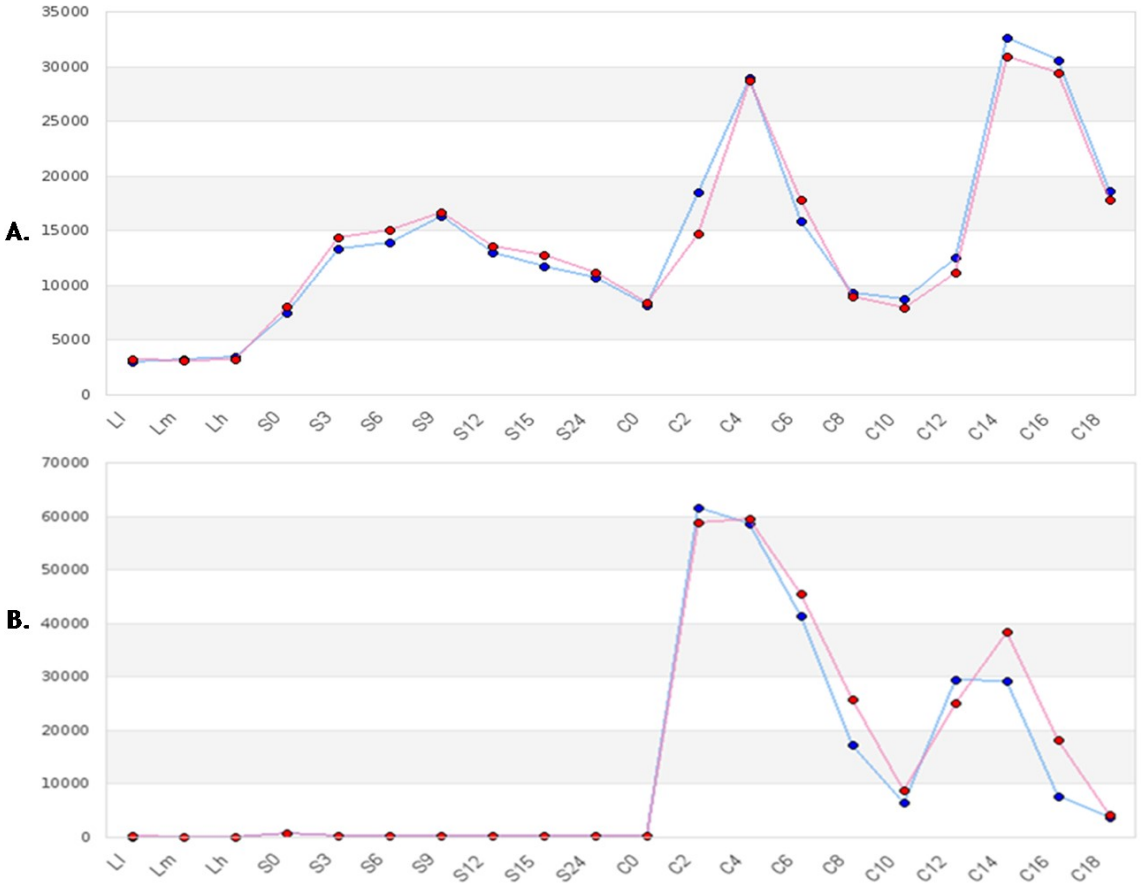

Figure 9. Microarray Expression Profiling Data for RAD51 and DMC1.
Expression profile obtained from two independent experiments, displayed by blue and red lines. Each done in duplicated or triplicate for the points shown. For growing cells, L-l, L-m and L-h correspond respectively to ~1X10^5 cells/mL, ~3.5X10^{5}cells/mL and ~1*10^6 cells/mL. For starvation, ~2X10^5 cells/ml were collected at 0 to 24 hours) referred to as S-0 toS-24. For conjugation, equal volumes of B2086 and CU428 cells were mixed, and samples were collected at 0 to 18 hours after mixing (referred to as C-0 to C-18)**. (A)** The expression profile for *RAD51*; **(B)** DMC1 microarray expression. (Xiong et al., 2011).

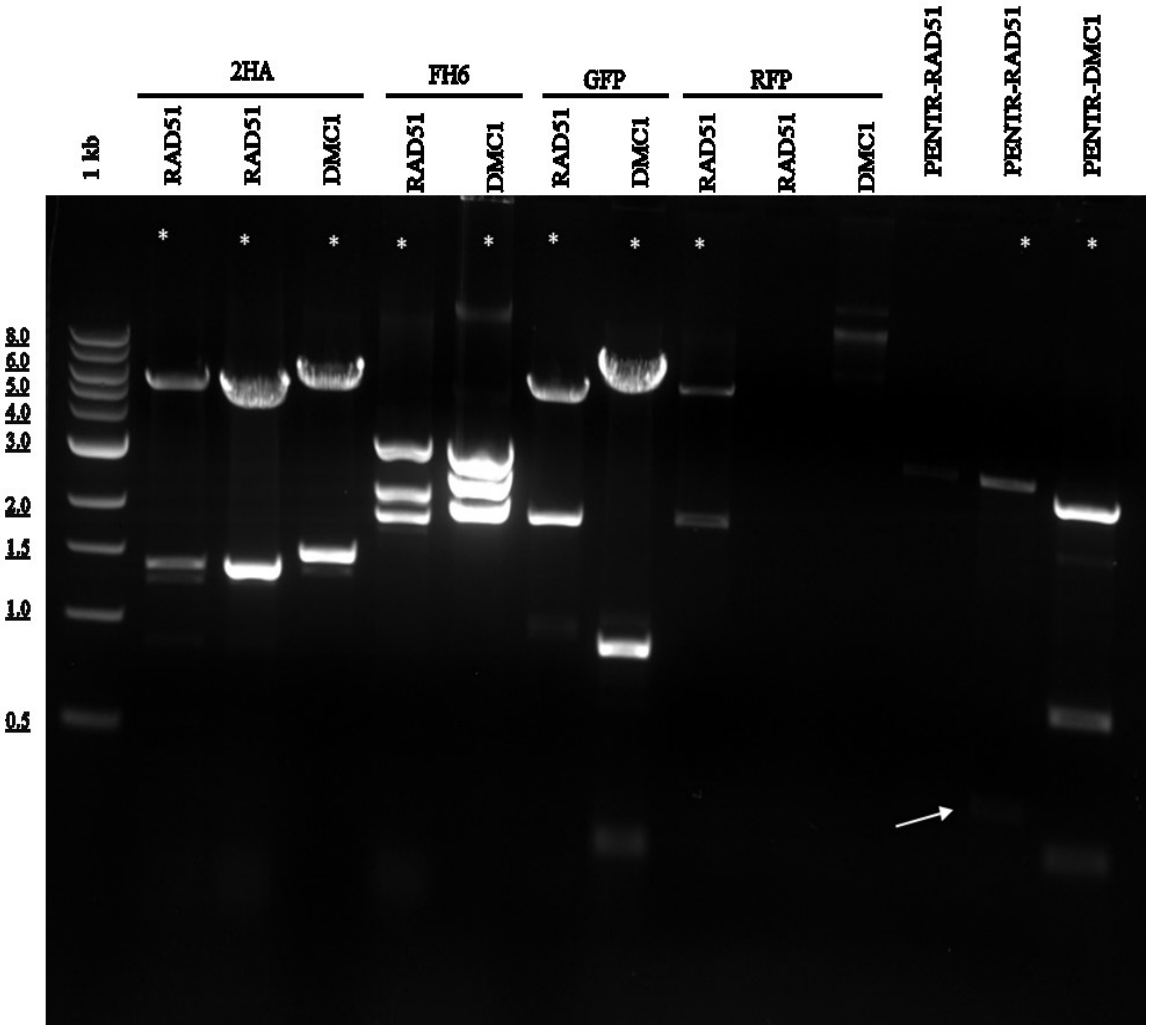

Figure 10. Confirmation digests for GFP, RFP, and HA constructs of RAD51 and DMC1. SnapGene program used to predict resulting fragment sizes. Purified samples were digested with restriction enzymes at 37℃ overnight and run on 1% agarose gel at 100 V for 58 min. Purified pENTR-DMC1 plasmid was digested with *NsiI* (predicted fragment sizes: 2892 bp, 784 bp, 266 bp); pENTR-RAD51 was digested with *EcoRI* (predicted fragment sizes: 3485 bp, 390 bp); 2HA-RAD51, RFP-RAD51, GFP-RAD51 plasmids were digested with *PstI* and *BamHI* with (predict fragment sizes: 6351 bp, 1524 bp;6440 bp, 2034 bp; 6435 bp, 2013 bp respectively). The purified RFP-DMC1 plasmid was digested with *SphI* (predict fragment sizes: 7249 bp, 1292 bp); GFP-DMC1 digested with *HindIII* (predict fragment sizes: 7436 bp, 901 bp, 178 bp), 2HA-DMC1 digested with *BamHI* (predict fragment sizes: 6351 bp, 1524 bp), FH6-RAD51 digested with *PstI* and *SpeI* (predict fragment sizes: 3211 bp, 2810 bp, 1992 bp), and FH6-DMC1 digested with *SpeI* to predict (predict fragment sizes: 3211 bp, 2575 bp, 2080 bp).The asterisk denotes to the sample that was transformed into *T. thermophila* for further experimentation and the correct bands were observed.

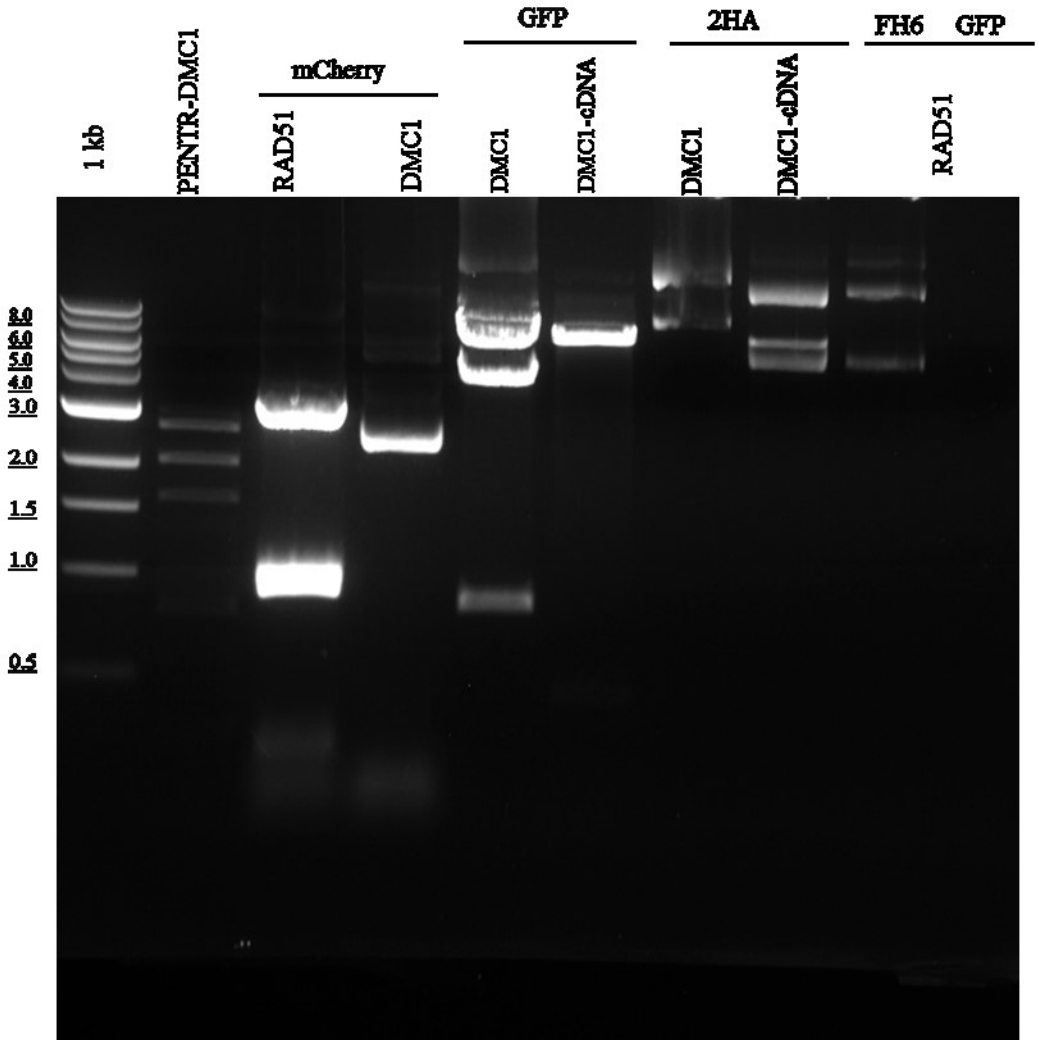

Figure 11. Confirmation digests for mCherry, GFP, FH6, and HA of RAD51 and DMC1 tagged constructs. SnapGene program was used to predict resulting fragment sizes. Purified samples were digested with restriction enzymes at 37 ℃ overnight and run on 1% agarose gel at 100 V for 50 min. Purified PENTR-DMC1 plasmid was digested with NsiI and predicted fragment size was (2892 bp, 784 bp, 266 bp); purified GFP-and GFP cDNA of DMC1 were digested with EcoR1 and predicted fragment sizes (7747 bp, 2561 bp) and (7681 bp, 2346 bp) respectively; purified 2HA and 2HA-cDNA of DMC1 were digest with BamHI and predicted fragments were (6351 bp, 1524 bp) and (6135 bp, 1458 bp) respectively; purified FH6-RAD51 was digested with SpeI and PstI to predict fragment sizes (3211 bp, 2810 bp, 1992 bp); GFP-RAD51 digested with PstI to predict fragment sizes (6872 bp, 2347 bp, 736 bp); mCherry-RAD51 digested with PstI and Bg1II to get (6692 bp, 3362 bp) and mCherry-DMC1 digested with SphI to predict (6870 bp, 2591 bp, 658 bp). Correct bands were not observed for any construct.

DMC1 (Figure 10). A separate electroporation for RFP-DMC1 was repeated multiple times and successfully confirmed clones were identified (Figure 12). Constructs were purified and quantified for transformation into *T. thermophila*. Linearization of the plasmid prior transformation is a required step to release the sequence containing the tag, MTT promoter, and either RAD51 or DMC1 genes, flanked by the BTU5' and BTU3'-NTS that allow for homologous recombination into the MAC btu-1 (K350M) locus of *T. thermophila.* Purified constructs were linearized with the restriction enzymes *KpnI* and *SacI* (Figure 13). FH6-RAD51, FH6-DMC1, GFP-RAD51, and GFP-DMC1 were transformed into *T. thermophila* CU725 strain, and 2HA-RAD51, 2HA-DMC1, GFP-RAD51, and RFP-DMC1 were transformed into *T. thermophila* CU522 strain. GFP and RFP tags were used for localization studies; FH6 and HA tags were used for western blot analysis.

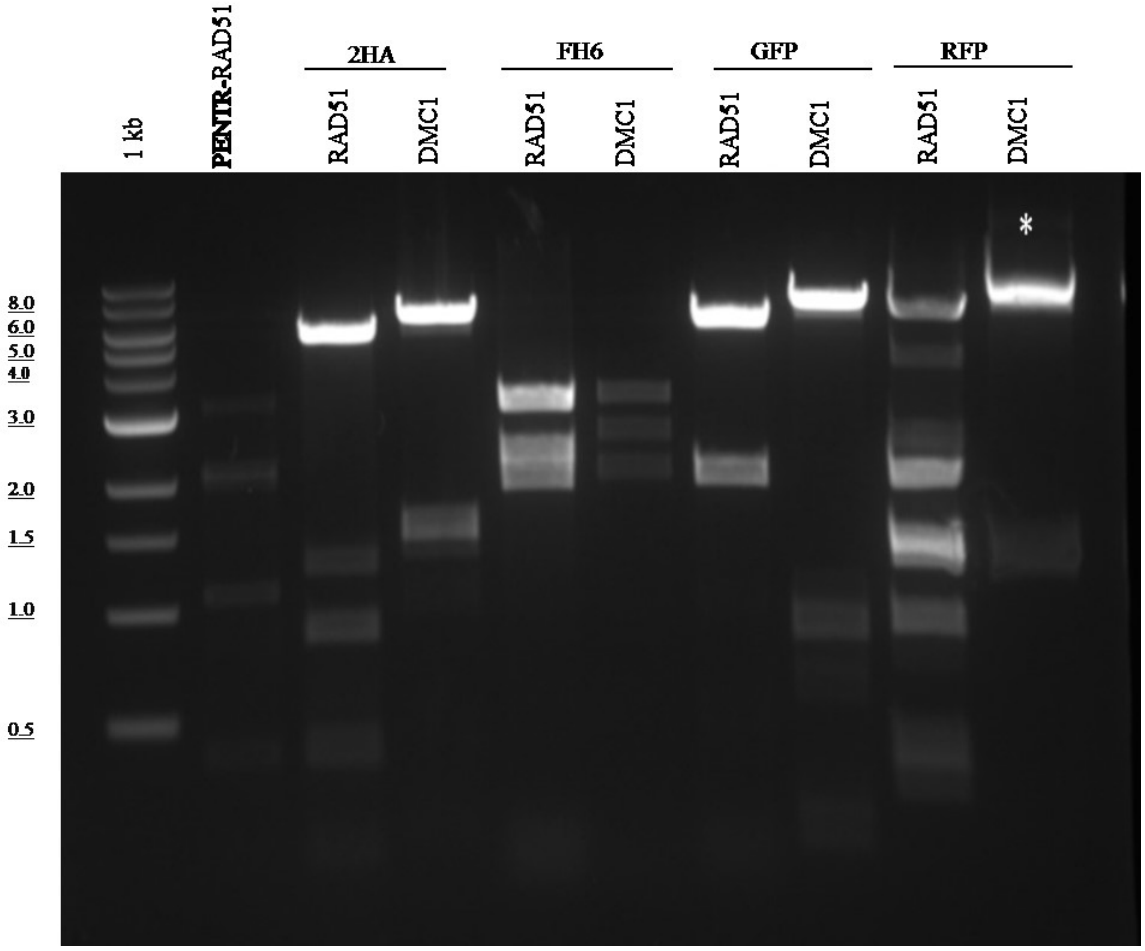

Figure 12. Expected band sizes observed in restriction enzyme digestion of RFP-DMC1 construct. SnapGene program was used to predict resulting fragment sizes. Purified samples were digested with SphI at 37 ℃ overnight and run on 1% agarose gel at 100 V for 58 min. the predicted fragment sizes (7249 bp, 1292 bp);The asterisk denotes the correct sample that was transformed into *Tetrahymena*.

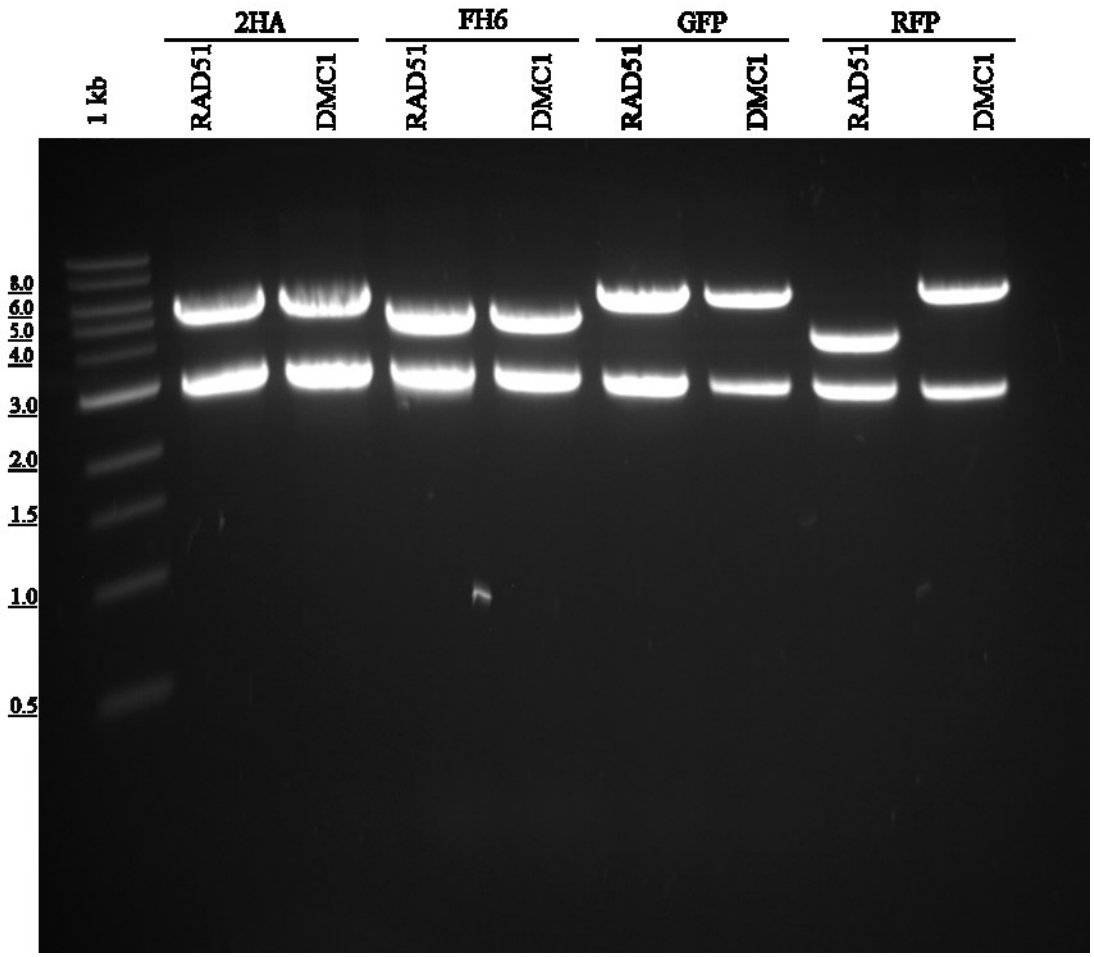

Figure 13. Restriction digest with KpnI and SacI to linearize DNA constructs for transformation into *T. thermophila*. The DNA samples were purified by phenol: chloroform extraction and ethanol precipitation and run on 1% agarose gel at 115 V. 1 kb ladder used to estimate the fragment's sizes. SnapGene was used to predict resulting fragment sizes of 2HA-RAD51 (4645 bp, 2876 bp), 2HA-DMC1 (4999 bp, 2876 bp), FH6-RAD51 (4637 bp, 2876 bp), FH6-DMC1 (4990 bp, 2876 bp), GFP-RAD51 (5572 bp, 2876 bp), GFP-DMC1 (5639 bp, 2876 bp), RFP-RAD51 (5598 bp, 2876 bp), and RFP-DMC1 (5665 bp, 2876 bp).

Primer Optimization

To determine if *RAD51* and *DMC1* have a role in DNA damage repair processes, primers were designed for qRT-PCR and run with GoTaq PCR in order to identify their optimum annealing temperature. These primers had to be tested to determine their specificity and optimal annealing temperature before they could be used experimentally. The optimal annealing temperatures of the primer sets were determined to be 56°C (Table.2) and the results of the GoTaq RT-PCR product specificity and product size was observed by agarose gel electrophoresis (Figure 14).

Two sets of DMC1 primers were designed: DMC1-1spans the first intron and DMC1-2 spans the third and the fourth introns. The optimal annealing temperatures for all primers was determined previously in the lab as 56°C. Using GoTaq PCR, gDNA and cDNA of DMC1-2 are amplified to produce the same product sizes (Figure 14). DMC1-1 primer set shows amplification of the gDNA and cDNA at the predicted sizes. RAD51-1 primer set spans the first intron and RAD51-2 spans the second intron. Both primer sets showed predicted amplification (Figure 14). Rad51-1 shows two bands in gDNA lane; one band has the same size as gDNA and the band is the same size of cDNA (Figure 14).

The primers were then tested in qRT-PCR using the same annealing temperature of 56°C using SsoFast Evagreen (SybrGreen PCR mix). Melt curve of DMC1-1 shows two peaks (Figure 15), but DMC1-1 shows one sharp peak. Also, RAD51-2 is amplified to two peaks and with a single peak for RAD51-1 primer set. The resulted products were run on the gel to check the amplification of the gDNA and cDNA of all primers (Figure 16). RAD51-1 and DMC1-2 primer sets were chosen for all subsequent qRT-PCR experiments. Based on RNAseq expression data for DMC1 (Figure 8), DMC1-2 maybe

amplifying an alternatively spliced form of it in which the first intron is not spliced out of the mRNA.

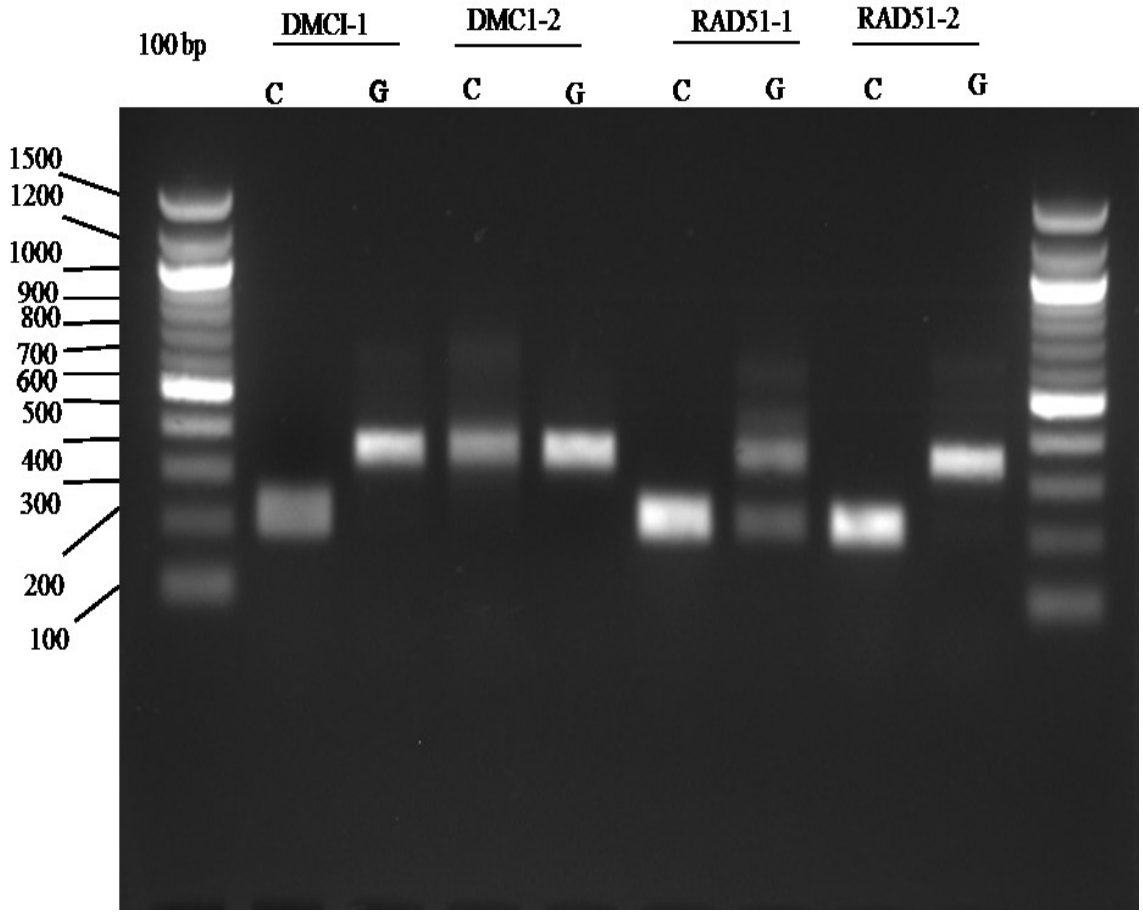

Figure 14. Confirmation of *RAD51* and *DMC1* primers in GoTaq PCR.
T. thermophila gDNA and cDNA amplified using *RAD51* and *DMC1* primer sets at 56°C. the expected gDNA product sizes for DMC1-1, DMC1-2, RAD51-1, and RAD51-2 were 281 bp, 334 bp, 335 bp, and 340 bp respectively. The expected cDNA product sizes for DMC1-1, DMC1-2, RAD51-1, and RAD51-2 were 202 bp, 197 bp, 204 bp, and 210 bp respectively. NOTE: RAD51-1 amplifies an additional band in the gDNA and gDNA and cDNA of DMC1-2 have the same size.

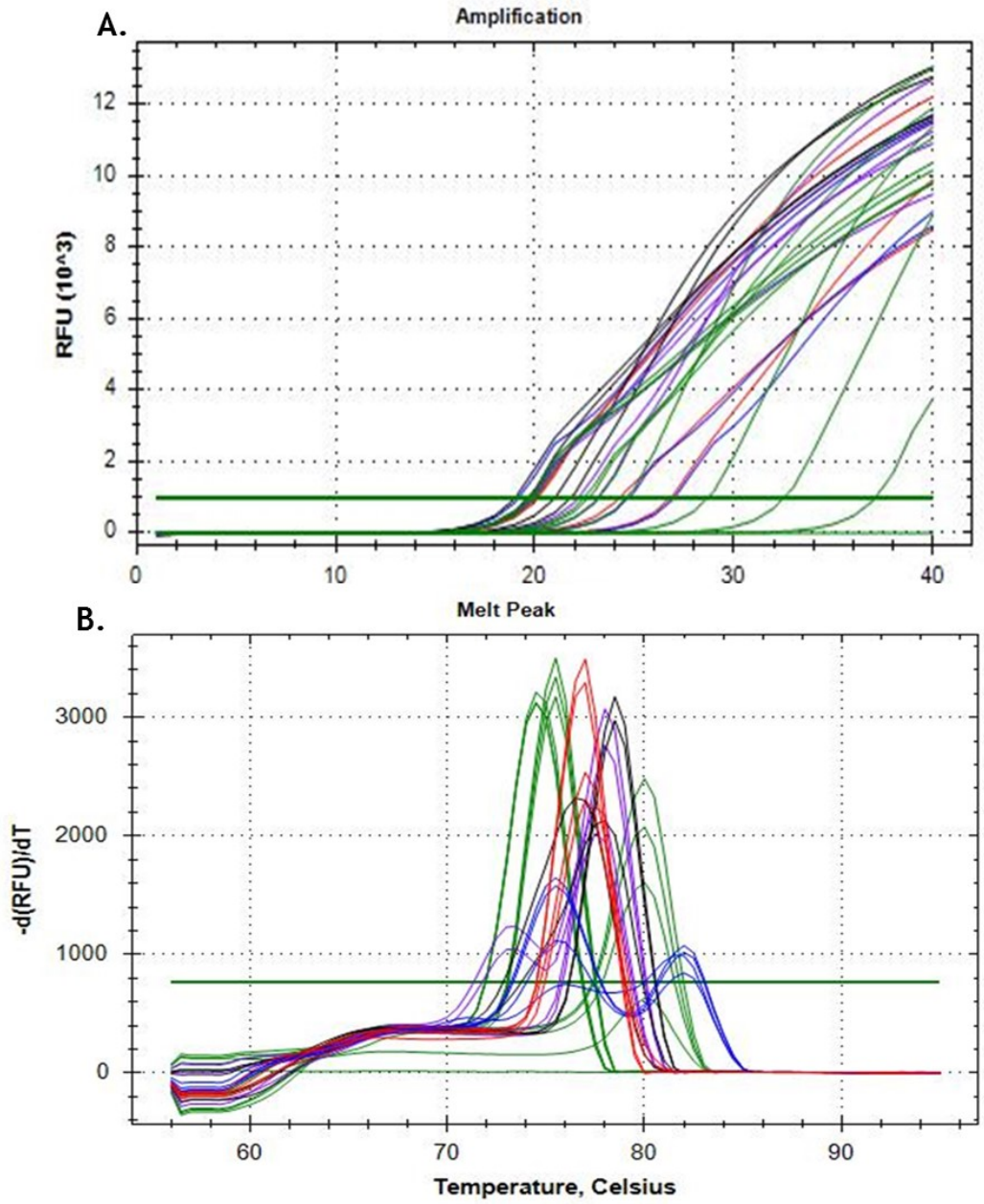

Figure 15. Melt and amplification curves for *RAD51* and *DMC1* primers. (A) amplification curve for all reactions. **(B).** The melt peak of the qRT-PCR reactions were analyzed. A single, sharp peak indicates a single product, and two peaks indicates two products. Red corresponds to DMC1-1 with one peak; purple corresponds to DMC1-2 with two peaks; black represents RAD51-1 with one product; blue represents RAD51-2 with two peaks. The horizontal green bar is representative of the threshold. Each melt peak is representative of all qRT-PCR performed using indicated primer and each peak is composed of triplicates.

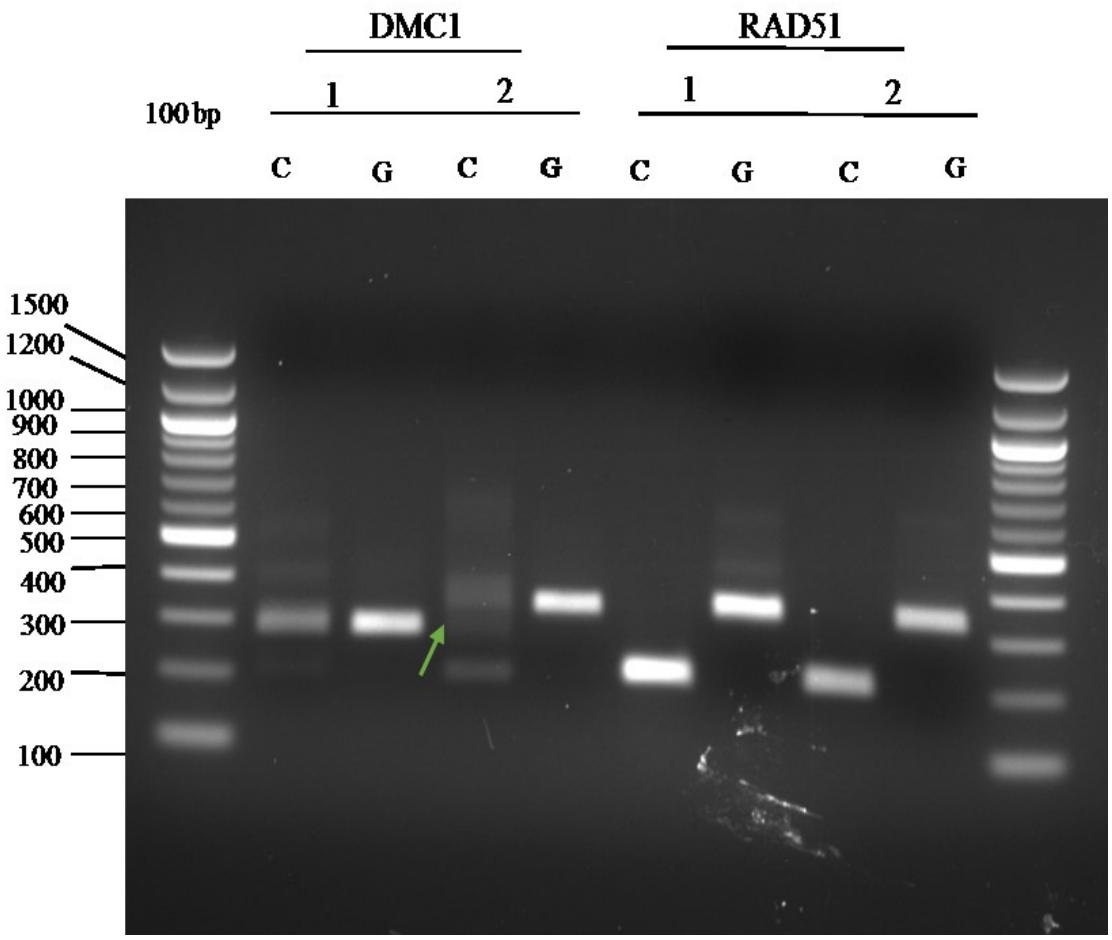

Figure 16. Confirmation of SsoFast Evagreen qRT-PCR products. Products from qRT-PCR run on a 1.5% agarose gel with EtBr. *T. thermophila* gDNA and cDNA amplified using *RAD51* and *DMC1* primer sets at 56°C. The expected gDNA product sizes for DMC1-1, DMC1-2, RAD51-1, and RAD51-2 were 281 bp, 334 bp, 335 bp, and 340 bp respectively. The expected cDNA product sizes for DMC1-1, DMC1-2, RAD51-1, and RAD51-2 were 202 bp, 197 bp, 204 bp, and 210 bp respectively. Both *RAD51* primers amplify as expected. RAD51-1 DMC1-2 primer sets were used for all subsequent qRT-PCR experiments. NOTE: DMC1-2 primer set amplifies additional band in the cDNA lane (green arrow).

RAD51 and DMC1 DNA Damage Expression After Various Damaging Agents

In order to determine the potential functional role of Rad51 and Dmc1 in DNA damage repair processes, quantitative real-time polymerase chain reaction (qRT-PCR) was conducted using cDNA, which was generated from the CU428 strain. These RNAs were treated every hour for four hours with either 100 J/m^2 of UV radiation, 10 mM Methyl Methanesulfonate (MMS), or 0.5 mM Hydrogen Peroxide (H_2O_2). UV radiation was utilized to induce CPD's and (6-4) photoproducts, which are repaired by Nucleotide Excision Repair (NER). To induce Base Excision Repair (BER), H_2O_2 was used to stimulate the damage of individual bases on the DNA, which leads to stall the replication. The MMS treatment was used to induce DSBs, which can be repaired through different repair mechanisms, specifically HRR that utilize Rad51 and potentially its paralog Dmc1. The expression of Rad51 and Dmc1 following exposure to genotoxic stressors was quantified from the results of the qRT-PCR (Figures 17-25).

In response to H_2O_2 damage, both homologs show an induced expression (Figures 17-19). *RAD51* expression peaks at 2 hours after treatment with H_2O_2 to approximately 9-fold (Figure 17). This pattern seems similar for *DMC1* peaking the most 3 hours after treatment with H_2O_2 to approximately 23-fold (Figure 18). For *DMC1* there is a greater induction of expression that is slightly later than *RAD51* and a more rapid decrease in the expression at 4 hours after treatment (Figure 19).

Under MMS treatment, the homologs exhibit the same pattern of expression, with increased expression during the three and four-hour time points (Figure 20-22). *RAD51* expression dramatically increases one hour after MMS treatment to 65-fold and continue to remain increased even four hours after treatment (Figure 20). This pattern for *DMC1*, although the degree of the increase is much smaller, increases about 2-fold after 3 hours

and remains elevated even at 4 hours (Figure 21). When *RAD51* and *DMC1* expression levels are compared under MMS treatment, *RAD51* expression is significantly more induced than *DMC1* (Figure 22). After UV treatment, *RAD51* and *DMC1* levels are obviously similar in terms of their increasing and decreasing patterns of expression (Figure 23-25). Expression of *RAD51* peaked two to three hour after UV treatment to around 15-fold and then decreased to 6-fold at four hours after treatment (Figure 23). Expression of *DMC1* followed a similar patter increasing approximately 6-fold at three hours, and decreases to about 4-fold four hours after UV treatment (Figure 24).

Fluorescent Microscopy of Rad51 and Dmc1

Localization study have shown that Dmc1 localizes to the micronucleus during meiosis, when crossing-over takes place (Howard et al., 2011). *T. thermophila* is a good organism to track the expression of Dmc1 and Rad51 during DSBs. If they were involved in DNA repair, they would localize to the macronucleus and/or micronucleus. The GFP and RFP tags were used to observe Rad51 and Dmc1 localization within living *T. thermophila* under fluorescent microscope (Figure 26). Nucleic acids were stained using DAPI to reveal the relative locations of macronucleus and micronucleus. The GFP and RFP tagged Rad51 and Dmc1 reveal that both proteins are not localizing to the macronucleus in undamaged cells. Merged images of GFP and RFP-Rad51 show their presence out of the nuclei (Figure 26). GFP and RFP-Dmc1 did not localize to the macronucleus but may be present in the micronucleus but due to the cell moving merging of the image with DAPI was not conclusive (Figure 26). Phase images were compared with the DAPI and GFP/RFP tagged cells; the shape and the size of the cells expressing GFP and RFP tagged proteins are normal.

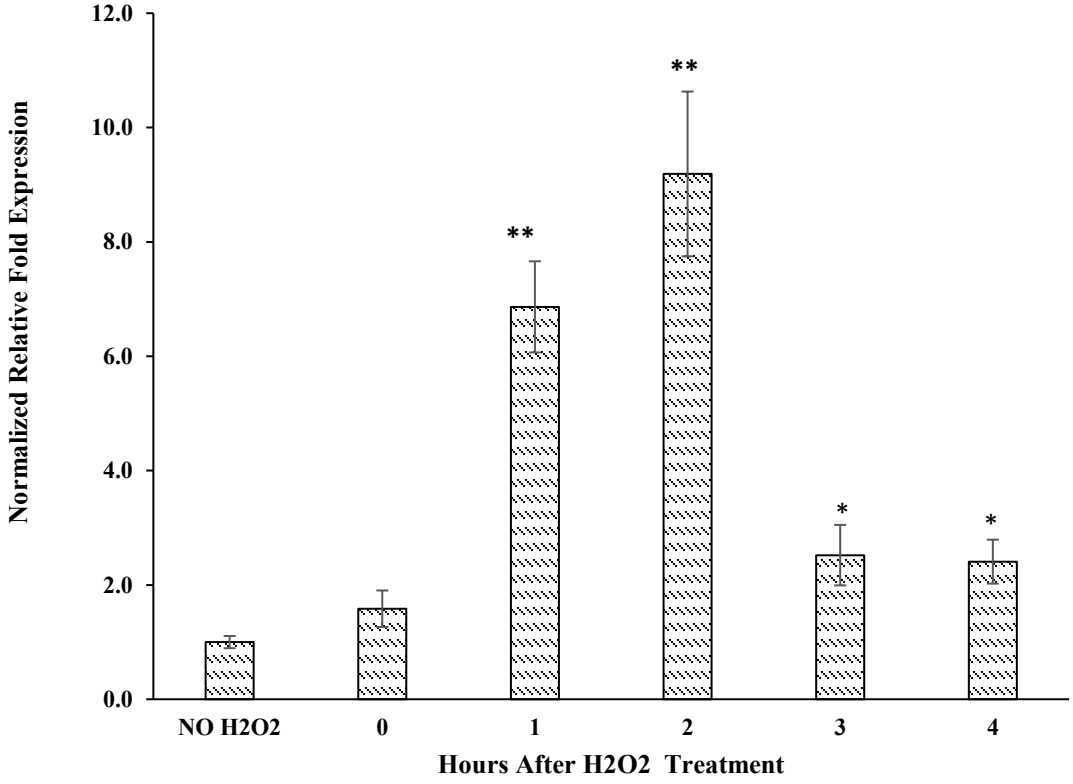

Figure 17: qRT-PCR expression profile analysis of the transcription of Rad51 in response to H_2O_2 treatment. Samples were treated with 10Mm H_2O_2; striped represents H_2O_2 treatment at time points. All samples were normalized to expression levels of the housekeeping gene HHP1 and set relative to an untreated cDNA control with the same primers. Values represent mean of five trials with error bars of ±SEM. *p<0.05, **p<0.01, ***p<0.001 vs. untreated samples as measured by two-tailed, paired sample t-test.

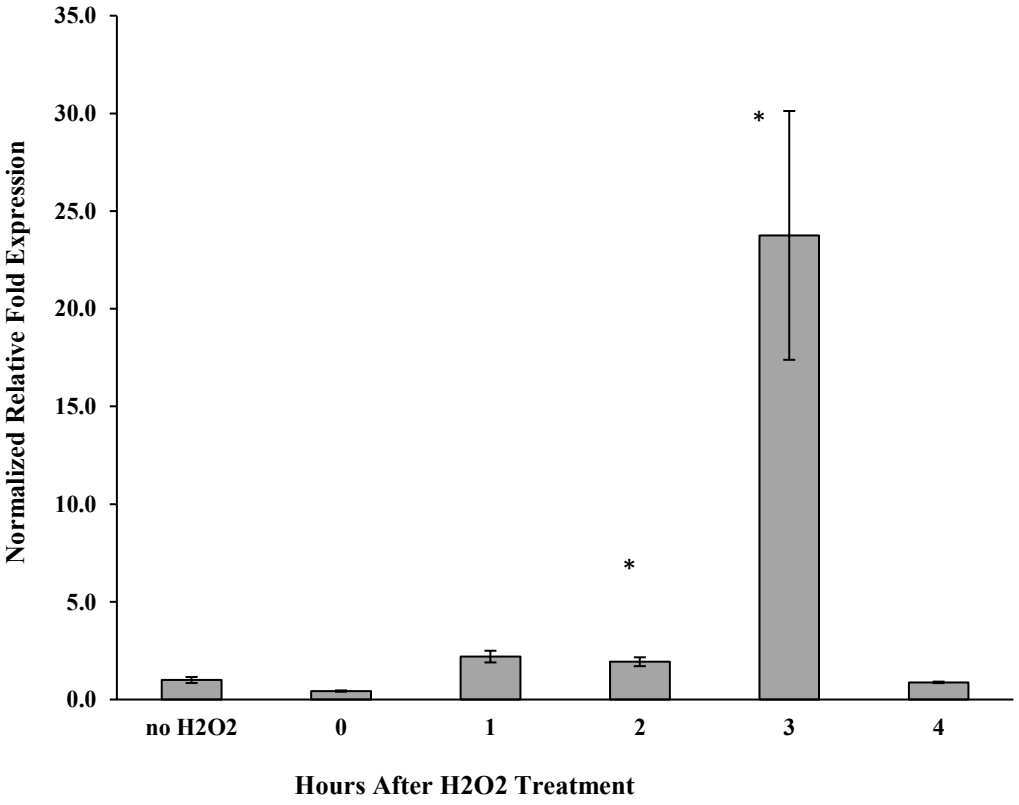

Figure 18: qRT-PCR expression profile analysis of the transcription of Dmc1 in response to H_2O_2 treatment. Samples were treated with 10Mm H_2O_2; gray represents H_2O_2 treatment at time points. All samples were normalized to expression levels of the housekeeping gene HHP1 and set relative to an untreated cDNA control with the same primers. Values represent mean of five trials with error bars of ±SEM. *$p<0.05$, **$p<0.01$, ***$p<0.001$ vs. untreated samples as measured by two-tailed, paired sample t-test.

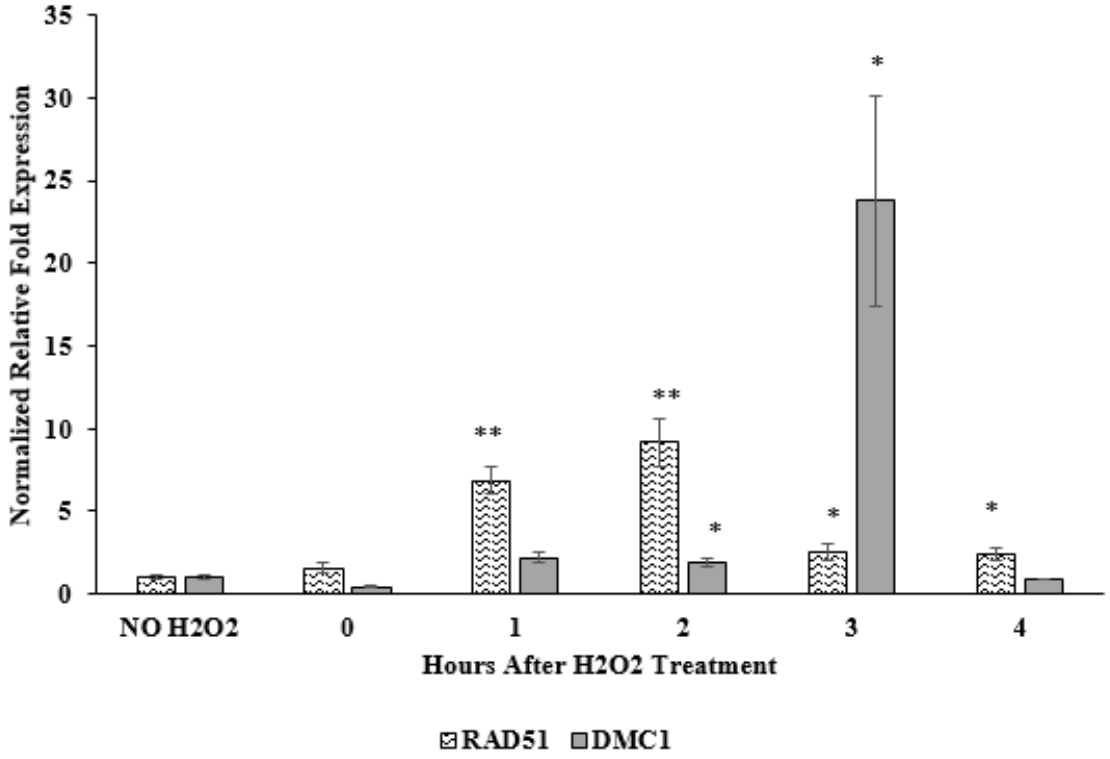

Figure 19. qRT-PCR expression profile analysis of the transcription of Rad51 and Dmc1 in response to H_2O_2 treatment. Samples were treated with 10Mm H_2O_2; striped represents Rad51; gray represents Dmc1 expression levels at different time points. All samples were normalized to expression levels of the housekeeping gene HHP1 and set relative to an untreated cDNA control with the same primers. Values represent mean of five trials with error bars of ±SEM. *p<0.05, **p<0.01, ***p<0.001 vs. untreated samples as measured by two-tailed, paired sample t-test.

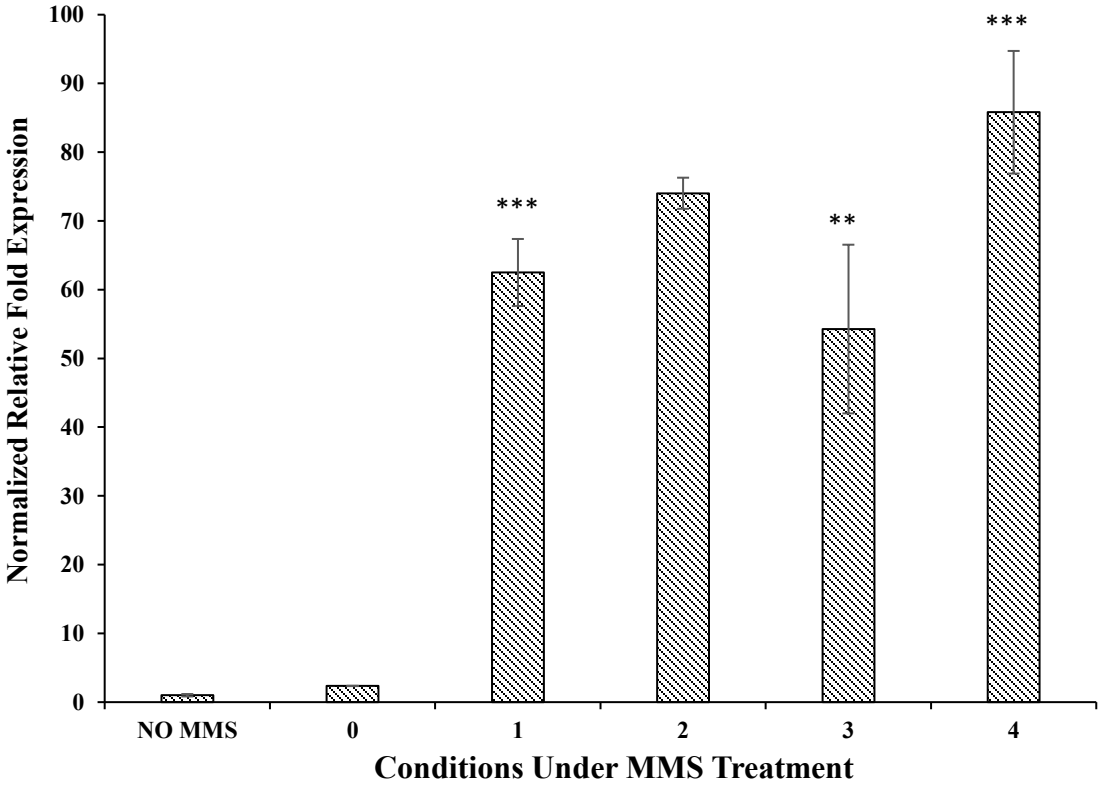

Figure 20. qRT-PCR expression profile analysis of the transcription of Rad51 in response to MMS treatment. Samples were treated with MMS; striped represents Rad51at different time points. All samples were normalized to the expression levels of the housekeeping gene HHP1 and set relative to an untreated cDNA control with the same primers. Values represent mean of six trials with error bars of ±SEM. *$p<0.05$, **$p<0.01$, ***$p<0.001$ vs. untreated samples as measured by two-tailed, paired sample t-test.

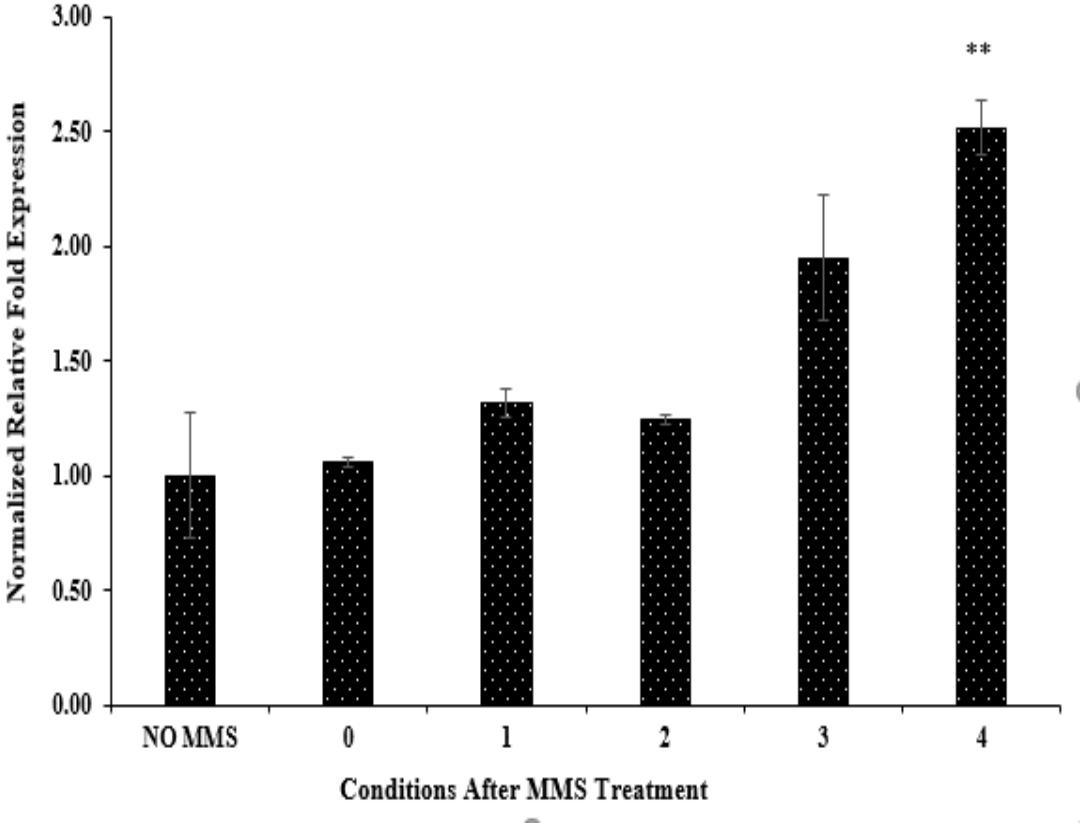

Figure 21. qRT-PCR expression profile analysis of the transcription of Dmc1 in response to MMS treatment. Samples were treated with MMS; black represents Dmc1 at different time points. All samples were normalized to the expression levels of the housekeeping gene HHP1 and set relative to an untreated cDNA control with the same primers. Values represent mean of six trials with error bars of ±SEM. *$p<0.05$, **$p<0.01$, ***$p<0.001$ vs. untreated samples as measured by two-tailed, paired sample t-test.

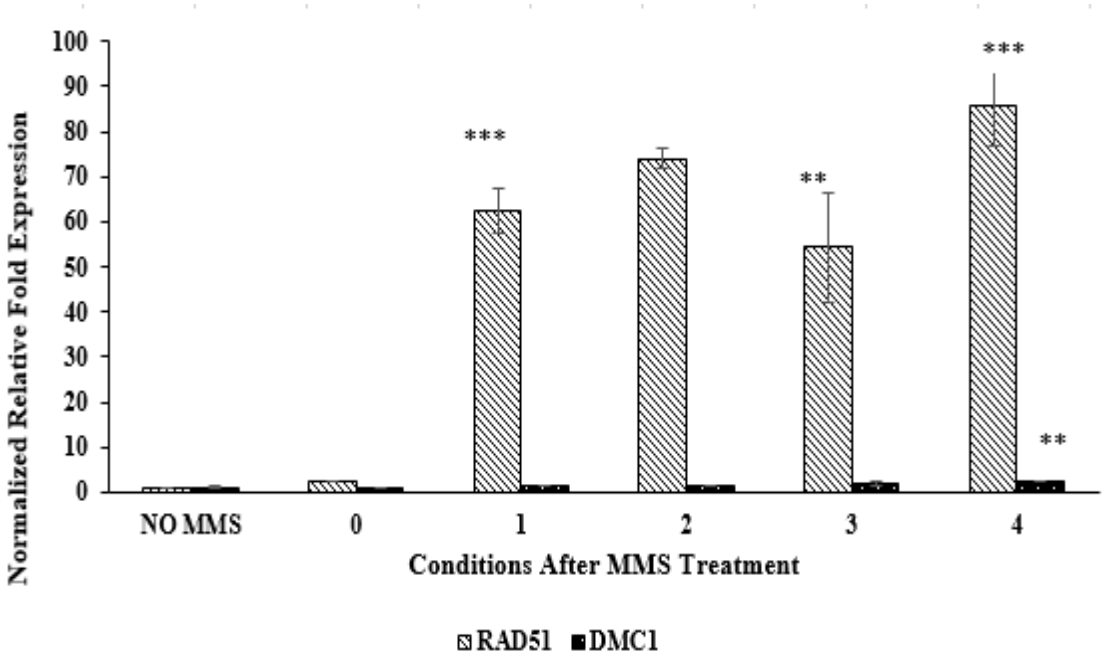

Figure 22. qRT-PCR expression profile analysis of the transcription of Rad51 and Dmc1 in response to MMS treatment. Samples were treated with MMS; striped represents Rad51; black represents Dmc1at different time points. All samples were normalized to the expression levels of the housekeeping gene HHP1 and set relative to an untreated cDNA control with the same primers. Values represent mean of six trials with error bars of ±SEM. *p<0.05, **p<0.01, ***p<0.001 vs. untreated samples as measured by two-tailed, paired sample t-test.

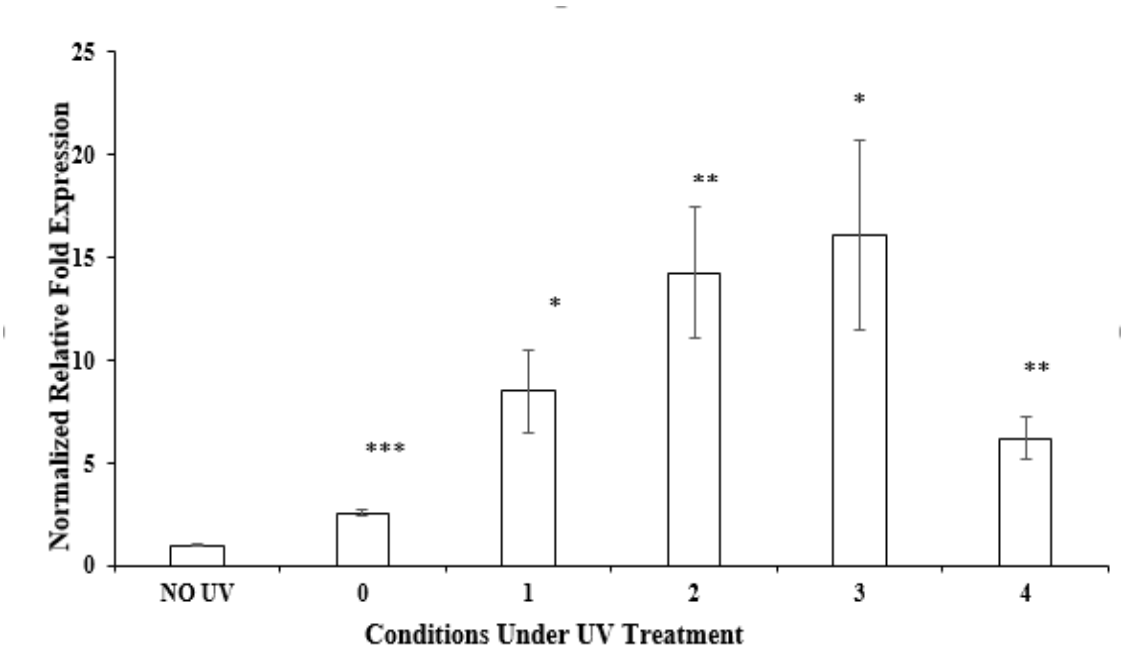

Figure 23. qRT-PCR expression profile analysis of the transcription of Rad51 in response to UV treatment. Samples were treated with UV; white represents Rad51at different time points. All samples were normalized to the expression levels of the housekeeping gene HHP1 and set relative to an untreated cDNA control with the same primers. Values represent mean of six trials with error bars of ±SEM. *p<0.05, **p<0.01, ***p<0.001 vs. untreated samples as measured by two-tailed, paired sample t-test.

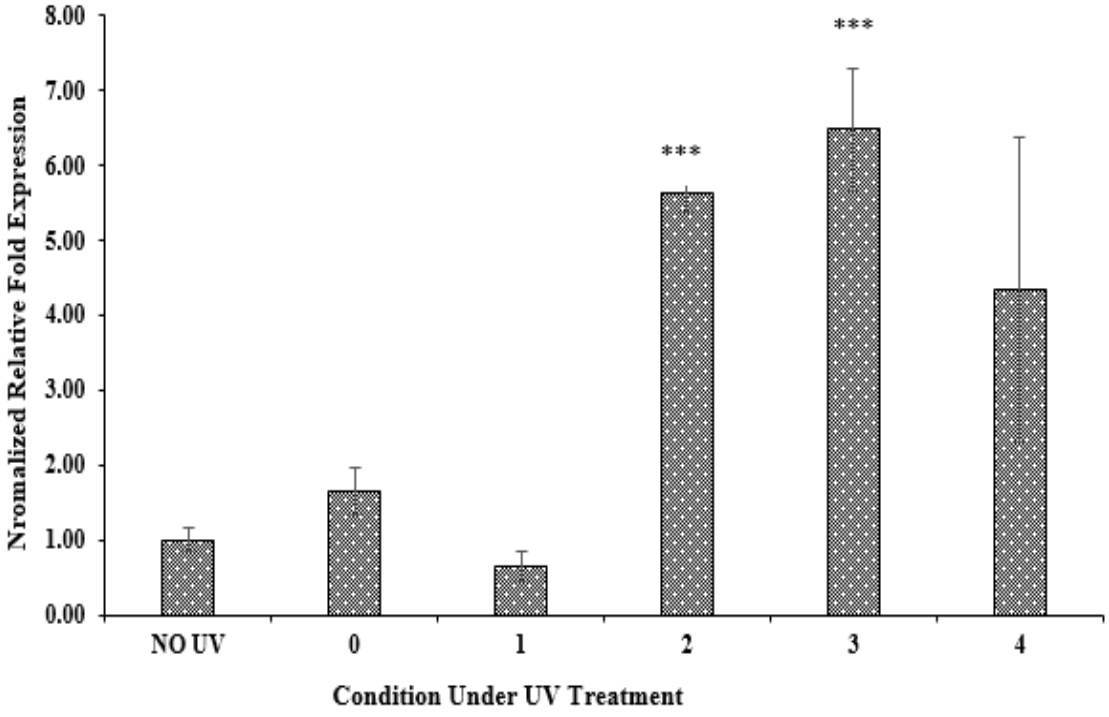

Figure 24. qRT-PCR expression profile analysis of the transcription of Dmc1 in response to UV treatment. Samples were treated with UV; striped represents Dmc1 at different time points. All samples were normalized to the expression levels of the housekeeping gene HHP1 and set relative to an untreated cDNA control with the same primers. Values represent mean of six trials with error bars of ±SEM. *p<0.05, **p<0.01, ***p<0.001 vs. untreated samples as measured by two-tailed, paired sample t-test.

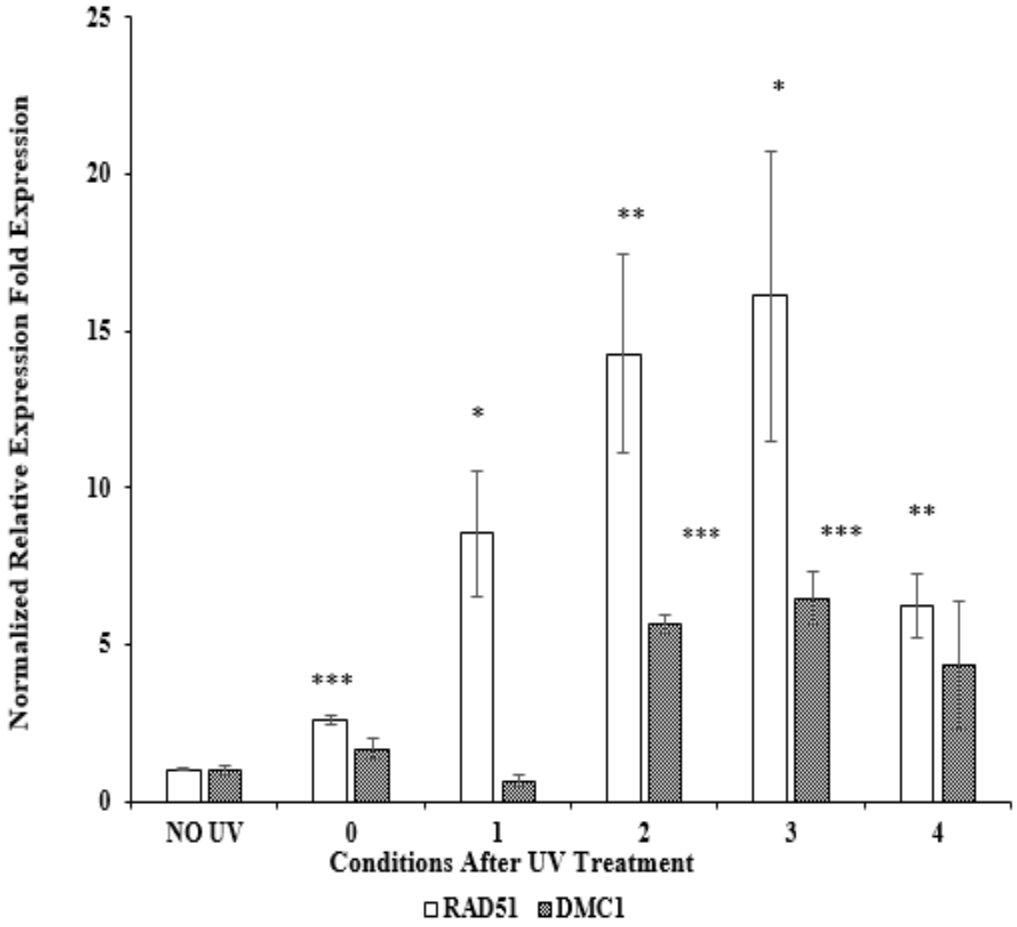

Figure 25. qRT-PCR expression profile analysis of the transcription of Rad51 and Dmc1 in response to UV treatment. Samples were treated with UV; white represents Rad51; striped represents Dmc1 at different time points. All samples were normalized to the expression levels of the housekeeping gene HHP1 and set relative to an untreated cDNA control with the same primers. Values represent mean of six trials with error bars of ±SEM. *p<0.05, **p<0.01, ***p<0.001 vs. untreated samples as measured by two-tailed, paired sample t-test.

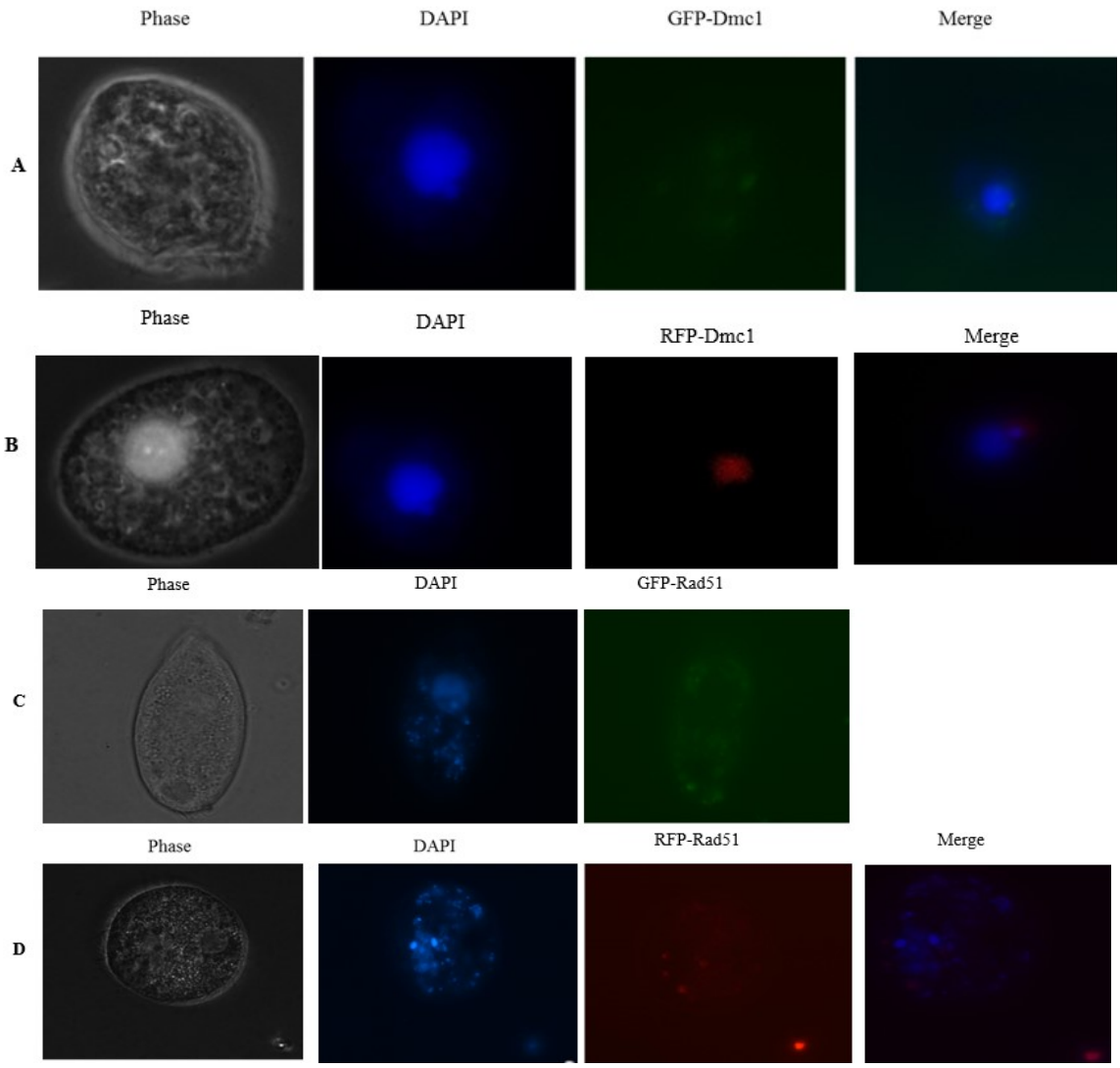

Figure 26. Fluorescent Microscopy images of Rad51 and Dmc1.The cells were stained with DAPI to view the nucleus. (A) Cells containing GFP-Dmc1. (B) Cells containing RFP-Dmc1. (C) Cells containingGFP-Rad51. (D) Cells containing RFP-Rad51. Rad51 and Dmc1 were distributed within the cytoplasm.

Rad51 and Dmc1 Localization in Response to DNA Damage

Localization of GFP-Rad51 and Dmc1 was observed after MMS treatment (Figure 27 & 28). Rad51 and Dmc1 expression is very sensitive to MMS. A concentration of 10 mM MMS was used to treat tagged cells for 1, 2, 3, and 4 hours. After one hour of MMS treatment, GFP-Dmc1 did not localize to either nucleus; it disappeared and GFP fluorescent was not expressed (Figure 27). Two hours later, GFP-Dmc1 started to show without localization to the nuclei; localization of GFP-Rad51 was seen throughout the cytoplasm. The pattern of localization for GFP-Dmc1 and GFP-Rad51 did not change when they were treated with MMS after three hours (Figures 27 & 28). The distribution of GFP-Dmc1 and GFP-Rad51 were observed throughout the cytoplasm after four hours of MMS treatment (Figures 27 & 28).

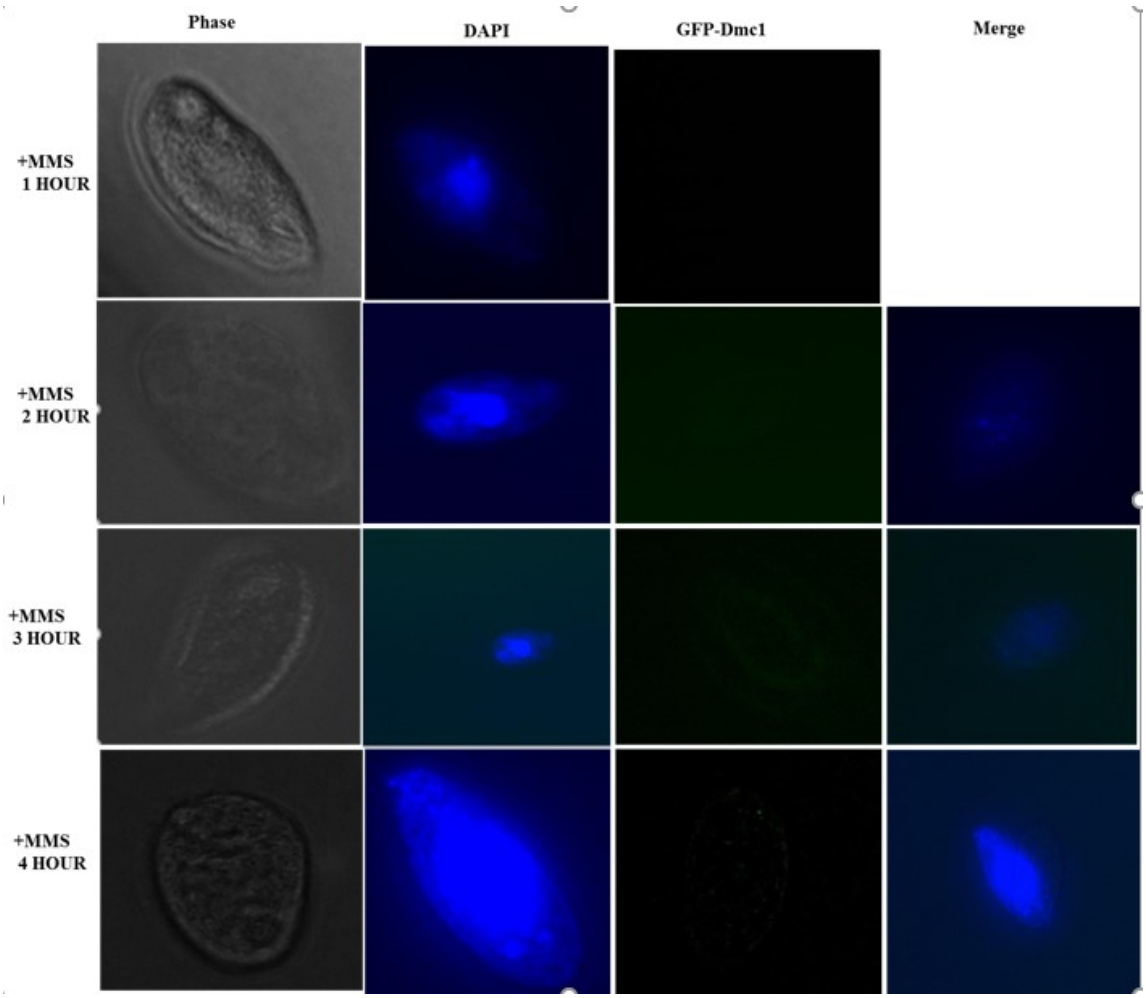

Figure 27. Dmc1 does not localize to nucleus following MMS treatment. Cells containing GFP-Dmc1 at log phase of growth (1 x 10^5 cells/mL). Then, Cells containing GFP-Dmc1 were treated with 10 mM MMS for 1-4 hours. In all panels cells were stained with DAPI and imaged at 1000x with oil immersion

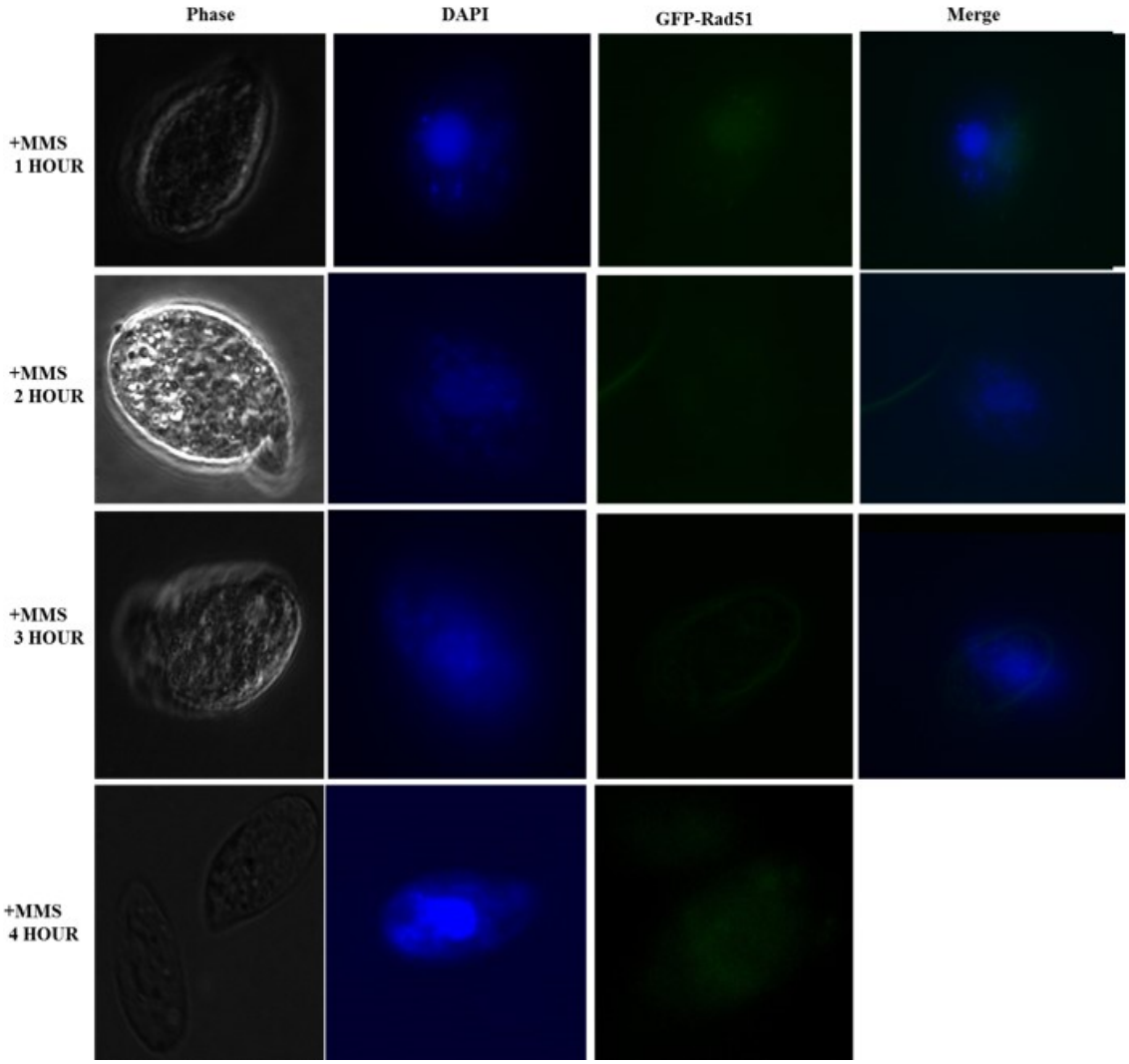

Figure 28. Rad51 does not localize to nucleus following MMS treatment. Cells containing GFP-Rad51 at log phase of growth (1 x 10^5 cells/mL). Then, Cells containing GFP-Rad51 were treated with 10 mM MMS for 1-4 hours. In all panels cells were stained with DAPI and imaged at 1000x with oil immersion.

DISCUSSION

Eukaryotic cells contain two recombinases paralogs, Rad51 and Dmc1 that are closely related to the bacterial RecA protein. RecA is a part of a DNA-dependent ATPase superfamily of proteins, which bind DNA and maintain genomic stability. RecA is the recombinase required for repair of DSBs in prokaryotic cells and Rad51 possesses a similar recombination function in eukaryotic cells. In eukaryotic cells they go through a specialized cell division for sexual reproduction and thus contain a meiosis-specific recombinase called Dmc1 that is used during non-sister chromatid DSB exchange (crossing-over), which happens in meiotic prophase I. The goal of this project was characterize the *T. thermophila* RecA homologs, Rad51 and Dmc1, and investigate their role in the response to DNA damaging agents.

Bioinformatics

Phylogenetic analysis of Rad51 and Dmc1 homologs revealed that both are highly conserved although in some organisms including *T. thermophila* the Dmc1 protein is more divergent away from the other eukaryotic RecA homologs (Figure s 7, B1, & B2). he phylogenetic tree identified that Rad51 and Dmc1 homologs were RecA family proteins (Figure 7). Some organisms have a more divergent Dmc1 while others the two paralogs were highly conserved and examples of both a divergent and highly conserved Rad51/Dmc1 was seen in examples across the four different eukaryotic kingdoms (Plantae, Fungi, Animalia, and Protista). This finding may help in identifying the unique characteristics and functions that these paralogs have in their role in the cell. In some paralogs there may be a loss of redundancy in function when the other is missing or a

separation of the functional roles. Studying the roles of Dmc1 and Rad51 in both P. tetraurelia T. thermophila both complex single-cell protozoa could elucidate the purpose for the divergence.

In addition to the similarity between Rad51 and Dmc1 at the whole protein level, they also were highly conserved within their functional domains and motifs and all RecA homologs contained two conserved ATPase domains (RECA2 and RECA3; Figure 6). The RECA2 domains is located in the N-terminal region and required for ATP hydrolysis and the RECA3 is located in the C-terminal region required for ATP binding. All RecA homologs also contained the highly conserved Walker A and Walker B motifs located in the RECA2 domain of both Rad51 and Dmc1 paralogs (Appendix B - Figures B1 & B2). The *T. thermophila* Dmc1 scored 87%, and *T. thermophila* Rad51 scored 92% similarity in their overall alignment further suggesting that Dmc1 may have a unique function in the cell.

Expression of *RAD51* and *DMC1* was observed through three methods, which included RNAseq, expression microarray, and qRT-PCR. The microarray data for *RAD51* indicated a ubiquitous basal expression during vegetative growth with induced expression during conjugation and starvation conditions (Figure 9A). Interestingly, *DMC1* was only expressed during the conjugation and emphasizes the role of Dmc1 has in meiosis (Figure 9B). Rad51 could function in both meiosis and mitosis, which has been documented in previous experiments where *RAD51* overexpression causes the macronucleus to not divide creating amacronucleate cells (Figure 5). Expression of both *RAD51* and *DMC1* increased in a bimodal pattern during conjugation, peaking between 2-4 hours corresponding to meiotic prophase I when crossing-over occurs and later between 12-16 hours during the time when the new macronuclei are developing from

zygotic micronuclei (micronuclear-limited sequences are eliminated, chromosomal fragmentation of 5 MIC chromosomes to 218 MAC chromosomes, and duplication of each MAC chromosome to 45 copies (2N to 45C). This suggests either an overlapping function, specific recombinational roles, or a complex interaction of Rad51 and Dmc1 in *T. thermophila* conjugation. Previously published work on the knockouts of *RAD51* and *DMC1* show deletion of either will halt conjugation in meiotic prophase but only removal of *RAD51* has a cell division phenotype causing arrest of micronuclear mitosis creating amicronucleate cells (Howard-Till et al., 2011; Marsh et al., 2000; Marsh et al., 2001). This suggests that the role is either recombinationally specific or a complex interaction between Rad51 and Dmc1.

Figure 8 shows the predicted annotation of *RAD51* to contain three exons and two introns, and *DMC1* to contain five exons and four introns and the RNAseq coverage data confirms the RAD51 exons and introns (Figure 8A). The RNAseq coverage data for *DMC1* confirms the exons and introns but there is a low level of coverage detected over the second intron (Figure 8B) and this could explain the multiple products produced from DMC1-2 primers over this intron (Figure 16).

In addition to Rad51 and Dmc1 homologs of Hop2 and Mnd1 proteins that are found to interact with each other and Rad51 and Dmc1 to promote efficient homologous recombination were identified and bioinformatics analysis conducted. The Hop2 and Mnd1 proteins families are typically represented by one homolog in most eukaryotes, but in *T.* thermophila two *HOP2* and two *MND1* homologs were found (Appendix B - Table B1 and data not shown). The meiosis-specific expression of HOP2 and the more ubiquitous expression of HOPP2 which peaks also during starvation and conjugation has been experimentally confirmed through RT-PCR (Mochizuki et al.,2008). There is a

higher ubiquitously expression of MNDP1 whereas MND1 is only expressed at very low levels in the cell (data not shown). Since Hop2 and Mnd1 act as a complex together in Dmc1 and Rad51 homologous pairing The linked patterns of expression could indicate that Hop2 functions with Dmc1 while Hopp2 functions with Rad51 or that a specific Hop2-Mnd1 complex interacts with Rad51 during mitosis and DNA repair while another Hop2-Mnd1 complex functions during conjugation.

Expression of *RAD51* and *DMC1* Following DNA Damage in *T. thermophila.*

Analysis of *DMC1* and *RAD51* PCR products from two sets of primers for each gene (each spanning across an intron) showed amplification of proper size product when using genomic DNA as the template (Figure 14 & 16). Both RAD51-1 and RAD51-2 showed the correct size PCR product using cDNA as the template, but RAD51-1 primers amplified a little better with the SsoFast Evagreen qPCR mix (Figure 16) so was used for all of the DNA damage expression experiments. Mixed results were seen with the *DMC1* primer sets when cDNA was used as the template. When the Gotaq PCR master mix was used a single band the correct size corresponding to the cDNA size was only seen with the DMC1-1 primer set and the DMC1-2 primers showed a product the same size as the genomic DNA (Figure 14). When the SsoFast Evagreen qPCR master mix was used DMC1-1 primers yielded a band that corresponded to the size of genomic DNA while DMC1-2 primers yielded two bands one corresponding to the size for cDNA and the other had the same size as gDNA (Figures 15 & 16). Since cDNA from vegetatively growing cells was used the lack of template cDNA may have caused the amplification of any genomic DNA contamination or in the case of the products in DMC1-2 there may be an alternatively spliced form that includes the second intron being that RNAseq showed

some coverage over that intron (Figure 8). The reasoning for a genomic DNA sized band with DMC1-1 primers is most likely genomic DNA contamination since it was not seen with GoTaq but was with qPCR which has more cycles in the PCR protocol. If alternative splicing occurs leaving the second intron in the cDNA a truncated protein of 194 amino acids instead of 356 would be made and it would only have a truncated portion of the RECA2 domain and lack the RECA3 domain (this would render it nonfunctional as a DNA-dependent ATPase. The activity of this form of Dmc1 is unknown, but it could be used as a decoy receptor to bind away proteins that can interact with both Rad51 and Dmc1 to turn off the recombination activity at the later part of DNA repair or when not needed during meiosis. Since the DMC1-2 set of primers gave a band at the predicted size in cDNA (even though other products were present) this set of primers were used for *DMC1* expression analysis after various DNA damaging agents.

Further qRT-PCR experiments were conducted to identify the expression patterns of *RAD51* and *DMC1* in response to DNA damaging agents. The qRT-PCR expression data revealed an increased expression of *RAD51* and *DMC1* in response to DNA damage by UV irradiation (Figure 25). The expression continued to increase as the time went on, but it dropped down at the 4-hour time point. The similarity of the expression of Rad51 and Dmc1 after UV treatment, peaking to 17-fold for Rad51 and 6.5-fold for Dmc1 at the 3-hour time point, strongly suggested both Rad51 and Dmc1 have a functional role in the UV induced DNA repair process (Figure 25). UV irradiation causes the production of DNA adducts, which can result in DSBs that could be repaired by homologous recombination (Rolfsmeier M et al.,2010). This explains the increased expression after two hours of treatment. Interestingly, MMS is known to cause DBSs that are repaired by HHR, which similar showed only a large induction of the expression of *RAD51* (70-fold

induction) while after 1-hour treatment *DMC1* only reached 2-fold induction and that was not until 4-hours after treatment (Figure 22). The drastic difference in expression illustrates that Rad51 and not Dmc1play a significant role in HRR DNA repair from damaged caused by MMS (Figure 22). Additionally, a similar pattern of expression was observed for *RAD51* after treatment with H_2O_2 as was with UV but *DMC1* expression was unique with a slight increase 2-hours after treatment and a drastic spike inducing 25-fold 3-hours after with a subsequent decrease back down 4-hours after treatment with H_2O_2 (Figure 19). Hydrogen peroxide results in radical damage and there may either be a role for both of these RecA homologs in the repair or it may be related to a cell cycle specific expression since with both UV and H_2O_2 the cells may arrest preventing progression through division and this increase is just a result of cell synchronization. Analysis of the qRT-PCR data shows that *DMC1* induction after DNA damage is always delayed compared to *RAD51* expression (Figures 19, 22, & 25) and it is possible that Dmc1 acts differently to stabilize the DNA repair done by Rad51 or as a mechanism to turn of the Rad51 repair by competing for interacting proteins like the Hop2-Mnd1 complex.

Epitope and Fluorescent Tagged Rad51 and Dmc1 Expression and Localization

T. thermophila transformants containing 2HA-Rad51, 2HA-Dmc1, FH6-Rad51, and FH6-Dmc1 were made, and Total protein extracts were isolated from multiple transformants to be used to confirm the expression of the epitope tagged Rad51 and Dmc1 through western blot analysis. This experiment was not completed and isolated protein extracts were stored at –80° C for future research. Transformation of GFP-Rad51, RFP-Rad51, RFP-Dmc1, and GFP-Dmc1 into *T.* thermophila was completed and

expression of the GFP and RFP tagged Rad51 and Dmc1 was confirmed by fluorescent microscopy in growing cells and all showed fluorescence in the cytoplasm confirming positive expression of the fusion proteins (Figure 26). The GFP expression was easier to visualize so GFP-Rad51 and GFP-Dmc1 transformants were treated with MMS to observe if there was a change in localization following DSBs (Figure 28). Transformants expressing GFP/RFP-Rad51 and GFP/RFP-Dmc1 exhibited the fluorescence protein in the cytoplasm and not within the macronucleus but only Dmc1 in the micronucleus (Figure 26). The localization in the micronucleus could not be confirmed by merging the DAPI with the GFP/RFP because even when the cells were not moving the organelles were still moving around in the cell slightly distorting the data between pictures. In response to MMS damage, Rad51 and Dmc1 did not localize to either the macronucleus or the micronucleus. After one hour of MMS treatment, Dmc1 was not detectible, but Rad51 showed a slight expression. It is known that Rad51 localizes to the nuclei to repair the DSBs caused by MMS (Campbell & Romero, 1998) but, localization was not observed. This may have occurred due to the high concertation of MMS, 10 mM MMS, which is known to turn off the MTT1 promoter which is driving the inducible expression of the fluorescently tagged proteins. Another possibility is that the tag interferes with the normal function and thus does not localize or that it takes a longer time to localize to the nuclei then previously documented.

Future Directions

More research will be needed to find the interplay role between Rad51 and Dmc1. Rad51 and Dmc1 were tagged with Flag and HA epitope tags and the total protein were isolated from the cells to run western blot experiment. Western blot analysis could be

performed to confirm the tagged HA-Rad51 and HA-Dmc1 proteins. Once, they are confirmed, an immunoprecipitation could be utilized to identify proteins interacting with Rad51 and Dmc1. Pulling down the interacting proteins can help to elucidate the factors that control the activity of Rad51 and Dmc1 during the DNA damage process and to even determine if Rad51 can form a heteronucleofilament with Dmc1 during DNA repair, cell cycle, and conjugation. In addition, it would be beneficial to create HA-Hop2/HA-Hopp2 and FH6-Mnd1/FH6-Mndp1 constructs to further characterize their roles in DSB repair and interactions with Rad51 and Dmc1 and to determine which of the Hop2 and Mnd1 homologs interact with one another, Rad51, and Dmc1.As the localization studies were inconclusive, repeating fluorescent microscopy analysis with GFP-Rad51/RFP-Rad51 and GFP-Dmc1/RFP-Dmc1will help to visualize any actual localization for these proteins. To improve the likelihood of success, it would be ideal to decrease the concentration of MMS from 10 mM to 5 mM instead and look at the localization between 1-6 hours to conclude if localization can be found in either nucleus. In addition, it would be beneficial to treat the cells with UV and H_2O_2 to track any localization of Rad51 and Dmc1 to the nuclei. Expression profiles showed an increase in *RAD51* and *DMC1* expression in response to UV and H_2O_2 treatment and were much higher for *DMC1* with these two damaging agents compared to MMS. Expression of *RAD51* and *DMC1* using qRT-PCR could be done on synchronized cells or starved cells to elucidate the role of Rad51 and Dmc1 in cell cycle progression and mitosis as well as stress related to starvation. Microarray expression data showed that *RAD51* was expressed through all cell conditions where as *DMC1* was only expressed during conjugation (Figure 9). To determine whether Rad51 has a specific role in somatic cell division that is lacking for Dmc1 single and double knockouts (double knockout of *rad51* and *dmc1*and single

knockouts of *dmc1* or *rad51*) and a *DMC1* overexpression strain (currently have a *RAD51* overexpression strain) could be constructed. These strains could then be tested with the same DNA damaging agents used above to look at sensitivity. If the double knockout cells are more sensitive to a DNA damaging agent than the *rad51* knockout, and if the *dmc1*knockout has no sensitivity, that would confirm that Dmc1 plays some accessory role to help Rad51 in DNA repair damage. If the double knockout looks just the same as the *rad51* knockout we can conclude that there is no direct interaction between Rad51 and Dmc1 and that the increase in Dmc1 may be a way to turn off the repair process by sequestering interacting proteins away from Rad51.

Additional FH6-Dmc1 could clarify the interplay role between both Rad51 and Dmc1. The protein extracts made from the FH6- Dmc1 cells compared to wild-type (CU428) cells that are induced and uninduced with DNA damaging agents and extracts made between 2-4 hours after treatment could be analyzed by western blot analysis. Immunoprecipitation studies using FLAG antibody and a commercial Rad51 antibody, looking at UV and H_2O_2 damage and interaction in the FH6-Dmc1 transformants, can help to determine if there is a physical interaction between Rad51 and Dmc1 in a heteronucleofilament that has not been previously identified. These experiments will also tell if the commercial Rad51 antibody only detects *T. thermophila* Rad51 or if it cross-reacts and detects Dmc1 too. This can be seen since Dmc1 is tagged with FLAG-6xHis it will be larger in the tagged strain than the wild-type strain and could be observed by western blot analysis.

The overexpression *RAD51* and *DMC1* in cells can be a great way to visualize if the amacronucleate phenotype found with overexpression of *RAD51* (Figure 5) is also seen if *DMC1* was expressed when it normally is not active. Overexpression of RAD51

caused a defect in macronuclear elongation that resulted in some amacronucleate cells and some cells with extra macronuclear contents (Smith et al., Unpublished data; Figure 5). Being that *T. thermophila* Rad51 and Dmc1 are more divergent than other eukaryotes differences in overexpression phenotypes can help determine if there is a potential Rad51 motif required for its role in macronuclear division and cell cycle. Chimeric proteins exchanging the n-terminal portion of Rad51 and Dmc1 and overexpressing these can help to find the region that is causing the amacronucleate phenotype in the RAD51 overexpression cells.

REFERENCES

Altschul, S.F., Wootton, J.C., Gertz, E.M., Agarwala, R., Morgulis, A., Schaffer, A.A., and Yu, Y. (2005). Protein databases searches using compositionally adjusted substitution matrices FEBS J. 272:5101-5109.

Aerssens, J., Armstrong, M., Gilissen, R., and Cohen, N. (2001). The human genome: an introduction. Oncologist 6(1):100-9.

Bishop, D.K., Park, D., Xu, L., and Kleckner, N., (1992). DMC1: a meiosis specific yeast homolog of E. coli RecA required for recombination, synaptonemal complex formation, and cell cycle progression. Cell 69, 439–456.

Bishop, D.K. (1994). RecA homologs Dmc1 and Rad51 interact to form multiple nuclear complexes prior to meiotic chromosome synapsis. Cell 79, 1081–1092.

Brown, M.S., and Bishop, D.K. (2015). DNA strand exchange and RecA homologs in meiosis. CSH Perspect. Biol. 7, p. 016659.

Buchhop, S., Gibson, M.K., Wang, X.W., Wagner, P., Sturzbecher, H.W., and Harris, C.C. (1997). Interaction of p53 with the human Rad51 protein. Nuc. Acids Res. 25:3868–3874.

Bugreev, D.V., Huang, F., Mazina, O.M., Pezza, R.J., Voloshin, O.N., Camerini-Otero, R.D., and Mazin, A.V. (2014). HOP2-MND1 modulates RAD51 binding to nucleotides and DNA. Nat. Commun. 5:4198–4207.

Campbell, C., and Romero, D. P. (1998). Identification and characterization of the RAD51 gene from the ciliate *Tetrahymena thermophila.* Nuc. Acids Res. 26(13), 3165–3172.

Chang, H.Y., Liao, C.-Y., Su, G.-C., Lin, S.W., Wang, H.W., and Chi, P. (2015). Functional Relationship of ATP Hydrolysis, Presynaptic Filament Stability, and Homologous DNA Pairing Activity of the Human Meiotic Recombinase DMC1. J. Biol. Chem. 290(32), 19863–19873.

Chen, Y.K., Leng, C.H., Olivares, H., Lee, M.H., Chang, Y.C., Kung, W.M., Ti, S.C., Lo, Y.H., Wang, A.H., and Chang, C.S. (2004). Heterodimeric complexes of Hop2 and Mnd1 function with Dmc1 to promote meiotic homolog juxtaposition and strand assimilation. Proc. Natl Acad. Sci. U.S.A.101:10572–10577.

Chi, P., San Filippo, J., Sehorn, M. G., Petukhova, G. V., and Sung, P. (2007). Bipartite stimulatory action of the Hop2–Mnd1 complex on the Rad51 recombinase. Genes Dev. 21(14), 1747–1757.

Cloud, V., Chan, Y.L., Grubb, J., Budke, B., and Bishop, D.K. (2012). Rad51 is an accessory factor for Dmc1-mediated joint molecule formation during meiosis. Science 337(6099):1222–1225.

Choudhury, A., Zhao, H., Jalali, F., Al Rashid, S., Ran, J., Supiot, S., Kiltie, A.E., and Bristow, RG. (2009). Targeting homologous recombination using imatinib results in enhanced tumor cell chemo-sensitivity and radiosensitivity. Mol. Cancer Ther. 8:203–213.

Davis, A. J., Lee, K.J., and Chen, D. J. (2013). The N-terminal Region of the DNA-dependent Protein Kinase Catalytic Subunit Is Required for Its DNA Double-stranded Break-mediated Activation. J. Biol. Chem. 288(10), 7037–7046.

Dresser, M.E., Ewing, D.J., Conrad, M.N., Dominquez, A.M., Barstead, R., Jiang, H., and Kodadek, T. (1997). Dmc1 functions in a Saccharomyces cerevisiae meiotic pathway that is largely independent of the Rad51 pathway. Genetics 147, 533–544.

Eisen, J. A., Coyne, R. S., Wu, M., Wu, D., Thiagarajan, M., Wortman, J. R., . . . and Orias, E. (2006). Macronuclear Genome Sequence of the Ciliate *Tetrahymena thermophila*, a Model Eukaryote. PLoS Biology 4(9), e286.

Featherstone, C., and Jackson, S. P. (1999). DNA double-strand break repair. Current Biology. 9(20), R759-R761.

Gasior, S.L., Wong, A.K., Kora, Y., Shinohara A., and Bishop D.K. (1998). Rad52 associates with RPA and functions with Rad55 and Rad57 to assemble meiotic recombination complexes. Genes Dev. 12(14):2208–2221.

Hakem, R. (2008). DNA-damage repair; the good, the bad, and the ugly. EMBO J. 27(4), 589–605.

Hannay, J.A., Liu, J., Zhu, Q.S., Bolshakov, S.V., Li, L., Pisters, P.W., Lazar, A.J., Yu D., Pollock, R.E., and Lev, D. (2007). Rad51 overexpression contributes to chemo-resistance in human soft tissue sarcoma cells: a role for p53/activator protein 2 transcriptional regulation. Mol. Cancer Ther. 6:1650–1660.

Helleday, T., Eshtad, S., and Nik-Zainal, S. (2014). Mechanisms underlying mutational signatures in human cancers. Nat. Rev. Genet. 15(9), 585–598.

Henry, J.M., Camahort, R., Rice, D.A., Florens, L., Swanson, S.K., Washburn, M.P., and Gerton, J.L. (2006). Mnd1/Hop2 facilitates Dmc1-dependent interhomolog crossover formation in meiosis of budding yeast. Mol. Cell. Biol. 26:2913–2923.

Howard-Till, R. A., Lukaszewicz, A., and Loidl, J. (2011). The Recombinases Rad51 and Dmc1 Play Distinct Roles in DNA Break Repair and Recombination Partner Choice in the Meiosis of *Tetrahymena*. PLoS Genetics 7(3), e1001359.

Jackson, S. P. (2002). Sensing and repairing DNA double-strand breaks. Carcinogenesis 23:687-696.

Jasin, M. (2002). Homologous repair of DNA damage and tumorigenesis: The BRCA connection. Oncogene 21, 8981-8993.

Khanna, K.K., and Jackson, S. P. (2001). DNA double-strand breaks: signaling, repair and the cancer connection. Nat. Genet. 27:247-254.

Kim, P. M., Allen, C., Wagener, B. M., Shen, Z., and Nickoloff, J. A. (2001). Overexpression of human RAD51 and RAD52 reduces double-strand break-induced homologous recombination in mammalian cells. Nuc. Acids Res. 29(21), 4352–4360.

Koonin, E.V., Tatusov, R.L., and Rudd, K.E. (1995). Sequence similarity analysis of Escherichia coli proteins: functional and evolutionary implications. Proc. Natl. Acad. Sci. U.S.A. 92, 11921–11925, 5–74.

Koonin, E.V. (1993). A superfamily of ATPases with diverse functions containing either classical or deviant ATP-binding motif. J. Mol. Biol. 229, 11639.

Koonin, E.V. (1993b). A common set of conserved motifs in a vast variety of putative nucleic acid-dependent ATPases including MCM proteins involved in the initiation of eukaryotic DNA replication. Nuc. Acids Res. 21, 2541 – 2547.

Lee, J.Y., Terakawa, T., Qi, Z., Steinfeld, J.B., Redding, S., Kwon, Y., Gaines, W.A., Zhao, W., Sung, P., and Greene, E.C. (2015). Base triplet stepping by the Rad51/RecA family of recombinases. Science 349, pp. 977-981.

Leipe, D.D., Wolf, Y.I., Koonin, E.V., and Aravind, L. (2002). Classification and evolution of P-loop GTPases and related ATPases. J. Mol. Biol. 317, 41 – 72.

Leu, J.Y., Chua, P.R., and Roeder, G.S. (1998). The meiosis-specific Hop2 protein of S. cerevisiae ensures synapsis between homologous chromosomes. Cell 94:375–386.

Lieber, M. R. (2010). The Mechanism of Double-Strand DNA Break Repair by the Non homologous DNA End Joining Pathway. Annu. Rev. Biochem. 79, 181–211.

Liu, N. (2002). XRCC2 Is Required for the Formation of Rad51 Foci Induced by Ionizing Radiation and DNA Cross-Linking Agent Mitomycin C. J. Biomed. Biotech. 2(2), 106–113.

Li, X., and Heyer, W.D. (2008). Homologous recombination in DNA repair and DNA damage tolerance. Cell Res. 18(1), 99–113.

Li, X., and Heyer W.D. (2009). RAD54 controls access to the invading 30-OH end after RAD51-mediatedDNA strand invasion in homologous recombination in Saccharomyces cerevisiae. Nuc. Acids Res. 37(2):638–646.

Li, Y., Wang, W.Y., Xiao, J.H., Xu, F., Liao, D.Y., Xie, L., Wang, J., and Luo, F. (2017). Overexpression of Rad51 Predicts Poor Prognosis in Colorectal Cancer: Our Experience with 54 Patients. PLoS ONE 12(1): e0167868.

Loidl, J. and Scherthan, H. (2004). Organization and pairing of meiotic chromosomes in the ciliate *Tetrahymena thermophila*. J. Cell Sci. 117, 5791–5801.

Maréchal, A., and Zou, L. (2013). DNA Damage Sensing by the ATM and ATR Kinases. Cold Spring Harbor Perspectives in Biology 5(9), a012716.

Marsh, T. C., Cole, E. S., Stuart, K. R., Campbell, C., and Romero, D. P. (2000). RAD51 is required for propagation of the germinal nucleus in *Tetrahymena thermophila.* Genetics 154(4), 1587–1596.

Marsh, T.C., Cole, E.S., and Romero, D.P. (2001). The Transition from Conjugal Development to the First Vegetative Cell Division Is Dependent on RAD51 Expression in the Ciliate *Tetrahymena thermophile.* Genetics 157,1591-1598.

Masson, J. Y., and West, S. C. (2001). The Rad51 and Dmc1 recombinases: a non-identical twin relationship. Trends Biochem. Sci. 26, 131-136.

Mizuta, R., LaSalle, J.M., Cheng, H.L., Shinohara, A., Ogawa, H., Copeland, N., Jenkins, N.A., Lalande, M., and Alt. F.W. (1997). RAB22 and RAB163/mouse BRCA2: Proteins that specifically interact with the RAD51 protein Proc. Natl. Acad. Sci. USA 94: 6927-6932.

Mochizuki, K., Novatchkova, M., and Loidl, J. (2008). DNA double-strand breaks, but not crossovers, are required for the reorganization of meiotic nuclei in *Tetrahymena*. J. Cell Sci. 121(Pt 13), 2148–2158.

Neale, M.J., and Keeney, S. (2006). Clarifying the mechanics of DNA strand exchange in meiotic recombination. Nature 442:153–158.

Ogawa, T., Yu, X., Shinohara, A., and Egelman, E.H. (1993). Similarity of the yeast RAD51 filament to the bacterial RecA filament. Science 259:1896–1899.

Okorokov, A.L., Chaban, Y.L., Bugreev, D.V., Hodgkinson, J., Mazin, A.V., and Orlova, E.V. (2010). Structure of the hDmc1-ssDNA Filament Reveals the Principles of Its Architecture. PLoS ONE 5(1), e8586.

Orias E. (2012). *Tetrahymena thermophila* Genetics: Concepts and Applications Meth. Cell Biol. 109, 301-325.

Orias E. (2000).Toward sequencing the *Tetrahymena* genome: Exploiting the gift of nuclear dimorphism. J. Eukaryot. Microbiol. 47:328–333.

Peng, M., Bakker, J.L., Dicioccio, R.A., Gille, J.J., Zhao, H., Odunsi, K., Sucheston, L., Jaafar, L., Mivechi, N.F., Waisfisz, Q. and Ko, L. (2013). Inactivating mutations in GT198 in familial and early-onset breast and ovarian cancers. Genes Cancer. 4:15–25.

Peterson, D.S., Gao, Y., Asokan, K., and Gaertig, J. (2002). The circumsporozoite protein of Plasmodium falciparum is expressed and localized to the cell surface in the free-living ciliate *Tetrahymena thermophila.* Mol. Biochem. Parasitol. 122:119–126.

Petukhova, G.V., Romanienko, P.J., and Camerini-Otero, R.D. (2003). The Hop2 protein has a direct role in promoting interhomolog interactions during mouse meiosis. Dev. Cell 5:927–936.

Pezza, R.J., Petukhova, G.V., Ghirlando, R., and Camerini-Otero, R.D. (2006). Molecular activities of meiosis-specific proteins. Hop2, Mnd1, and the Hop2–Mnd1 complex. J. Biol. Chem. 281:18426–18434.

Pittman, D.L., Cobb, J., Schimenti, K.J., Wilson, L.A., Cooper, D.M., Brignull, E., Handel, M.A., and Schimenti, J.C. (1998). Meiotic prophase arrest with failure of chromosome synapsis in mice deficient for Dmc1, a germline-specific RecA homolog. Mol. Cell 1:697–705.

Ploquin, M., Petukhova, G.V., Morneau, D., Dery, U., Bransi, A., Stasiak, A., Camerini-Otero, R.D., and Masson, J.Y. (2007). Stimulation of fission yeast and mouse Hop2-Mnd1 of the Dmc1 and Rad51 recombinases. Nuc. Acids Res. 35:2719–2733.

Qiao, G.B., Wu, Y.L., Yang, X.N., Zhong, W.Z., Xie, D., Guan, X.Y., Fischer, D., Kolberg, H.C., Kruger, S., and Stuerzbecher, H.W. (2005). High-level expression of Rad51 is an independent prognostic marker of survival in non-small-cell lung cancer patients. Brit. J. Cancer 93(1), 137–143.

Ramsden, D.A., and Gellert, M. (1998). Ku protein stimulates DNA end joining by mammalian DNA ligases: a direct role for Ku in repair of DNA double-strand breaks. EMBO J., 17, 609-614.

Ray, C. (1956). Meiosis and nuclear behavior in *Tetrahymena pyriformis*. J. Protozool. 3, 88–96.

Reymer, A., Frykholm, K., Morimatsu, K., Takahashi M., and Nordén, B. (2009). Structure of human Rad51 protein filament from molecular modeling and site-specific linear dichroism spectroscopy. Proc. Natl. Acad. Sci. U.S.A. 106 (32) 13248-13253.

Ristic, D., Modesti, M., Heijden, T.V.D., Noort, J., Dekker, C., Kanaar, R., and Wyman, C. (2005). Human Rad51 filaments on double- and single-stranded DNA: correlating regular and irregular forms with recombination function. Nuc. Acids Res. 33 (10): 3292-3302.

Rockmill, B., Sym, M., Scherthan, H., and Roeder, G.S. (1995). Roles for two RecA homologs in promoting meiotic chromosome synapsis. Genes Dev. 9:2684–2695.

Rolfsmeier, M., Laughery, M.F., and Haseltine, C.A. (2010). Repair of DNA Double-Strand Breaks following UV Damage in Three Sulfolobus solfataricus Strains. J. Bacteriol. 192 (19): 4954-4962.

Rothkamm, K., Krüger, I., Thompson, L. H., and Löbrich, M. (2003). Pathways of DNA Double-Strand Break Repair during the Mammalian Cell Cycle. Mol. Cell. Biol. 23(16), 5706–5715.

Schwacha, A. and Kleckner, N. (1997). Interhomolog bias during meiotic recombination: meiotic functions promote a highly differentiated interhomolog only pathway. Cell 90, 1123–1135

Sebesta, M., Burkovics, P., Haracska, L., Krejci, L. (2011). Reconstitution of DNA repair synthesis in vitro and the role of polymerase and helicase activities. DNA Repair (Amst) 10(6):567–576.

Sebesta, M., and Krejci, L. (2016). Mechanism of Homologous Recombination (PDF Download Available) in DNA replication, recombination, and repair: molecular mechanisms and pathology. Tokyo: Springer. Retrieved Jan, 2017.

Seong, C., Sehorn, M.G., Plate, I., Shi, I., Song, B., Chi, P., Mortensen, U., Sung, P., and Krejci, L. (2008). Molecular anatomy of the recombination mediator function of *Saccharomyces cerevisiae* Rad52. J. Biol. Chem. 283(18):12166–12174.

Shang, Y., Li, B., and Gorovsky, M.A. (2002). *Tetrahymena thermophila* contains a conventional gamma-tubulin that is differentially required for the maintenance of different microtubule-organizing centers. J. Cell Biol.158:1195–1206.

Sharan, S.K., Morimatsu, M., Albrecht, U., Lim, D.S., Regel, E., Dinh, C., Sands, A., Eichele, G., Hasty, P., and Bradley, A. (1997). Embryonic lethality and radiation hypersensitivity mediated by Rad51 in mice lacking Brca2. Nature, 386: 804-810.

Shinohara, A., Ogawa, H., and Ogawa, T. (1992). Rad51 protein involved in repair and recombination in S. cerevisiae is a RecA-like protein. Cell 69, 457–470.

Shinohara, A., Gasior, S., Ogawa, T., Kleckner, N. and Bishop, D. K. (1997). *Saccharomyces cerevisiae* recA homologues RAD51and DMC1 have both distinct and overlapping roles in meiotic recombination. Genes to Cells, 2: 615–629.

Slupianek, A., Schmutte, C., Tombline, G., Nieborowska-Skorska, M., Hoser, G., Nowicki, M.O., Pierce, A.J., Fishel, R., and Skorski, T. (2001). BCR/ABL regulates mammalian RecA homologs, resulting in drug resistance. Mol. Cell. 8:795–806.

Smith, J.J., Cole, E.S., and Romero, D.P. (2004). Transcriptional control of RAD51 expression in the ciliate *Tetrahymena thermophila.* Nuc. Acids Res. 32(14), 4313–4321.

Sung, P. (1997). Yeast Rad55 and Rad57 proteins form a heterodimer that functions with replication protein A to promote DNA strand exchange by Rad51 recombinase. Genes Dev. 11(9):1111–1121.

Stover, N.A., Krieger, C.J., Binkley, G., Dong, Q., Fisk, D.G., Nash, R., Sethuraman, A., Weng, S., and Cherry J.M. (2006). Tetrahymena Genome Database (TGD): a new genomic resource for *Tetrahymena thermophile research*. Nuc. Acids Res. 34 (Database issue): D500-3.

Tanaka, K., Kagawa, W., Kinebuchi, T., Kurumizaka, H., and Miyagawa, K. (2002). Human Rad54B is a double-stranded DNA-dependent ATPase and has biochemical properties different from its structural homolog in yeast, Tid1/Rdh54. Nuc. Acids Res. 30(6), 1346–1353.

Tarsounas, M., Davies, A. A., and West, S. C. (2004). RAD51 localization and activation following DNA damage. Philosophical Transactions of the Royal Society B: Biological Sciences, 359(1441), 87–93.

Waters, R. (2006). Maintaining genome integrity. EMBO Reports, 7(4), 377–381.

Wolfe, J., Hunter, B. and Adair, W.S. (1976). A cytological study of micronuclear elongation during conjugation in *Tetrahymena*. Chromosoma 55, 289–308.

Xiong, J., Lu, X., Lu, Y., Zeng, H., Yuan, D., Feng, L., Chang, Y., Josephine, B., Gorovsky, M., Fu, C., and Miao, W. (2011). Tetrahymena Gene Expression Database (TGED): A resource of microarray data and co-expression analyses for Tetrahymena. Science China Life Sciences 54(1): 65-67.

Yoshida, K., Kondoh, G., Matsuda, Y., Habu, T., Nishimune, Y., and Morita, T. (1998) The mouse recA-like gene DMC1 is required for homologous chromosome synapsis during meiosis. Mol. Cell 1, 707–718.

Yu, X., Jacobs, S. A., West, S. C., Ogawa, T., and Egelman, E. H. (2001). Domain structure and dynamics in the helical filaments formed by RecA and Rad51 on DNA. Proc. Natl. Acad. Sci. U.S.A. 98(15), 8419–8424.

Zangen, D., Kaufman, Y., Zeligson, S., Perlberg, S., Fridman, H., Kanaan, M., Abdulhadi-Atwan, A., Abu Libdeh, A., Gussow, A., Kisslov, I., Carmel, L., Renbaum, P., and Levy-Lahad, E. (2011). XX Ovarian Dysgenesis Is Caused by a PSMC3IP/HOP2 Mutation that Abolishes Coactivation of Estrogen-Driven Transcription. Amer. J. Hum. Genet. 89(4), 572–579.

Zhao, W., Saro, D., Hammel, M., Kwon, Y., Xu, Y., Rambo, R.P., and Sung, P. (2014). Mechanistic insights into the role of Hop2–Mnd1 in meiotic homologous DNA pairing. Nuc. Acids Res. 42(2), 906–917.

Zhao, W., and Sung, P. (2015). Significance of ligand interactions involving Hop2-Mnd1 and the RAD51 and DMC1 recombinases in homologous DNA repair and XX ovarian dysgenesis. Nuc. Acids Res. 43(8), 4055–4066.

APPENDICES

Appendix A: *Tetrahymena* Rad51 and Dmc1 Epitope Tags Constructs.

SnapGene program was used to insert *RAD51* and *DMC1* from the pENTR cloning vector into GTW vectors containing GFP, RFP, HA, and FLAG tags. Tagged constructs of Rad51 and Dmc1 are shown in (Figure s A3-A10). Figure s A1 and A2 are pENTR maps used as entry clone containing the *RAD51* and *DMC1* genes. Each construct was confirmed using restriction enzymes that had sites within and out of the genes. Banding patterns resulted from gel electrophoresis were confirmed and compared with the stimulated gel. The plasmids were purified and transformed into *Tetrahymena* to use for further experimentation. Each construct was digested with unique restriction enzymes mentioned in the Figure legends.

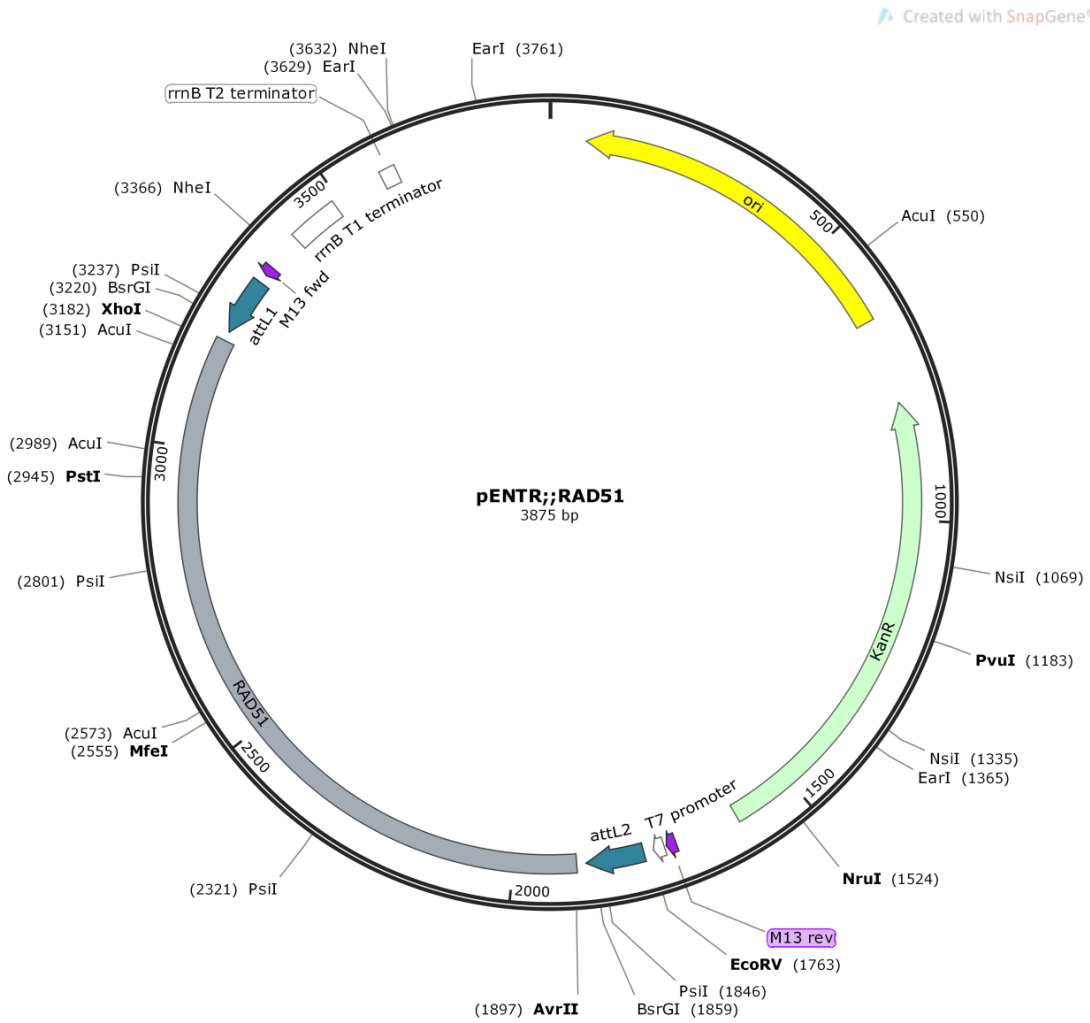

Figure A1. pENTR-RAD51 construct map. The Figure shows the features of pENTR-RAD51 displaying the following: restriction sites, the T7 promoter (purple), Kanamycin resistance gene (light green), RAD51 gene (gray), attL1 and attL2 sites (green) allow recombinational cloning of *RAD51* in the entry construct with a Gateway® destination vector. SnapGene was used to predict fragment sizes (3,485 bp, 390 bp) digested with EcoRI.

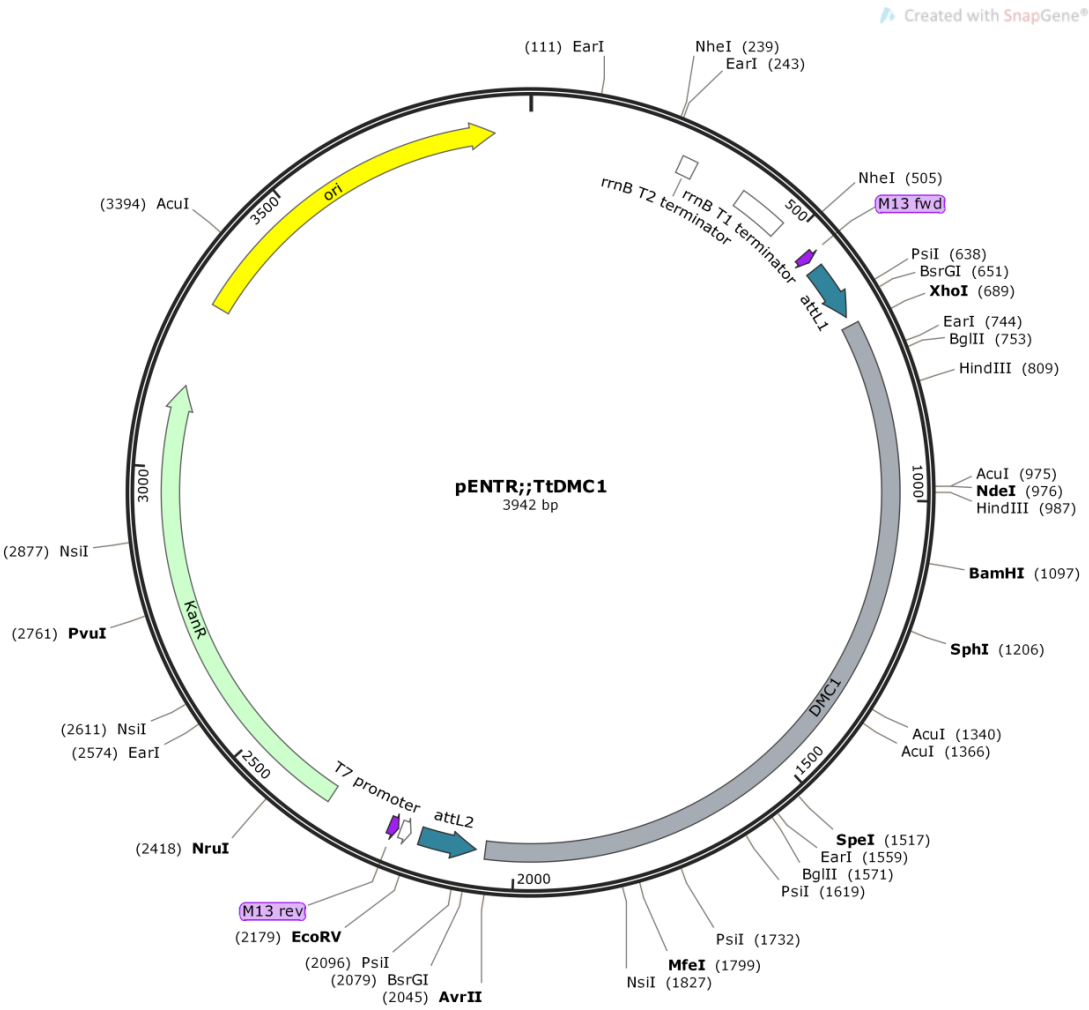

Figure A2. pENTR-DMC1 plasmid map. The Figure shows the features of pENTR-DMC1 displaying the following: restriction sites, the T7 promoter (purple), Kanamycin resistance gene (light green), *DMC1* gene (gray), attL1 and attL2 sites (green) allow recombinational cloning of *DMC1* in the entry construct with a Gateway® destination vector. SnapGene was used to predict fragment sizes (2,892 bp, 784 bp, 566 bp) digested with NsiI.

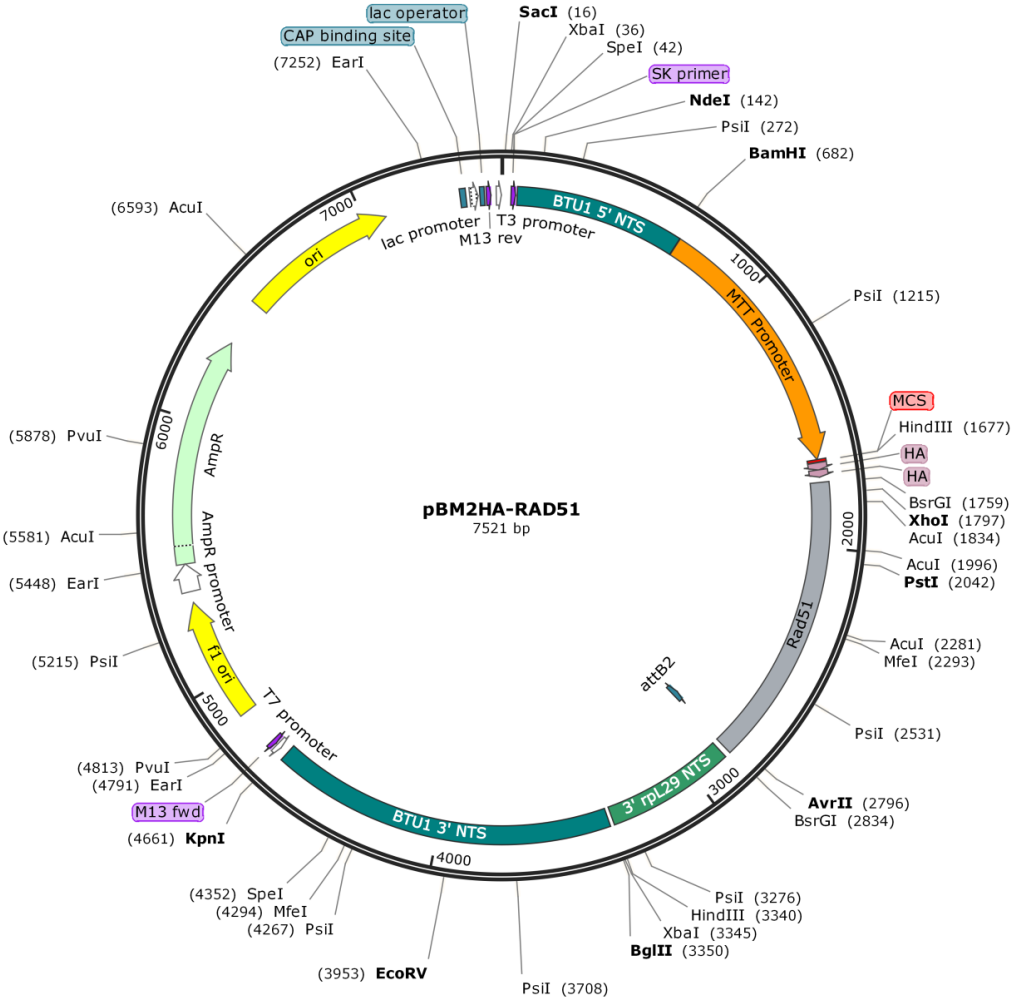

Figure A3. pBM2HA-RAD51 plasmid map. Map of 2HA-RAD51 shows the basic following features: *RAD51* gene (gray), the 2HA tag (pink), the MTT promoter (orange), Ampicillin resistance gene (light green), and BTU1-5' NTS and 3' NTS (blue). SnapGene predicted fragments sizes (6,169 bp, 1,352 bp) which was digested using PstI and BamHI restriction enzymes.

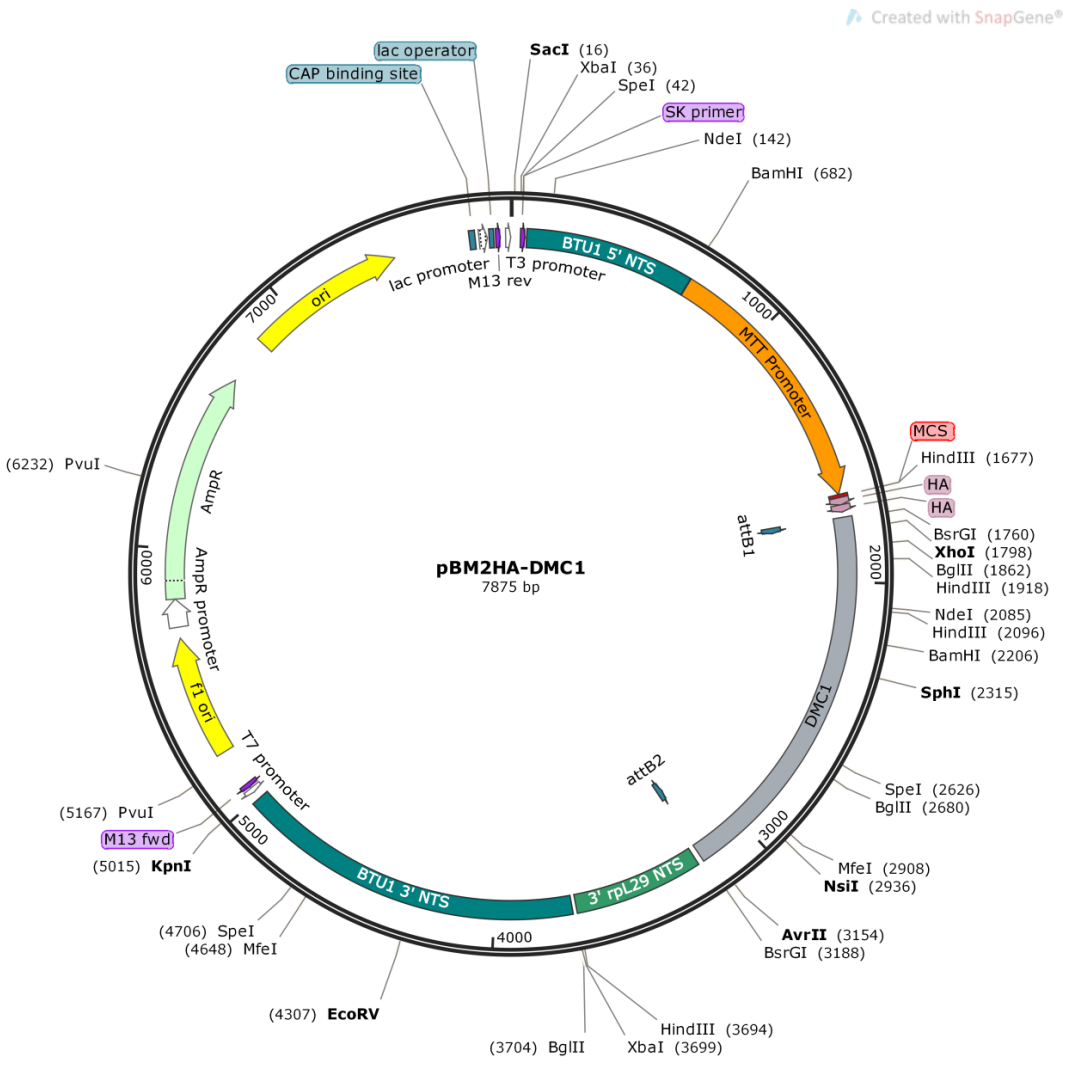

Figure A4. pBM2HA-*DMC1* plasmid map. Map of 2HA-DMC1 shows the basic following features: *DMC1* gene (gray), the 2HA tag (pink), the MTT promoter (orange), Ampicillin resistance gene (light green), and BTU1-5' NTS and 3' NTS (blue). SnapGene predicted fragment sizes (6,351 bp, 1,524 bp) which was digested using BamHI restriction enzyme.

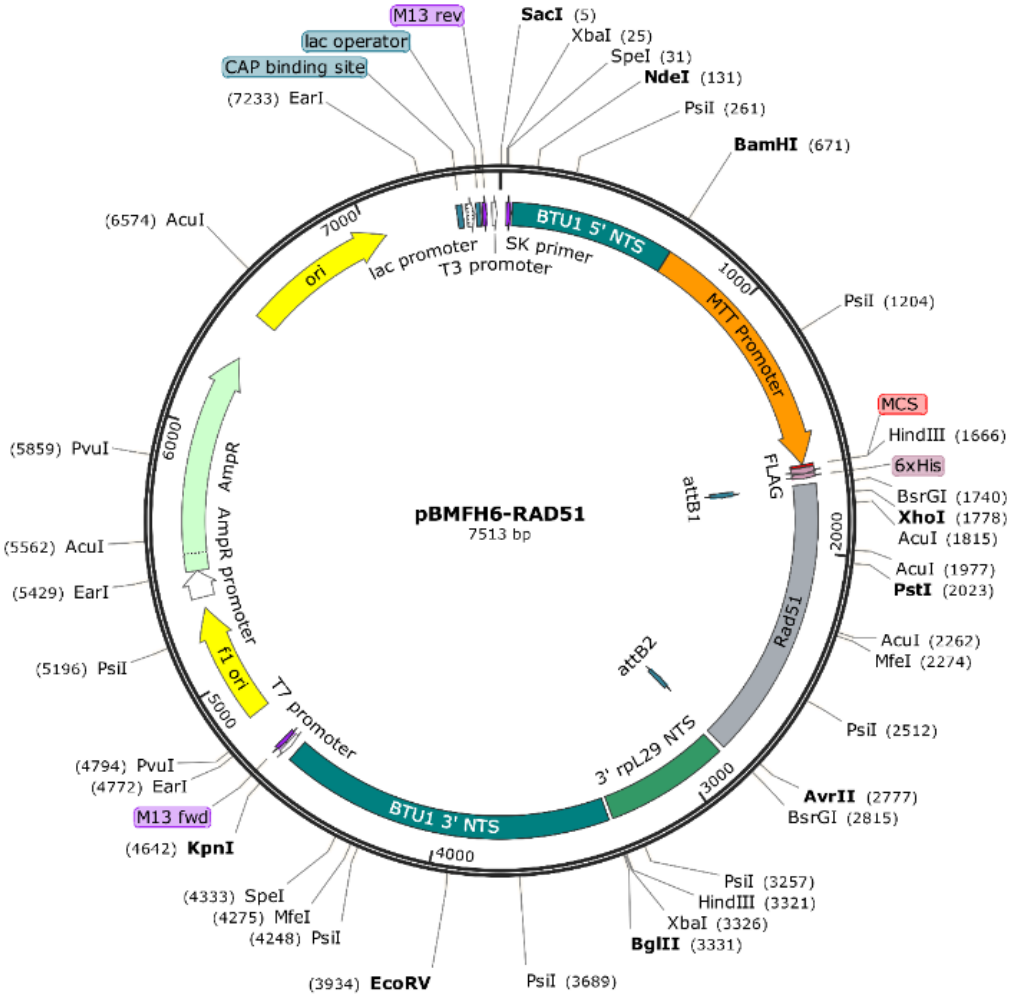

Figure A5. pBMFH6-*RAD51* plasmid map. The map shows the features of FH6-RAD51 displaying the following: *RAD51* gene (gray), the MTT promoter (orange), Ampicillin resistance gene (light green), Flag tag (light purple), and BTU1-5' NTS and 3' NTS (blue). SnapGene predicted fragment sizes (3,211 bp, 2,310 bp, 1,002 bp) which was digested using PstI and SpeI restriction enzymes.

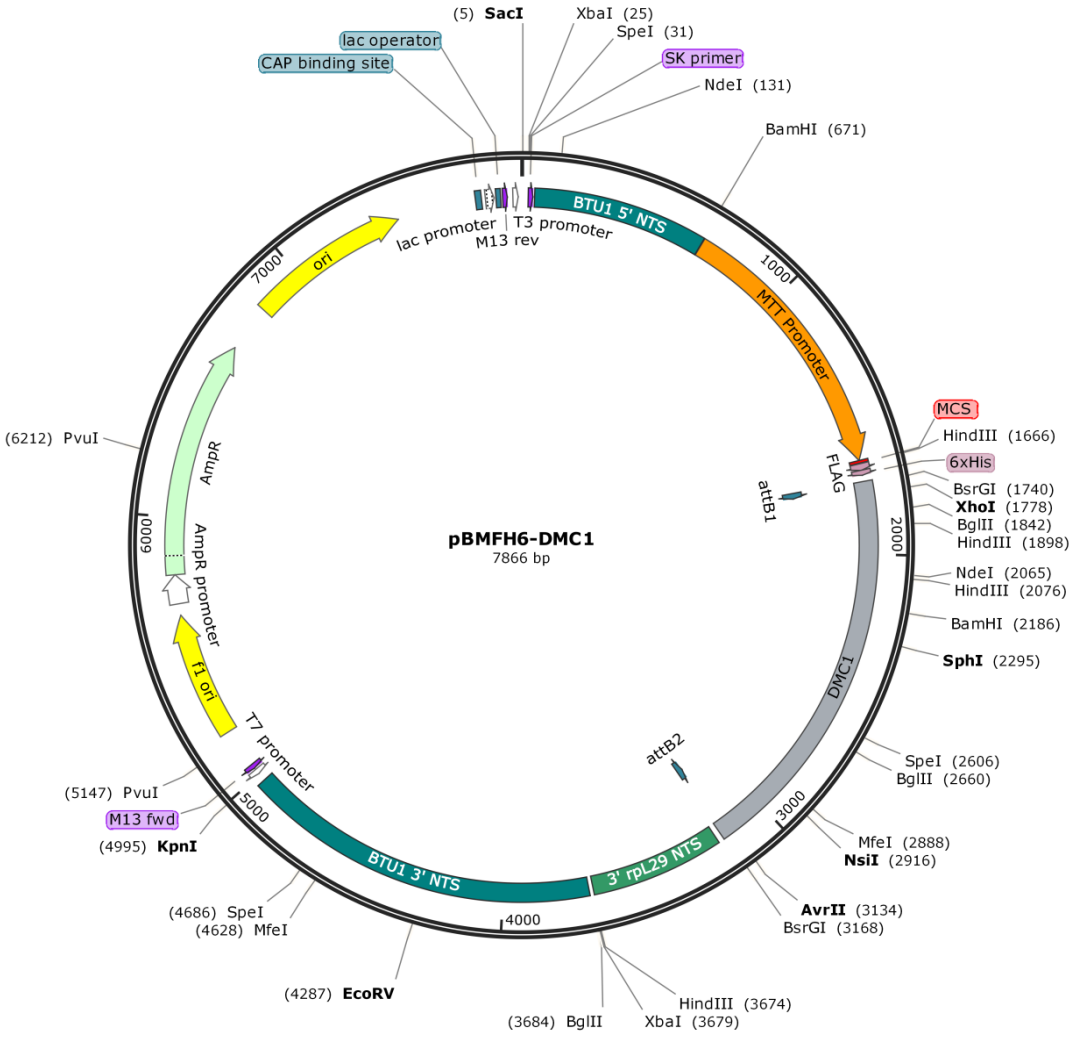

Figure A6. pBMFH6-*DMC1* plasmid map. The map shows the features of FH6-DMC1 displaying the following: *DMC1* gene (gray), the MTT promoter (orange), Ampicillin resistance gene (light green), Flag tag (light purple), and BTU1-5' NTS and 3' NTS (blue). SnapGene predicted fragment sizes (3,211 bp, 2,575 bp, 2,080 bp) which was digested using SpeI restriction enzymes.

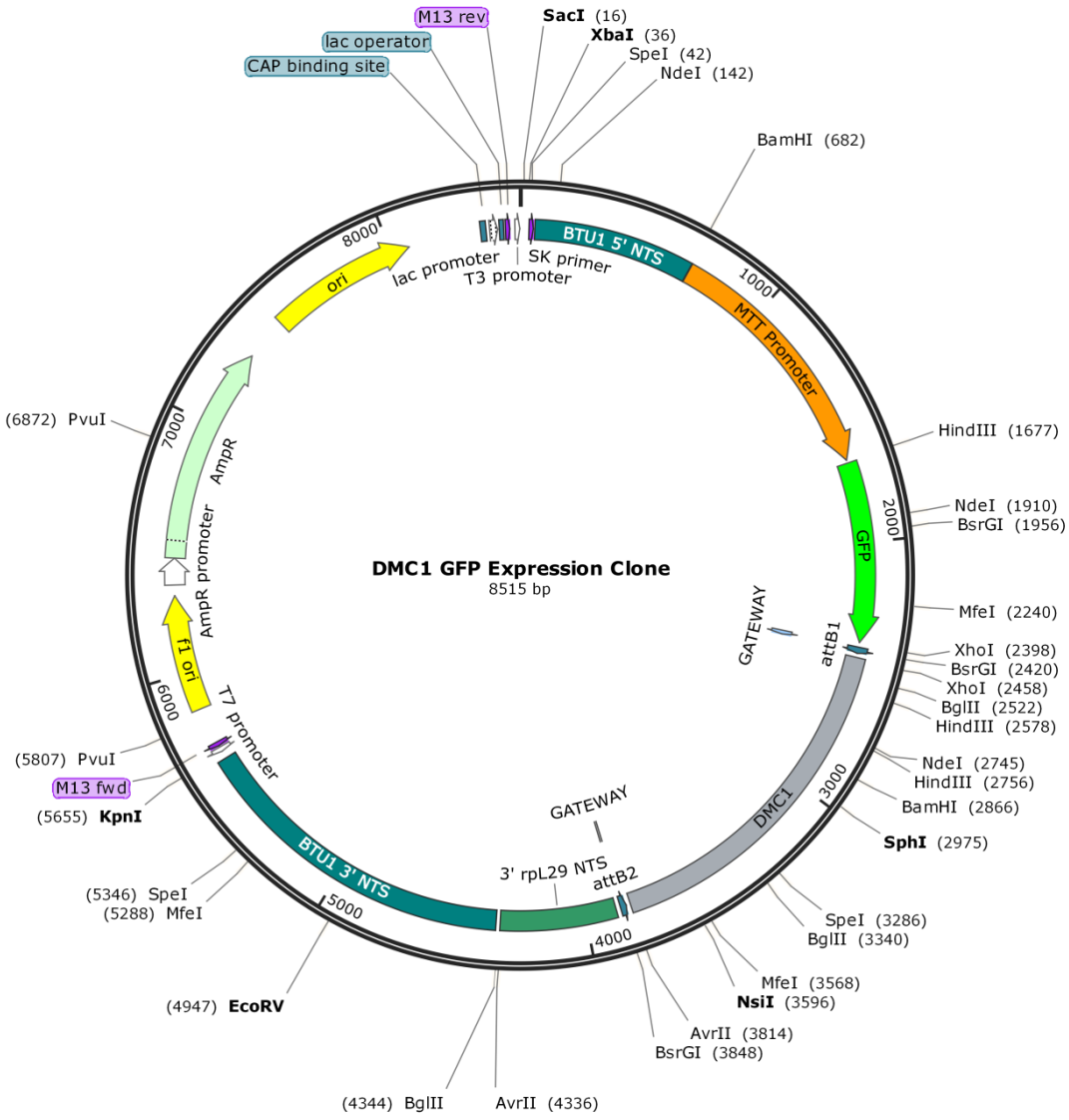

Figure A7. pBMGFP-*DMC1* plasmid map. The map shows the features of GFP-DMC1 displaying the following: restriction enzymes, *DMC1* gene (gray), the MTT promoter (orange), Ampicillin resistance gene (light green), GFP fluorescent tag (green), BTU1-5' NTS and 3' NTS (blue), and attB1 and attB2 sites for recombination cloning (blue). SnapGene predicted fragment sizes (7,436 bp, 901 bp, 178 bp) which was digested using HindIII restriction enzymes.

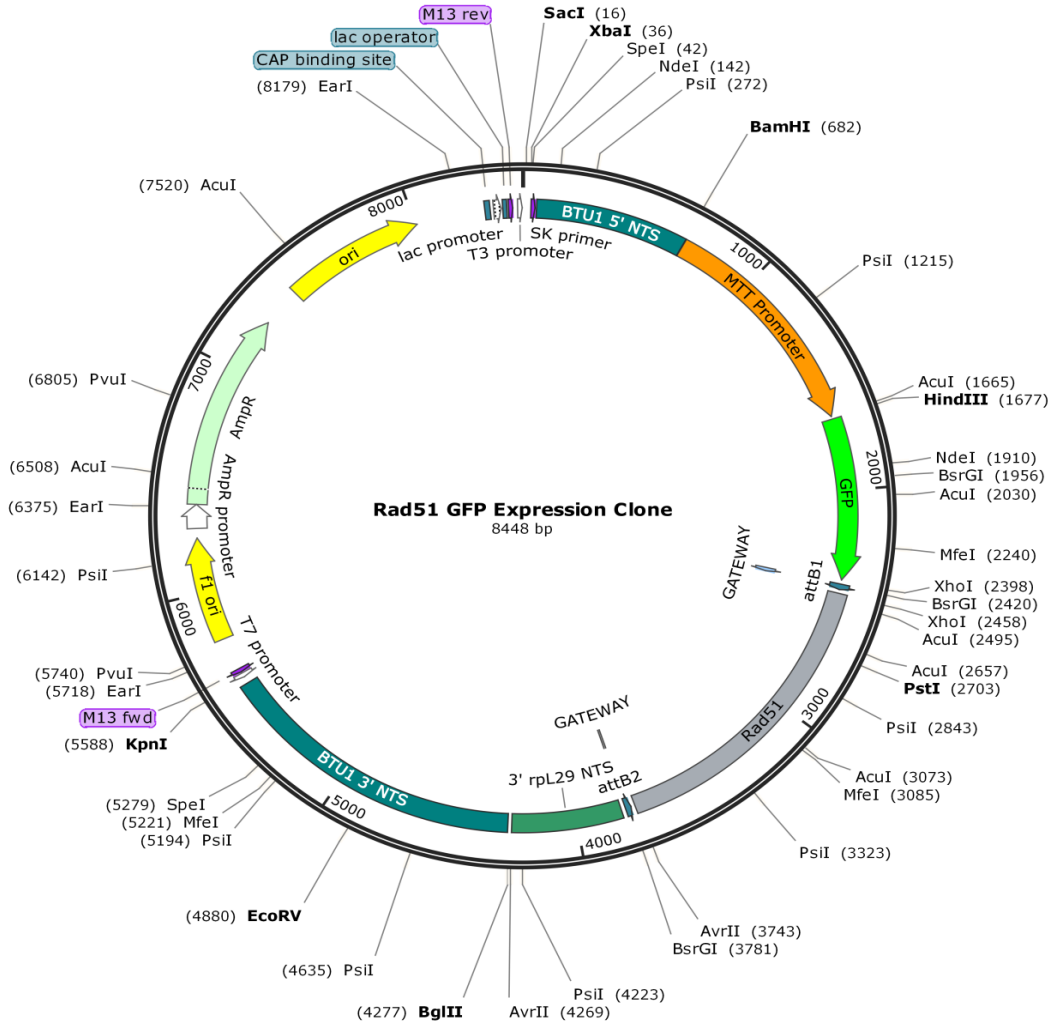

Figure A8. pBMGFP-*RAD51* plasmid map. The map shows the features of GFP-RAD51 displaying the following: restriction enzymes, RAD51 gene (gray), the MTT promoter (orange), Ampicillin resistance gene (light green), GFP fluorescent tag (green), BTU1-5' NTS and 3' NTS (blue), and attB1 and attB2 sites for recombination cloning (blue). SnapGene predicted fragment sizes (6,435 bp, 2,013 bp) which was digested using PstI and BamHI restriction enzymes.

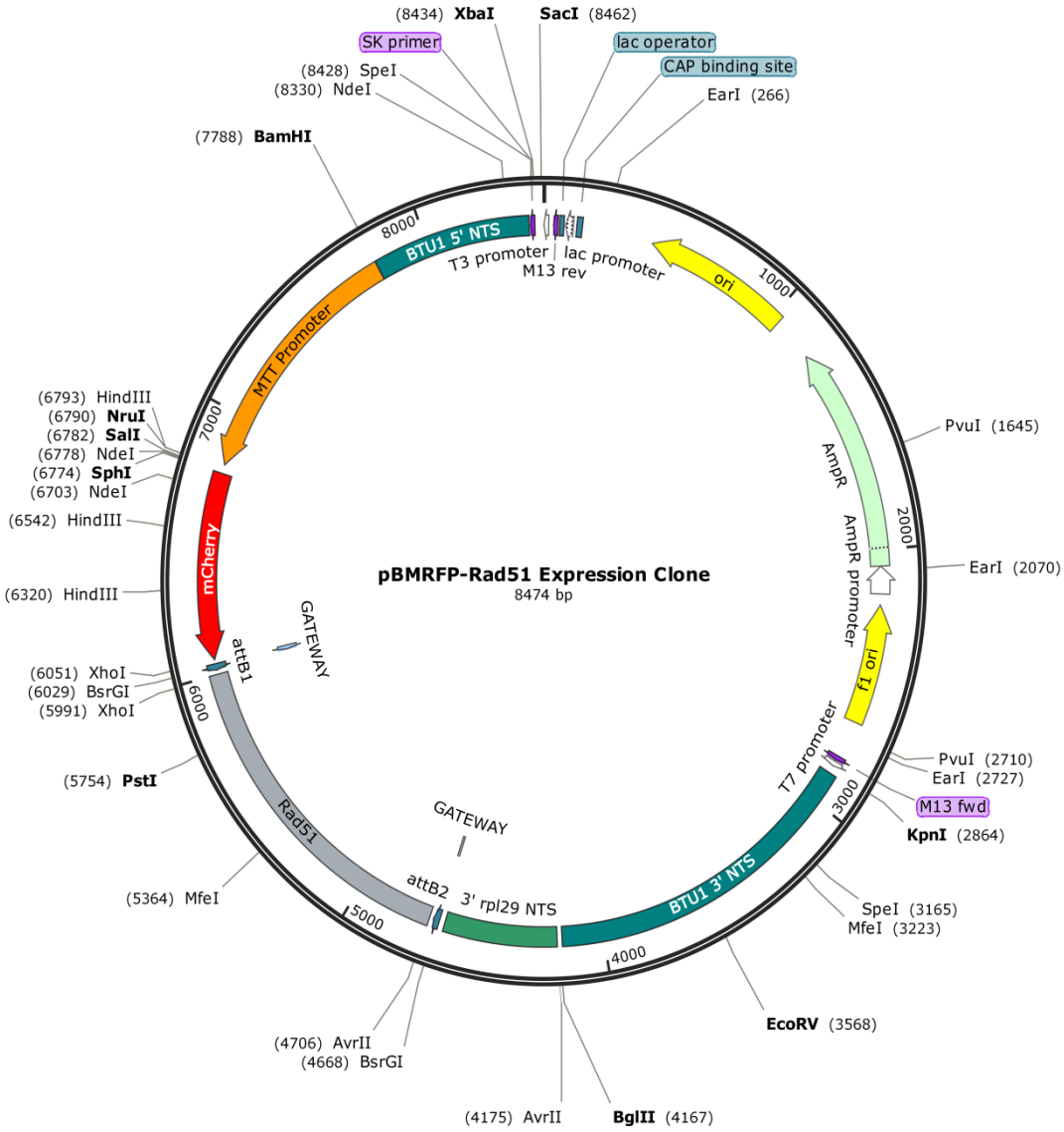

Figure A9. pBMRFP-*RAD51* plasmid map. The map shows the features of RFP-RAD51 displaying the following: restriction enzymes, RAD51 gene (gray), the MTT promoter (orange), Ampicillin resistance gene (light green), RFP fluorescent tag (red), BTU1-5' NTS and 3' NTS (blue), and attB1 and attB2 sites for recombination cloning (blue). SnapGene predicted fragment sizes (6,440 bp, 2,034 bp) which was digested using PstI and BamHI restriction enzymes.

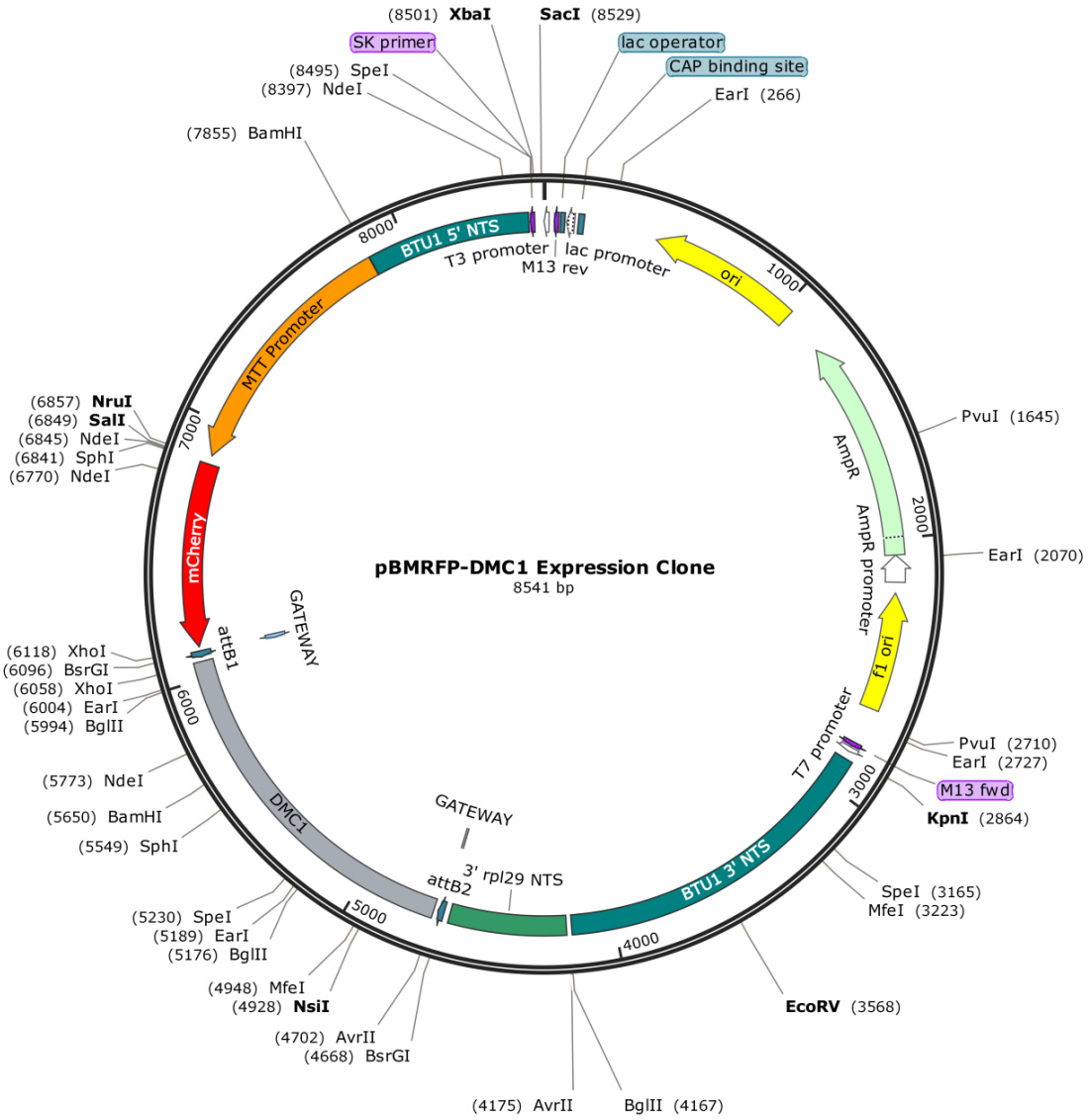

Figure A10. pBMRFP-*DMC1* plasmid map. The map shows the features of RFP-DMC1 displaying the following: restriction enzymes, DMC1 gene (gray), the MTT promoter (orange), Ampicillin resistance gene (light green), RFP fluorescent tag (red), BTU1-5' NTS and 3' NTS (blue), and attB1 and attB2 sites for recombination cloning (blue). SnapGene predicted fragment sizes (7,249 bp, 1,292 bp) which was digested using SphI restriction enzyme.

Appendix B: T-COFFEE Alignment and *T. thermophila* Hop2-Mnd1 Proteins.

Protein sequences were obtained for *T. thermophila* Rad51, Dmc1, Hop2, and Mnd1 using TGD website (www.ciliate.org). *T. thermophila* proteins were compared with homologs of various other organisms. A TCOFFEE alignment was obtained to show the best alignment, and if there are any conserved domains between different sequences. The Walker A and Walker B motifs, found in Rad51 and Dmc1, are conserved motifs among all species and RecA homolog shown in (Figure s B1 and B2)

Hop2 and Mnd1 protein sequences were obtained and two paralogs of each protein were identified in *T. thermophila* (Table B1). The two *T. thermophila* Hop2 (HOP2 and HOPP2) and Mnd1 (MND1 and MNDP1) paralogs were chosen as the best hit and had low E-values compared to their homologs in *Saccharomyes cerevisiae* (Table B1). Microarray data for the two *HOP2* paralogs show that *HOP2* is absent of expression except during conjugation whereas *HOPP2* has some increased expression during starvation as well as during conjugation and is expressed even during vegetative growth unlike *HOP2* (Figure B3). Microarray data for the two *MND1* paralogs shows that *MND1* has a low expression with some expression during conjugation but is minimal whereas *MNDP1* has a higher expression even during vegetative growth and increases during conjugation similar to *RAD51* and *DMC1* (Figure B3).

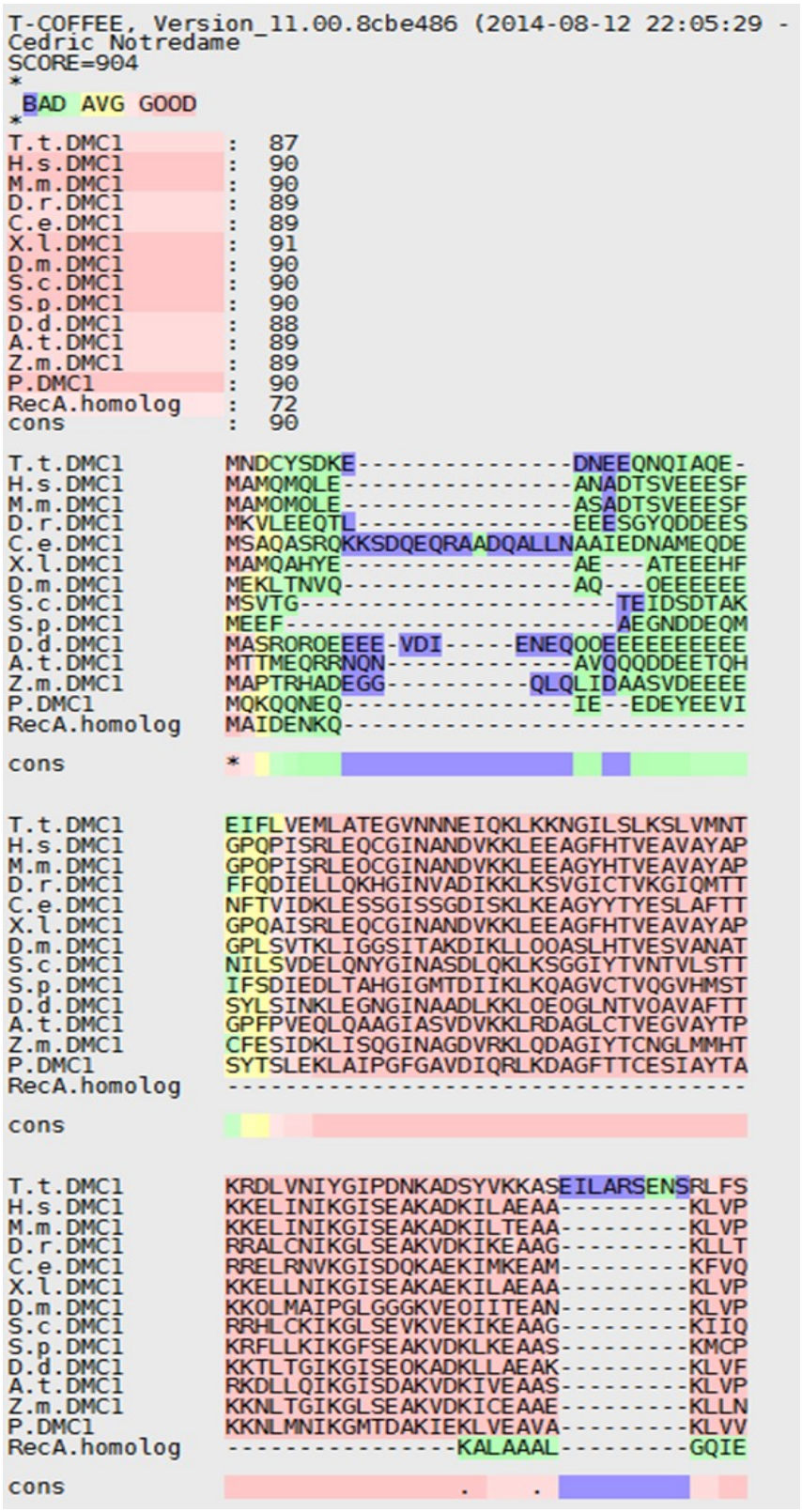
T-COFFEE, Version_11.00.8cbe486 (2014-08-12 22:05:29 -
Cedric Notredame
SCORE=904
BAD AVG GOOD
T.t.DMC1 : 87
H.s.DMC1 : 90
M.m.DMC1 : 90
D.r.DMC1 : 89
C.e.DMC1 : 89
X.l.DMC1 : 91
D.m.DMC1 : 90
S.c.DMC1 : 90
S.p.DMC1 : 90
D.d.DMC1 : 88
A.t.DMC1 : 89
Z.m.DMC1 : 89
P.DMC1 : 90
RecA.homolog : 72
cons : 90


T.t.DMC1
H.s.DMC1
M.m.DMC1
D.r.DMC1
C.e.DMC1
X.l.DMC1
D.m.DMC1
S.c.DMC1
S.p.DMC1
D.d.DMC1
A.t.DMC1
Z.m.DMC1
P.DMC1
RecA.homolog
cons
Walker A motif
Walker B m


Walker B motif
T.t.DMC1 VDSIMANFRCDFSGRGDLSERQQALGK-----FMSR
H.s.DMC1 VDSATALYRTDYSGRGELSARQMHLAR-----FLRM
M.m.DMC1 VDSATALYRTDYSGRGELSARQMHLAR-----FLRM
D.r.DMC1 IDSIMALFRVDFSGRGELAERQQKLAQ-----MLSR
C.e.DMC1 VDCATAHFRNEYTGRGDLAERQMKLSA-----FLKC
X.l.DMC1 VDSATALYRTDYSGRGELSARQMHLAR-----FLRM
D.m.DMC1 VDSAMALYRSDYIGRGELAARQNHLGL-----FLRM
S.c.DMC1 VDSIMANFRVDYCGRGELSERQQKLNQ-----HLFK
S.p.DMC1 VDSIMALFRVDYSGRGELSERQQKLNI-----MLAR
D.d.DMC1 VDSATALYRTDYAGRGELADRQKHLAR-----FLRT
A.t.DMC1 VDSATALYRTDFSGRGELSARQMHLAK-----FLRS
Z.m.DMC1 VDSVIALFRVDFSGRGELAERQQKLAQ-----MLSR
P.DMC1 VDSATALYRTDYLGRGELSARQNHLGK-----FLRN
RecA.homolog VDSVAALTP-KAEIEGEIGDSHMGLAARMMSQAMRK
cons :*. * . .*::. : *
T.t.DMC1 LQRMAAEFNIAVIITNQVMADPSGA-MTGGAIPQPK
H.s.DMC1 LLRLADEFGVAVVITNQVVAQVDGA-AMFA-ADPKK
M.m.DMC1 LLRLADEFGVAVVITNQVVAQVDGA-AMFA-ADPKK
D.r.DMC1 LQKISEEYNVAVFVTNQMTADPGAG-MTFQ-ADPKK
C.e.DMC1 LAKLADEYGVAVIITNQVVAQVDGGASMFQ-ADAKK
X.l.DMC1 LLRLADEFGVAVVITNQVVAQVDGA-AMFA-ADPKK
D.m.DMC1 LQRLADEFGVAVVITNQVTASLDGAPGMF---DAKK
S.c.DMC1 LNRLAEEFNVAVFLTNQVQSDPGAS-ALFASADGRK
S.p.DMC1 LNHISEEFNVAVFVTNQVQADPGAA-MMFA-SNDRK
D.d.DMC1 LQRLADEFGVAVVITNQVVASVDGAGGMFN-PDPKK
A.t.DMC1 LQKLADEFGVAVVITNQVVAQVDGS-ALFA-GPQFK
Z.m.DMC1 LTKIAEEFNVAVYITNQVIADPGGG--MFI-TDPKK
P.DMC1 LQRLADEFNVAVVITNQVMSQVEGT-MMAM-GDQKK
RecA.homolog LAGNLKQSNTLLIFINQIRMKIG---VMF--GNPET
cons * : . : . **: .
T.t.DMC1 PIGGHILAHASTQRLFMKKKT----------DNIRK
H.s.DMC1 PIGGNIIAHASTTRLYLRKGR----------GETRI
M.m.DMC1 PIGGNIIAHASTTRLYLRKGR----------GETRI
D.r.DMC1 PIGGHILAHASTTRISLRKGR----------AELRI
C.e.DMC1 PIGGHIIAHMSTTRLYLRKGK----------GENRV
X.l.DMC1 PIGGNIIAHASTTRLYLRKGR----------GETRI
D.m.DMC1 PIGGHIMAHSSTTRLYLRKGK----------GETRI
S.c.DMC1 PIGGHVLAHASATRILLRKGR----------GDERV
S.p.DMC1 PVGGHVMAHASATRLLLRKGR----------GEERV
D.d.DMC1 PIGGHIMAHSSTTRLSLRKGK----------GEMRI
A.t.DMC1 PIGGNIMAHATTTRLALRKGR----------AEERI
Z.m.DMC1 PAGGHVLAHAATIRLMLRKGK----------GEQRV
P.DMC1 PIGGNIMAHASTTRLYLRKGR----------GENRI
RecA.homolog TTGGNALKFYASVRLDIRRIGAVKEGENVVGSETRV
cons . **: : . :: *: ::: : *

Figure B1. T-COFFEE Alignment of DMC1. The protein sequence of *T. thermophila* and other species were entered into TCOFFEE alignment generator. Red shows the best alignment; yellow shows regions with average similarities between the sequences, then blue shows where there are no similarities between aligned sequences.

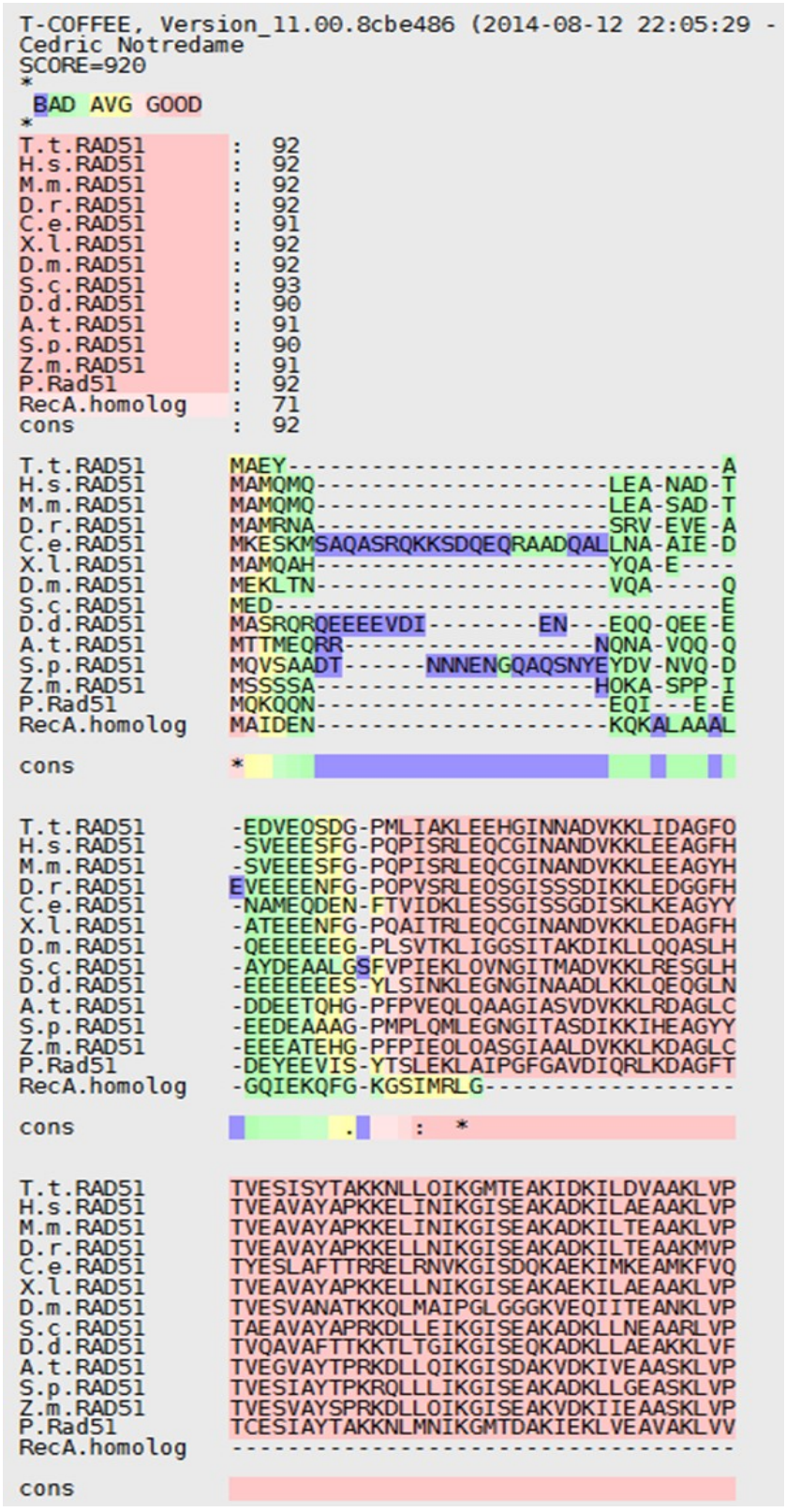
T-COFFEE, Version_11.00.8cbe486 (2014-08-12 22:05:29 -
Cedric Notredame
SCORE=920
BAD AVG GOOD
T.t.RAD51 : 92
H.s.RAD51 : 92
M.m.RAD51 : 92
D.r.RAD51 : 92
C.e.RAD51 : 91
X.l.RAD51 : 92
D.m.RAD51 : 92
S.c.RAD51 : 93
D.d.RAD51 : 90
A.t.RAD51 : 91
S.p.RAD51 : 90
Z.m.RAD51 : 91
P.Rad51 : 92
RecA.homolog : 71
cons : 92
T.t.RAD51 MAEY----------A
H.s.RAD51 MAMQMQ----------LEA-NAD-T
M.m.RAD51 MAMQMQ----------LEA-SAD-T
D.r.RAD51 MAMRNA----------SRV-EVE-A
C.e.RAD51 MKESKMSAQASRQKKSDQEQRAADQALLNA-AIE-D
X.l.RAD51 MAMQAH----------YQA-E----
D.m.RAD51 MEKLTN----------VQA-----Q
S.c.RAD51 MED----------E
D.d.RAD51 MASRQRQEEEEVDI--------EN---EQQ-QEE-E
A.t.RAD51 MTTMEQRR----------NQNA-VQQ-Q
S.p.RAD51 MQVSAADT------NNNENGQAQSNYEYDV-NVQ-D
Z.m.RAD51 MSSSSA----------HQKA-SPP-I
P.Rad51 MQKQQN----------EQI---E-E
RecA.homolog MAIDEN----------KQKALAAAL
cons *
T.t.RAD51 -EDVEQSDG-PMLIAKLEEHGINNADVKKLIDAGFQ
H.s.RAD51 -SVEEESFG-PQPISRLEQCGINANDVKKLEEAGFH
M.m.RAD51 -SVEEESFG-PQPISRLEQCGINANDVKKLEEAGYH
D.r.RAD51 EVEEEENFG-PQPVSRLEQSGISSSDIKKLEDGGFH
C.e.RAD51 -NAMEQDEN-FTVIDKLESSGISSGDISKLKEAGYY
X.l.RAD51 -ATEEENFG-PQAITRLEQCGINANDVKKLEDAGFH
D.m.RAD51 -QEEEEEEG-PLSVTKLIGGSITAKDIKLLQQASLH
S.c.RAD51 -AYDEAALGSFVPIEKLQVNGITMADVKKLRESGLH
D.d.RAD51 -EEEEEEES-YLSINKLEGNGINAADLKKLQEQGLN
A.t.RAD51 -DDEETQHG-PFPVEQLQAAGIASVDVKKLRDAGLC
S.p.RAD51 -EEDEAAAG-PMPLQMLEGNGITASDIKKIHEAGYY
Z.m.RAD51 -EEEATEHG-PFPIEQLQASGIAALDVKKLKDAGLC
P.Rad51 -DEYEEVIS-YTSLEKLAIPGFGAVDIQRLKDAGFT
RecA.homolog -GQIEKQFG-KGSIMRLG----------
cons . : *
T.t.RAD51 TVESISYTAKKNLLQIKGMTEAKIDKILDVAAKLVP
H.s.RAD51 TVEAVAYAPKKELINIKGISEAKADKILAEAAKLVP
M.m.RAD51 TVEAVAYAPKKELINIKGISEAKADKILTEAAKLVP
D.r.RAD51 TVEAVAYAPKKELLNIKGISEAKADKILTEAAKMVP
C.e.RAD51 TYESLAFTTRRELRNVKGISDQKAEKIMKEAMKFVQ
X.l.RAD51 TVEAVAYAPKKELLNIKGISEAKAEKILAEAAKLVP
D.m.RAD51 TVESVANATKKQLMAIPGLGGGKVEQIITEANKLVP
S.c.RAD51 TAEAVAYAPRKDLLEIKGISEAKADKLLNEAARLVP
D.d.RAD51 TVQAVAFTTKKTLTGIKGISEQKADKLLAEAKKLVF
A.t.RAD51 TVEGVAYTPRKDLLQIKGISDAKVDKIVEAASKLVP
S.p.RAD51 TVESIAYTPKRQLLLIKGISEAKADKLLGEASKLVP
Z.m.RAD51 TVESVAYSPRKDLLQIKGISEAKVDKIIEAASKLVP
P.Rad51 TCESIAYTAKKNLMNIKGMTDAKIEKLVEAVAKLVV
RecA.homolog ----------
cons

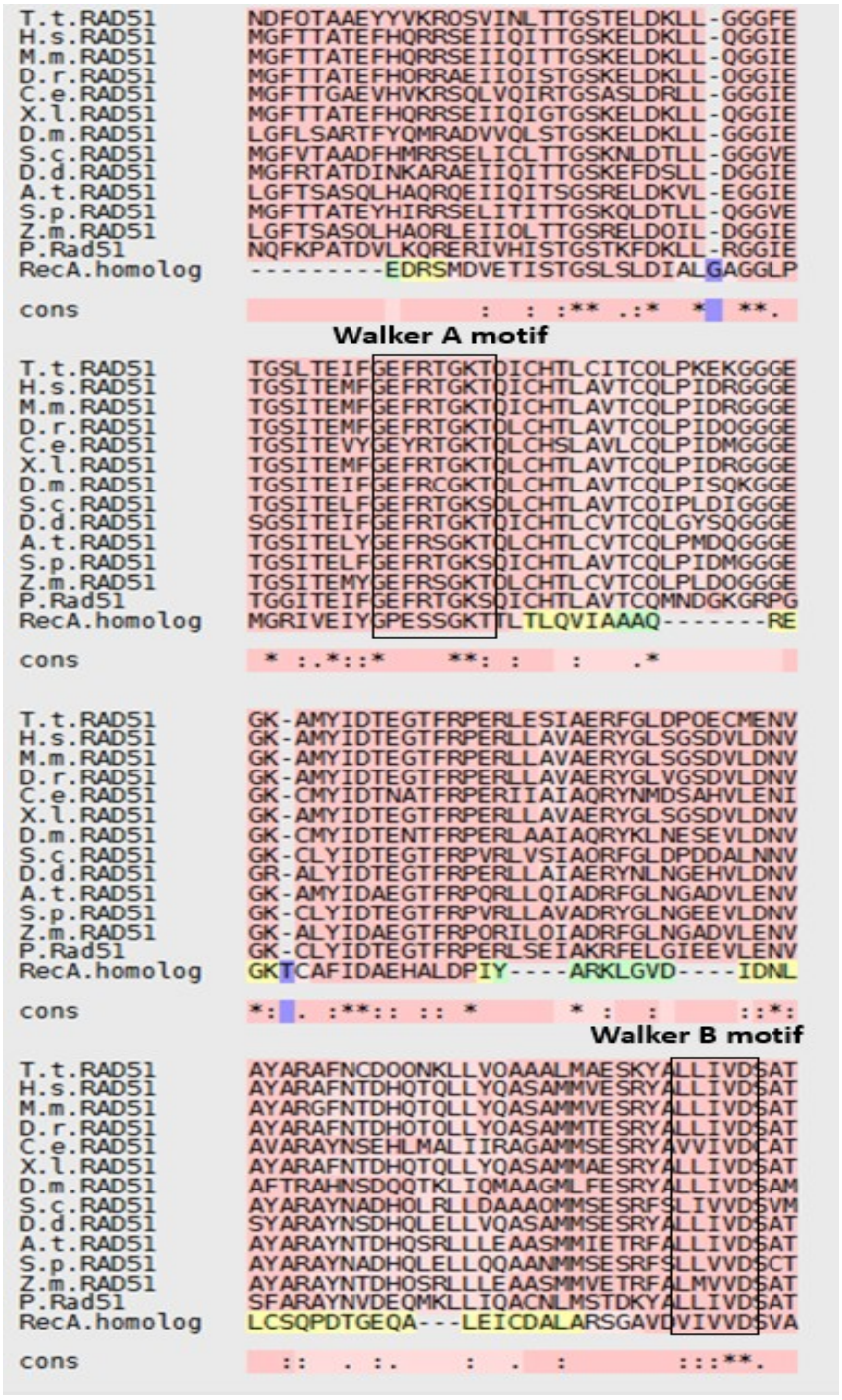
Walker A motif
Walker B motif

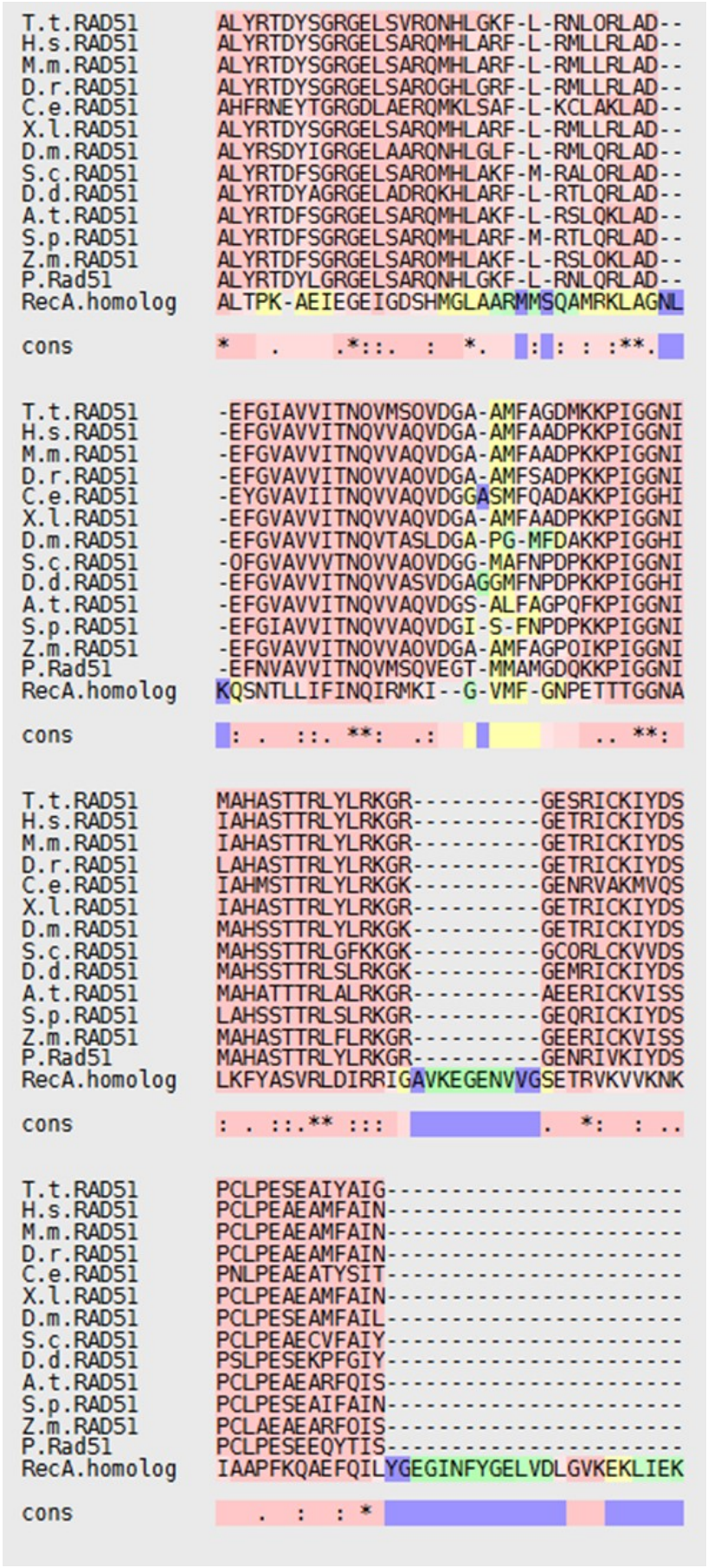
T.t.RAD51 ALYRTDYSGRGELSVRQNHLGKF-L-RNLQRLAD--
H.s.RAD51 ALYRTDYSGRGELSARQMHLARF-L-RMLLRLAD--
M.m.RAD51 ALYRTDYSGRGELSARQMHLARF-L-RMLLRLAD--
D.r.RAD51 ALYRTDYSGRGELSAROGHLGRF-L-RMLLRLAD--
C.e.RAD51 AHFRNEYTGRGDLAERQMKLSAF-L-KCLAKLAD--
X.l.RAD51 ALYRTDYSGRGELSARQMHLARF-L-RMLLRLAD--
D.m.RAD51 ALYRSDYIGRGELAARQNHLGLF-L-RMLQRLAD--
S.c.RAD51 ALYRTDFSGRGELSAROMHLAKF-M-RALQRLAD--
D.d.RAD51 ALYRTDYAGRGELADRQKHLARF-L-RTLQRLAD--
A.t.RAD51 ALYRTDFSGRGELSARQMHLAKF-L-RSLQKLAD--
S.p.RAD51 ALYRTDFSGRGELSARQMHLARF-M-RTLQRLAD--
Z.m.RAD51 ALYRTDFSGRGELSAROMHLAKF-L-RSLQKLAD--
P.Rad51 ALYRTDYLGRGELSARQNHLGKF-L-RNLQRLAD--
RecA.homolog ALTPK-AEIEGEIGDSHMGLAARMMSQAMRKLAGNL
cons * . .*::. : *. :: : : :**.
T.t.RAD51 -EFGIAVVITNQVMSQVDGA-AMFAGDMKKPIGGNI
H.s.RAD51 -EFGVAVVITNQVVAQVDGA-AMFAADPKKPIGGNI
M.m.RAD51 -EFGVAVVITNQVVAQVDGA-AMFAADPKKPIGGNI
D.r.RAD51 -EFGVAVVITNQVVAQVDGA-AMFSADPKKPIGGNI
C.e.RAD51 -EYGVAVIITNQVVAQVDGGASMFQADAKKPIGGHI
X.l.RAD51 -EFGVAVVITNQVVAQVDGA-AMFAADPKKPIGGNI
D.m.RAD51 -EFGVAVVITNQVTASLDGA-PG-MFDAKKPIGGHI
S.c.RAD51 -OFGVAVVVTNQVVAQVDGG-MAFNPDPKKPIGGNI
D.d.RAD51 -EFGVAVVITNQVVASVDGAGGMFNPDPKKPIGGHI
A.t.RAD51 -EFGVAVVITNQVVAQVDGS-ALFAGPQFKPIGGNI
S.p.RAD51 -EFGIAVVITNQVVAQVDGI-S-FNPDPKKPIGGNI
Z.m.RAD51 -EFGVAVVITNQVVAQVDGA-AMFAGPQIKPIGGNI
P.Rad51 -EFNVAVVITNQVMSQVEGT-MMAMGDQKKPIGGNI
RecA.homolog KQSNTLLIFINQIRMKI--G-VMF-GNPETTTGGNA
cons : . ::. **: .: .. **:
T.t.RAD51 MAHASTTRLYLRKGR----------GESRICKIYDS
H.s.RAD51 IAHASTTRLYLRKGR----------GETRICKIYDS
M.m.RAD51 IAHASTTRLYLRKGR----------GETRICKIYDS
D.r.RAD51 LAHASTTRLYLRKGR----------GETRICKIYDS
C.e.RAD51 IAHMSTTRLYLRKGK----------GENRVAKMVQS
X.l.RAD51 IAHASTTRLYLRKGR----------GETRICKIYDS
D.m.RAD51 MAHSSTTRLYLRKGK----------GETRICKIYDS
S.c.RAD51 MAHSSTTRLGFKKGK----------GCORLCKVVDS
D.d.RAD51 MAHSSTTRLSLRKGK----------GEMRICKIYDS
A.t.RAD51 MAHATTTRLALRKGR----------AEERICKVISS
S.p.RAD51 LAHSSTTRLSLRKGR----------GEQRICKIYDS
Z.m.RAD51 MAHASTTRLFLRKGR----------GEERICKVISS
P.Rad51 MAHASTTRLYLRKGR----------GENRIVKIYDS
RecA.homolog LKFYASVRLDIRRIGAVKEGENVVGSETRVKVVKNK
cons : . ::.** ::: . *: : ..
T.t.RAD51 PCLPESEAIYAIG----------
H.s.RAD51 PCLPEAEAMFAIN----------
M.m.RAD51 PCLPEAEAMFAIN----------
D.r.RAD51 PCLPEAEAMFAIN----------
C.e.RAD51 PNLPEAEATYSIT----------
X.l.RAD51 PCLPEAEAMFAIN----------
D.m.RAD51 PCLPESEAMFAIL----------
S.c.RAD51 PCLPEAECVFAIY----------
D.d.RAD51 PSLPESEKPFGIY----------
A.t.RAD51 PCLPEAEARFQIS----------
S.p.RAD51 PCLPESEAIFAIN----------
Z.m.RAD51 PCLAEAEARFQIS----------
P.Rad51 PCLPESEEQYTIS----------
RecA.homolog IAAPFKQAEFQILYGEGINFYGELVDLGVKEKLIEK
cons . : : *

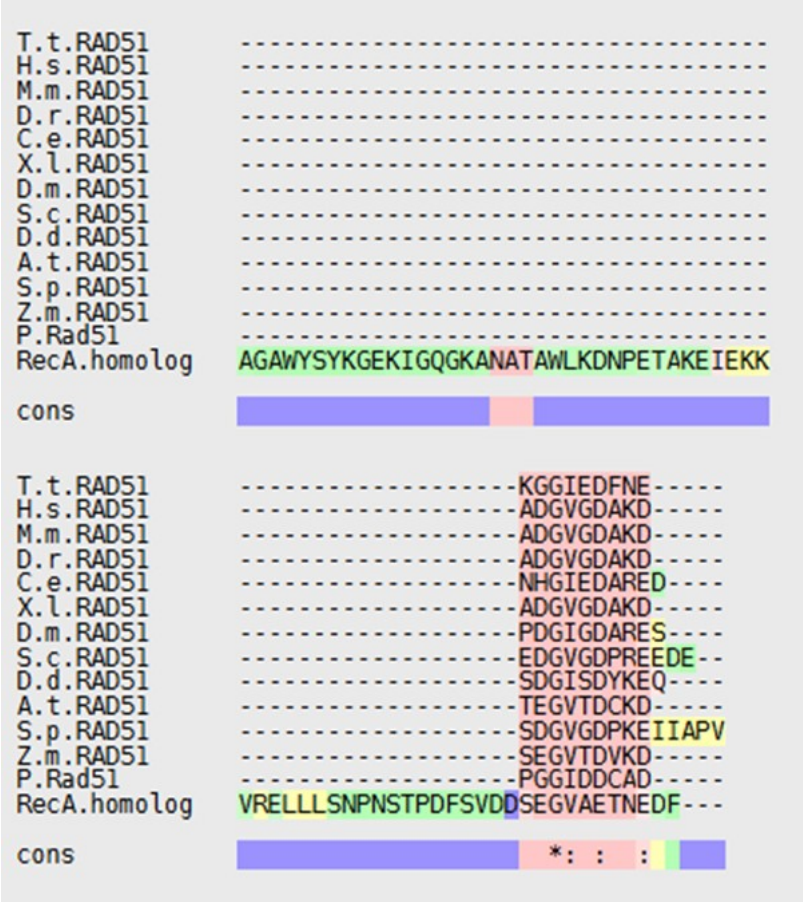

Figure B2. T-COFFEE Alignment of RAD51. The protein sequence of *T. thermophila* Rad51 and other species were entered into TCOFFEE alignment generator. Red shows the best alignment; yellow shows regions with average similarities between the sequences, then blue shows where there are no similarities between aligned sequences.

Table B1. *T. thermophila* Hop2-Mnd1 homologs.

T. thermophila Gene Name	Gene Identification (TTHERM_#)	S. cerevisiae BLAST E-value	Gene Description
HOP2	TTHERM_00794620	5e-05	HOP2 has a role in chiasmata and meiotic bivalent formation.
HOPP2	TTHERM_01190440	1e-10	Ubiquitously expressed paralog of the meiotically expressed gene HOP2 (TTHERM_00794620). Essential for vegetative growth.
MND1	TTHERM_00300659 (Formerly TTHERM_00300660 before annotation correction)	8e-12	The Mnd1 protein forms a complex with Hop2 to promote homologous chromosome pairing and meiotic DSB repair. Mnd1 requires Hop2 to localize to chromosomes. It is a meiotic version.
MNDP1	TTHERM_00382290	8e-14	The Mnd1 protein forms a complex with Hop2 to promote homologous chromosome pairing and meiotic DSB repair. Mnd1 requires Hop2 to localize to chromosomes. It's a ubiquitously expressed version copy